Doctoral Dissertation

Fundamental Investigation on High Quality Hole Drilling of CFRP (Carbon Fiber Reinforced Plastic) Using a Tilted Helical Milling Technique

チルトヘリカル加工による **CFRP**（炭素繊維強化プラスチック）の高品質穴開けに関する基礎研究

By

Qiang Wang

Akita Prefectural University
Akita, Japan

September 2018

This page intentionally left blank.

CONTENTS

Abstract

Carbon fiber reinforced plastic (CFRP) is used for various mechanical structures because of its superior mechanical and physical properties. A lot of drilling is demanded during the processing and manufacturing of CFRP components. However, characterized by nonuniformity, anisotropy and high hardness, CFRP is susceptible to bearing following defects when processed with conventional drilling technology: entrance cleavage, exit laceration, delamination, and burrs. The aforesaid defects may affect the service life of CFRP components and even cause scrapping of such components.

To solve the problem, this paper has investigated and compared all sorts of CFRP drilling techniques in terms of processing efficiency and quality, and it was found that the conventional helical milling (CHM) technology was advantageous than others in both processing efficiency and quality. But CHM was still faced with a few problems such as zero-point in cutting speed of cutting tool terminal, delamination at hole exit due to extruding of material at hole bottom, and inner surface scratch of the hole caused by friction between side edge of cutting tool and inner hole wall. Therefore, this study proposed a novel method for drilling holes in CFRP products. This new method is performed by replacing the revolving motion of the tool in CHM with conical pendulum motion in which the tool axis is tilted towards the hole axis at a certain angle, consequently it was called tilted helical milling (THM). With THM processing, when the cutting tool revolves on its own axis, its axis keeps tilting in relation to the hole axis at a certain angle and maintains screw-feed along the hole axis.

Firstly, an experimental device of THM was designed and manufactured for verifying the effectiveness of the proposed method, then a theoretical analysis of the hole forming process and material removal rate during THM was performed and experiments were conducted to verify its basic processing properties and strengths. Further, the exit formation of the hole was studied, and the inhibition mechanism of the hole exit formation on the exit delamination defect was figured out. The obtained results revealed that the obtained results revealed that during hole drilling by THM, a

circumferential V-groove exists between the end face of the tool and the bottom of the hole, whereas in CHM this phenomenon does not occur. This fact is beneficial to timely chip removal, drilling force reduction and zero cutting speed point problem avoidance. Moreover, the hole exit formation in THM was divided into two stages: formation of small-diameter hole and hole enlargement processing. The extruded layer resulting from the first stage would be removed through hole diameter enlargement in the second one to inhibit the generation of delamination at the hole exit.

Both cutting force and cutting temperature can produce a significant effect on the CFRP processing quality. Therefore, this paper established a mechanical model about the cutting force of THM to study the factors performing on the cutting force. A string of plans was adopted to measure the cutting temperature during THM processing, and the effects of cutting force and cutting temperature were analyzed in different machining conditions. Lastly, the processing quality of hole entrance, exit and inner surface in different processing conditions was assessed to optimize the processing conditions and provide guidance for potential industrial application. The research results indicate the THM can generate high-quality holes on CFRP at a high efficiency.

According to the above results, THM was proven to have such strengths as speed zero-point evading, delamination inhibition, smooth cuttings discharge, strong heat radiation capacity, and low thrust force. Subsequently, high quality holes can be successfully obtained with high efficiency by THM.

Chapter I
Introduction

1.1 CFRP

With features such as light weight and high strength, high resistance to strain and abrasion, and extremely low shrinkage and expansion against heat, carbon fiber reinforced plastic (CFRP) is widely used in aerospace, defense industry, transportation, wind power and other fields [1, 2]. With the continued maturation of material preparation processes and equipment, the comprehensive cost of composite materials has been continuously optimized, which has promoted the rapid development of CFRP applications in the industrial field. In recent years, the requirements for energy saving, emission reduction and environmental protection have been continuously improved, prompting CFRP to rapidly replace traditional metal materials as the preferred material for structural materials [2].

Although the application prospect of CFRP is very good and the potential demand is huge, it will be popularized and popularized in the industrial field. The requirements for CFRP material preparation technology and CFRP component manufacturing process will inevitably become more stringent. In the application of CFRP products, the joining process of CFRP parts is essential, and usually three methods are available: mechanical fastening (such as riveting and bolting), bonding, and a combination of mechanical fastening and bonding [3, 4]. Because mechanically fastened CFRP parts are convenient to repair/access, and mechanical fasteners are not sensitive to surface preparation, service temperature, or humidity, the mechanical fastening method has been used more extensively when compared to the other two methods [5]. Therefore, drilling holes in CFRP parts is essential for mechanical fastening.

However, CFRP is a multiphase structure made of carbonized propylene fiber and epoxy resin, which has the characteristics of non-homogeneity, anisotropy, high hardness, and is difficult to cut. Conventional drilling techniques are prone to splitting at the entrance, tearing at the exit, burrs, delamination, radial crushing, micro-cracks

and other damage [6]. These defects will affect the service life of the components, even serious Lead to the retirement of the overall structure [7,8]. This has become a bottleneck in the promotion and application of CFRP, and it is urgent to seek solutions to it.

1.2 Current drilling techniques

At present, the hole making process of CFRP mainly adopts the method of mechanical drilling. High processing efficiency is its greatest advantage. But poor machinability of CFRP poses considerable problems in the drilling process when using a drill or milling cutting tool. Because of anisotropy, highly heterogeneous nature, weak bonding strength between layers, low thermal conductivity, and small fracture strain, uncut fibers and delamination occur frequently, resulting in reduced fatigue strength, poor assembly tolerance, and compromised structural integrity [9-11]. Thus, burrs, chippings, and delamination have been considered to be the major challenges with CFRP materials with a drill or milling cutting tool.

To face the existing problems above-mentioned, in recent years, many researchers have made their efforts to study the drilling mechanism and adopt the strategies of improving the hole quality by experiments and simulation, and consequently proposed several novel techniques such as abrasive water jet and laser processing to solve the problems in CFRP drilling (Fig. 1.1). In some respects, they have certain advantages, but there are many limitations; for example, abrasive water. Jets tend to form tapered holes with poor surface roughness and risk of delamination; laser holes are prone to thermal damage due to high temperature and high heat. Therefore, mechanical drilling is still widely used in CFRP hole making.

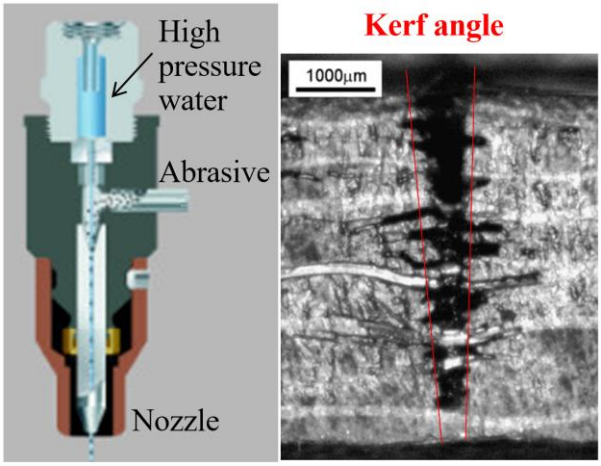

(a)Jet machining

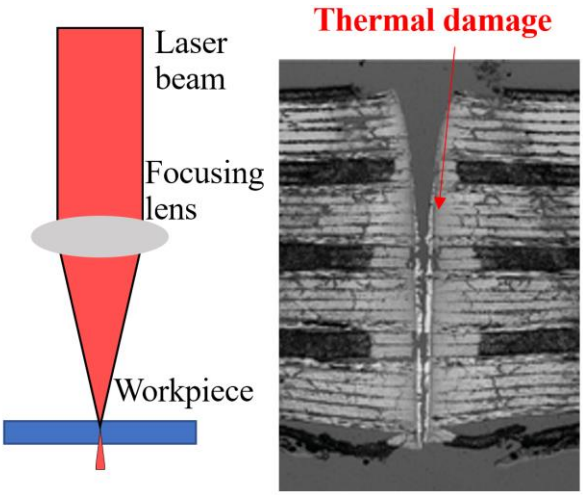

(b)Laser machining

Fig. 1.1 Comparison of hole cross-section shapes in various CFRP hole making methods

In the conventional drilling process, the zero-speed problem of the chisel edge is the main cause of the axial cutting force, and 40%~60% of the general axial force is due to it [12]. In addition, the chisel edge is the main factor that causes the outlet side of the hole to push out the delamination when the CFRP hole is made (see Fig. 1.2). By using pre-processed guide holes, the influence of the chisel edge can be eliminated, the axial force can be reduced, and the stratification at the outlet side of the hole can be avoided [12-19]. However, this method requires an additional pre-drilling step, which reduces the production efficiency and increases the processing cost.

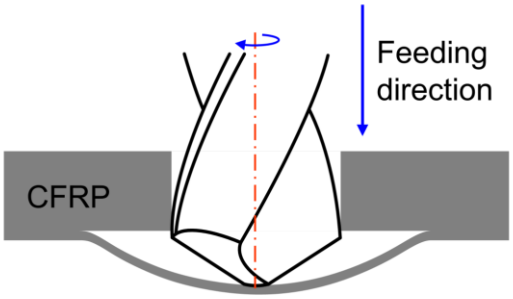

Fig. 1.2 Problem of push out delamination in CFRP drilling process

For this reason, a promising technique known as “helical milling” which not only exploited the advantages of high mechanical drilling efficiency, but also overcome many of the deficiencies caused by the slow-speed zero point of the chisel edge for CFRP drilling and has already been extensively employed in practical cases [20]. In this method, a tool, usually an end mill, the axis of which is parallel to that of the hole to be drilled, rotates around its own axis and exhibits planetary motion around the hole axis. Simultaneously, when the tool is fed downward along the hole axis, it moves along a helical path (see Fig. 1.3).

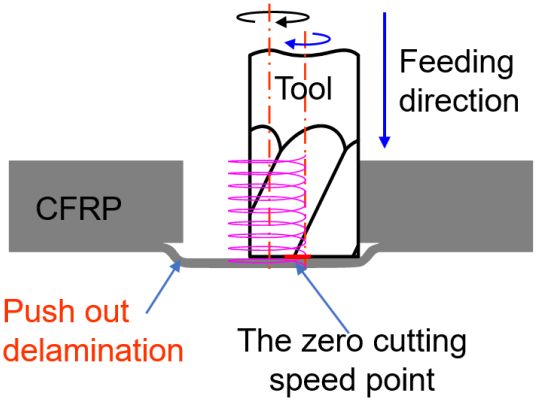

Fig. 1.3 Illustration of the conventional helical milling

Eventually, a through-hole is created once the tool end face fully penetrates the workpiece. In this process, the diameter of the drilled hole is certainly greater than that of the tool, resulting in a gap between the tool and the hole wall. One benefit of this gap is that chips can be easily removed from the cutting zone. Another benefit is that the cutting edges on the side of the tool impose intermittent cutting action, which promotes

heat dissipation. Therefore, the helical milling method does have many advantages over conventional drilling methods in terms of cutting temperature, hole quality, and processing efficiency. In order to further improve the performance of this method, the kinematic mechanism of the helical milling process was researched and the obtained result revealed that it was actually a combination of drilling and milling processes [21-24]. The influence of the tool deformation caused by the cutting force on deviations in the hole diameter was discussed [25]. The effects of cutting parameters on the cutting forces, based on the shape of the model about the unreformed chip were analyzed [26]. A heat transfer model was proposed to research the temperature distribution during the helical milling of CFRP [27]. The helical milling method was applied to drill holes in CFRP/Ti materials and the result confirmed that the occurrence of delamination can be considerably restrained [28].

1.3 Proposal of Tilted Helical Milling technique

However, there are still several weaknesses in CHM. The cutting edges on the end of the tool perform cutting action constantly during drilling, which results in high cutting temperature and heavy cutting-edge wear. At the hole entrance, the entire end of the tool is cut into the workpiece at almost the same time. Similarly, at the hole exit, these cutting edges cut out the workpiece suddenly. This phenomenon results in a sharp increase and decrease in cutting force at the hole entrance and exit, which leads to the frequent occurrence of burrs and chipping. The stiffness of the part under the tool end cutting edges is also suddenly reduced, eventually leading to the occurrence of uncut fibers. In addition, the chisel edge problem in CHM, i.e., the existence of zero cutting speed point, not only accelerates tool wear, but also becomes a big factor that affects the delamination at the edges of the CFRP hole. This results in the deterioration of hole quality and a reduction in machining efficiency.

To address these problems, a tilted helical milling (hereafter referred to as THM) technique [29-30] was proposed, respectively, based on the CHM. The THM technique is performed by tilting the tool against the workpiece at a small angle during CHM. An

in-house rotary worktable capable of rotating the workpiece to obtain planetary/revolution motion was mounted on a 3-axis CNC milling machine with a tilt angle to perform a THM operation. Drilling experiments were carried out on the produced rig. The obtained results showed that on both the entrance and the exit of the hole obtained by THM, the number of burrs and the instances of delamination were dramatically less than those produced while using CHM. In addition, a higher surface quality was achieved on the hole wall by THM compared with CHM. These results successfully validate the proposed THM method for drilling holes in CFRP. The experimental results showed that few burrs and few instances of delamination remained on the workpiece. Therefore, it should be of significant importance to give priority to the development of the THM technique.

1.4 Objective of the study

As a step toward the development of the THM technique, in this paper, the machining characteristics of CFRP high-quality drilling technology have been studied in THM.

First, the relative motion between the tool and the workpiece was analyzed theoretically, and the material removal mechanism and hole machining process in the CHM and THM were compared. The results show that with the new method, the zero point of the bottom edge of the tool in the CHM can be avoided, the discharge of the chips can be facilitated, and high-quality drilling can be performed. Next, an experimental apparatus was constructed by manufacturing a rotary table capable of tilting and rotating the workpiece and mounting it on a CNC milling machine. Then, the experimental results of the pore generation process were determined experimentally, and systematic studies on the effects of machining conditions such as workpiece tilt angle and tool eccentricity on cutting resistance, cutting temperature, and tool wear were conducted experimentally, and theoretical analysis was also thoroughly performed. Finally, by experimentally studying the effect of processing conditions on the quality of the entrance side and exit side of the hole, the superiority of the THM processing has been confirmed, and the guidance for optimizing the processing conditions has been

given.

This paper aims to establish a new type of CFRP drilling technology that has not yet been seen so far. By grasping the characteristics of basic processing, clarifying the processing mechanism, finding the best processing conditions, and obtaining a large amount of knowledge and results, we have a high practical value for engineering. Can also be expected to lead to practical applications.

1.5 Thesis organization

The thesis is made up of the introductory chapter along with other 6 chapters:

Chapter I briefly reviews the CFRP and the drilling technology of CFRP. Prevailing technologies and emerging ones for drilling CFRP is outlined.

Chapter II details the related experimental devices that were employed in the work. An experimental apparatus was constructed by manufacturing a rotary table capable of tilting and rotating the workpiece and mounting it on a CNC milling machine. After that, the experimental conditions under which the experiments were performed are listed.

Chapter III performed a theoretical analysis of the hole forming process and material removal rate during THM and conducted THM experiment to verify its basic processing properties and strengths. Next further the exit formation of the hole was studied, and finally the inhibition mechanism of the hole exit formation on the exit delamination defect was figured out.

Chapter IV established a mechanical model about the cutting force of THM to study the factors affecting the cutting force. A string of plans was adopted to measure the cutting temperature during THM processing, and the effects of cutting force and temperature were analyzed in different processing conditions.

Chapter V, the processing quality of hole entrance, exit and inner surface in different processing conditions was assessed to optimize the processing conditions and provide guidance for potential industrial application.

Chapter VI, the last chapter summarizes and advises the work and outlines the

prospects of the CFRP drilling techniques together with utilization of CFRP in state-of-the-art precision drilling fields.

References

[1] Wang HJ, Sun J, Zhang DD, Guo K, Li JF (2016) The effect of cutting temperature in milling of carbon fiber reinforced polymer composites. Compos Part A Appl S 91:380–387.

[2] Brinksmeier E, Fangmann S, Rentsch R (2011) Drilling of composites and resulting surface integrity. CIRP Annals-Manuf Technol 60:57-60.

[3] Wei JC, Jiao GQ, Jia PR, Huang T (2013) The effect of interference fit size on the fatigue life of bolted joints in composite laminates. Compos Part B Eng 53:62–68.

[4] Alberdi A, Artaza T,Suarez A, Rivero A,Girot F (2016) An experimental study on abrasive waterjet cutting of CFRP/Ti6Al4V stacks for drilling operations. Int J Adv Manuf Technol 86:691–704.

[5] Thoppul SD, Finegan J, Gibson RF (2009) Mechanics of mechanically fastened joints in polymer–matrix composite structures –A review. Compos Sci Technol 69(3–4):301–329.

[6] D. F. Liu, Y. J. Tang, W. L. Cong. A review of mechanical drilling for composite laminates. Composite Structures, 2012, 94:1265-1279.

[7] R. Zitoune, L. Crouzeix, F. Collombet. Behaviour of composite plates with drilled and moulded hole under tensile load. Composite Structures, 2011, 93(9):2384-2391.

[8] H. Hocheng, C. C. Tsao. The path towards delamination-free drilling of composite materials. Materials Processing Technology, 2005, 167:251-264.

[9] Xu WX, Zhang LC (2016) Mechanics of fibre deformation and fracture in vibration-assisted cutting of unidirectional fibre-reinforced polymer composites. Int J Mach Tool Manuf 103:40–52.

[10] Abrao AM, Faria PE, Campos Rubio JC, Reis P, Davim JP (2007) Drilling of fiber reinforced plastics: a review. J Mater Process Tech 186(1–3):1–7.

[11] Zitoune R, Crouzeix L, Collombet F, Grunevald YH (2011) Behaviour of composite plates with drilled and moulded hole under tensile load. Compos Struct 93(9):2384–2391.

[12] Cong WL, Pei ZJ, Treadwell C (2014) Preliminary study on rotary ultrasonic machining of CFRP/Ti stacks. Ultrasonics 54(6):1594–1602.

[13] H. Hocheng, C. C. Tsao. The path towards delamination-free drilling of composite materials. Materials Processing Technology, 2005, 167:251-264

[14] L. M. Durao, A. G. Magalhaes, J. M. R. S. Tavares, A. T. Marques. Analyzing objects in images for estimating the delamination influence on load carrying capacity of composites laminates. Electronic Letters on Computer Vision and Image Analysis, 2008, 7:11-21

[15] C. C. Tsao, H. Hocheng. The effect of chisel length and associate pilot hole on delamination when drilling composite materials. Int J Mach Tool Manuf, 2003, 43:1087-1092

[16] C. C. Tsao. Effect of pilot hole on thrust force by saw drill. Int J Mach Tool Manuf, 2007, 47:2172-2176

[17] V. Tagliaferri, G. Caprino, A. Diterlizzi. Effect of drilling parameters on the finish and mechanical properties of GFRP composites. J Mach Tool Manufact, 1990, 30:77-84

[18] A. Velayudham, R. Krishnamurthy. Effect of point geometry and their influence on thrust and delamination in drilling of polymeric composites. J Materials Processing Technology, 2007, 185:204-209

[19] M. S. Won, C. K. H. Dharan. Chisel Edge and Pilot Hole Effects in Drilling Composite Laminates. J Manufacturing Science and Engineering, 2002, 124:242-247

[20] Pereira RBD, Brandao LC, Paivab AP, Ferreira JR, Davim JP (2017) A review of helical milling process. Int J Mach Tool Manuf 120:27-48.

[21] Wang H Y, Qin XD, Li H, Tan YQ (2016) A comparative study on helical milling of CFRP/Ti stacks and its individual layers. Int J Adv Manuf Technol 86(5):1973–1983.

[22] Li ZQ, Liu Q, Ming XZ, Wang X, Dong YF (2014) Cutting force prediction and analytical solution of regenerative chatter stability for helical milling operation. Int J Adv Manuf Technol 73(1):433–442.

[23] Wang HY, Qin XD (2016) A mechanistic model for cutting force in helical milling of carbon fiber-reinforced polymers. Int J Adv Manuf Technol 82(9):1485–1494.

[24] Li ZL, Ding Y, Zhu LM (2017) Accurate cutting force prediction of helical milling operations considering the cutting tool runout effect. Int J Adv Manuf Technol. doi: 10.1007/s00170-017-0464-1.

[25] Deitert L. Orbital drilling, Sae Tech Pap. doi:10.4271/2011-01-2533.

[26] Denkena B, Boehnke D, Dege JH (2008) Helical milling of CFRP-titanium layer compounds. CIRP J Manuf Sci Technol 1(2):64–69.

[27] Liu J, Chen G, Ji CH (2014) An investigation of workpiece temperature variation of helical milling for carbon fiber reinforced plastics (CFRP). Int J Mach Tool Manuf 86:89–103.

[28] Lindqvist R, Eriksson I, Wolf M (2011) Orbital drilling of sandwich constructions for space applications. Sae Technical Papers. doi: 10.4271/2001-01-2571.

[29] Wu YB, Wang Q, Nomura M (2016) Proposal of tilt helical milling method for hole creation of carbon fiber reinforced plastic (CFRP). Adv Mater Res 1136:190–195.

[30] Q. Wang, Y. Wu, T. Bitou. Proposal of a tilted helical milling technique for high quality hole drilling of CFRP. Kinetic analysis of hole formation and material removal. Int J Adv Manuf Technol, 2017, Doi: 10.1007/s00170-017-1106-3.

Chapter II
Experiment apparatus and details

2.1 Introduction

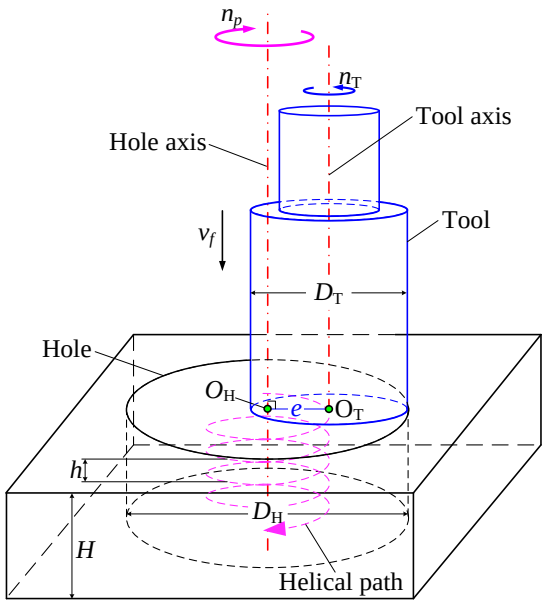

(a) CHM

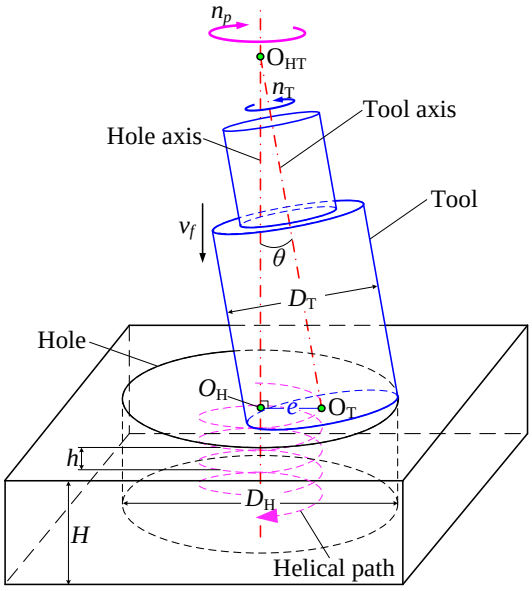

(b) THM

Fig. 2.1 Illustrations of the hole drilling process using CHM and THM

Figs. 2.1 (a) and (b) illustrate the hole drilling processes by the CHM and the THM technique, respectively. In CHM (Fig. 2.1 (a)), the axis of the tool, usually an end mill with a diameter of D_T, positioned parallel to that of the hole, and the distance between the two axes, i.e., the eccentricity of the tool, is e. During drilling, the tool rotates around its own axis at a speed of n_T, has planetary motion around the hole axis at a speed of n_p, and is simultaneously fed downward along the hole axis at a feed rate of v_f. Eventually, the tool moves along a helical path with a pitch of $h = v_f T_p$, where $T_p = 60/n_p$ is the time period for one revolution of the tool. The unwanted materials in the wall and at the bottom of the hole are cut off with the side and end of the tool at the same time. As a result, a through-hole is created once the end face of the tool has penetrated through the workpiece with thickness of H. Evidently, owing to the tool eccentricity, e, the hole diameter, D_H, can be determined by the relationship $D_H = D_T + 2e$, in the case of assuming that the employed drilling equipment is a perfectly rigid body, i.e., all the geometric interferences between the tool and the workpiece are 100% removed. This indicates that holes with different diameters can be obtained by adjusting the value of e.

In contrast, the THM technique (Fig. 2.1 (b)) is performed by tilting the tool against the hole at a small angle, θ, in CHM. That is, the tool rotates around its own axis at the speed, n_T, and exhibits conical pendulum motion around the hole axis at a speed of n_p. It is fed downward along the hole axis simultaneously at a feed rate of v_f. Eventually, the tool moves along a helical path similar to that in CHM to create a through-hole with a diameter of $D_H = 2e + D_T\cos\theta$. e is the distance from the tool end face center, O_T, to the hole axis. In contrast to CHM where the tool axis is constantly parallel to the hole axis, the tool attitude in THM is adjusted momentarily so that the tool axis is always tilted against the hole axis with the tilt angle, θ, due to the conical pendulum motion. A point, O_{HT}, on the hole axis, where the tool axis crosses the hole axis, moves downward as the tool is fed downward along the hole axis.

This chapter focuses mainly on the theory and design of THM and experiments. In order to study the processing characteristics of CFRP high quality drilling technology in THM, it is necessary to design and manufacture THM experimental device to verify the effectiveness of the proposed method. In addition, the detailed experimental conditions are also listed out along with temperature measurement method. Lastly, the device and method for hole quality evaluation were introduced.

2.2 Experimental setup, conditions and procedure

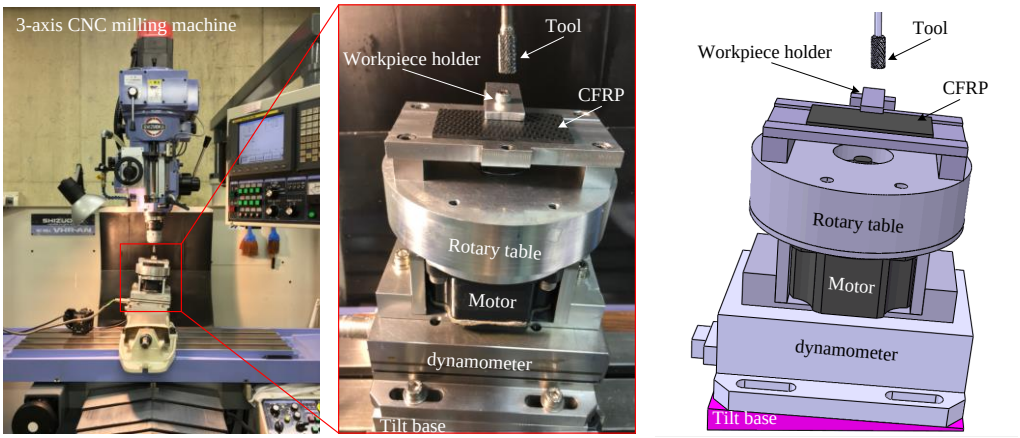

(a) Whole view of experimental apparatus (b) Illustration of the work-holding unit

Fig. 2.2 Experimental setup

Although a 5-axis CNC machining center is preferred for performing THM, as the purpose of the current work was solely to confirm the validity of the proposed THM method and its superiority to the CHM method, a more affordable 3-axis CNC milling machine (Vhr-an by Shizuoka machine tool Co., Ltd., Japan) was used. Therefore, a work-holding unit capable of securing the workpiece and obtaining the revolution motion of tool produced in our previous work was installed on the worktable of the 3-axis CNC milling machine.

Figs. 2.2 (a) and (b) show the illustration and a picture of the main portion of the setup, respectively. The work-holding unit mainly consists of a workpiece holder, a rotary table, a motor, and a wedge-shaped tilt base for tilting the workpiece at the given tilt angle, θ. A dynamometer (9257B by Kistler Co., Ltd., Switzerland) was fixed below the unit to measure the drilling force. Thus, by utilizing this setup, the conical pendulum

motion of the tool around the hole axis is available and the revolution speed, n_p, can be provided by the rotation of the rotary worktable. If the wedge-shaped tilt base is replaced with a flat plate, the hole drilling by CHM could be performed.

2.3 Metrology and characterization

2.3.1 Optical image of hole entrance/exit side and bottom section profile

Fig. 2.3 Micro-focus digital camera

As shown in Fig. 2.3, a micro-focus digital camera (Micro Nikkor 40 by Nikon Corp.) was used to observe the hole cross section at different moments in CHM and THM, respectively. In addition, this micro-focus digital camera was also used to observe hole entrance/exit sides to evaluate the delamination defect.

2.3.2 Hole entrance and exit side defects enlarged observation

Fig. 2.4 Electron microscope

As shown in Fig. 2.4, an electron microscope (VHK-200 by Keyence Corp.) was used to observe the entrances and exits of the drilled holes, and the burr/chipping areas were quantitatively obtained to compare the hole qualities in CHM and THM.

2.3.3 Three-dimensional laser scanning microscope

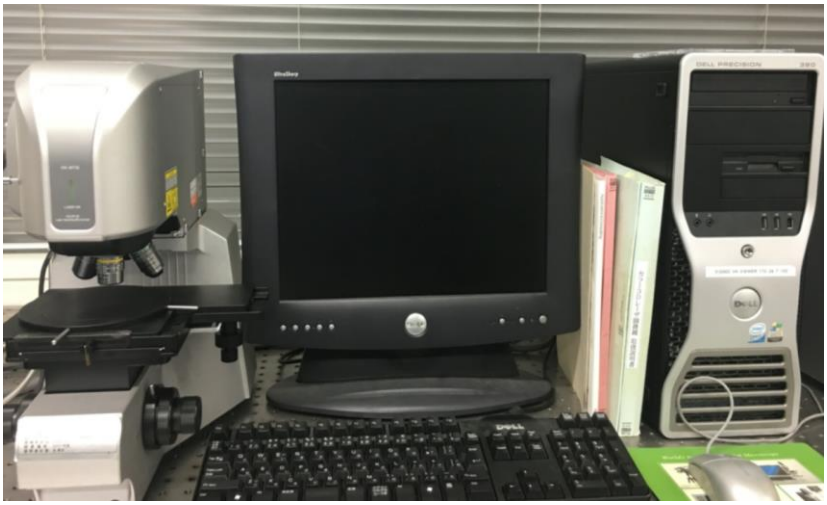

Fig. 2.5 3D laser microscope

As shown in Fig. 2.5, damage of the surface of the pore was observed using a 3D laser microscope (VK-8710 by Keyence Corp.). The volume calculation function of the 3D laser microscope used obtains the total volume of the formed pits to quantitatively evaluate the damage.

2.3.4 Analyze qualitatively the structure of the finished holes

Fig. 2.6 Micro-computer tomography (CT) scans

As shown in Fig. 2.6, micro-computer tomography (CT) scans (Inspe Xio SMX-225 CT FPD HR, Shimadzu Co., Ltd. Japan) have been executed to analyze qualitatively the structure of the finished holes. During the experiment, a plate detector, which ran at 200 kV tube voltage, was used to measure the hole entrances. Further, an industrial micro-CT system was used at 225 kV accelerating voltage and 4μm resolution ratio to scan the holes by CHM and THM. The scanning data was visualized using software (VG Studio MAX 3.0).

2.3.5 Tool wear observations

Fig. 2.7 Scanning electron microscope

As the figure shows, the scanning electron microscope (3D-SEM SM-200 by Elionix Co., Ltd.) was used to measure the tool wear because of its large stroke in the z-direction.

2.3.6 Surface quality characterization

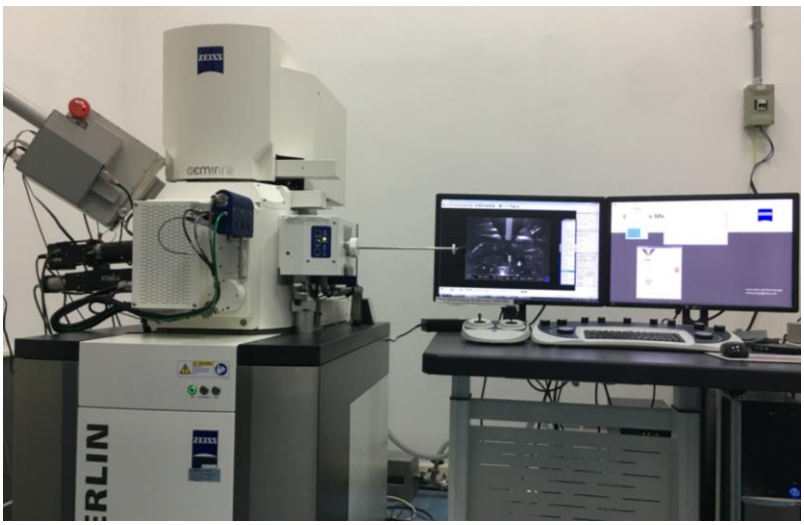

Fig. 2.8 Scanning electron microscope

As shown in Fig. 2.8, the scanning electron microscope (3D-SEM Merlin by Zeiss Co., Ltd.) was used to observe the damage of hole surface such as the fiber bending and fiber matrix debending.

2.3.6 Hole wall straightness and surface roughness

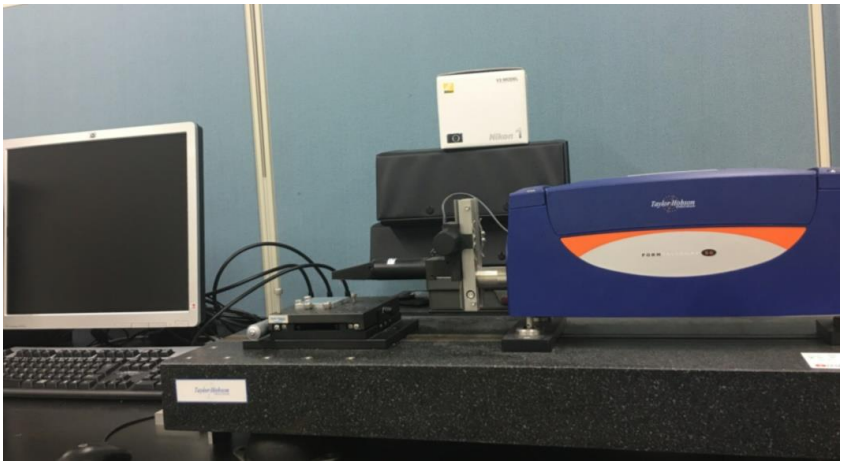

Fig. 2.9 A stylus-based profilometer

As shown in Fig. 2.9, a stylus-based profilometer **(**Form Talysurf Intra by Taylor Hobson Inc.) was used to measure the longitudinal profile of the holes in a direction parallel to the axis of the hole.

2.4 Summary

This chapter first introduces the processing principle of THM. Secondly, in order to realize THM processing, a processing device is designed and manufactured. In addition, hole processing characteristics were evaluated, and hole quality evaluation equipment was introduced.

Chapter III
Kinetic analysis of Tilted Helical Milling technique

3.1 Introduction

As a step toward the development of the THM technique, its advantages over CHM is abstracted through the kinetic comparison of hole formation, material removal, and the problem of zero cutting speed point at the cutting edges on the end of the tool. Then, drilling experiments were conducted on the existing rig to confirm the kinetic analysis on the hole formation by observing the cross sectional profiles of the hole at different moments during drilling. Next, the variation in the cutting force during drilling was experimentally obtained to confirm the predicted material removal behavior. Subsequently, the hole quality in THM was experimentally compared with that in CHM, in terms of burrs/chippings on hole entrances and exits. Finally, the chip removal during the THM process was also compared with that of CHM process by observing chip adhesion on the cutting edges on the end of the tool.

In addition, the delamination phenomenon in the drilling of CFRPs has been recognized as one of the critical problems. It is mainly defined as an inter-laminar or -ply failure behavior of the CFRP composites. The hole exit delamination occurs more severely at the bottom-most surface of CFRP materials (Dharan et al., 2000). It has a critical influence on the final quality of the components and their (sub) assemblies (Tsao et al., 2005). As a step towards the development of the THM technique, it is crucial to analyze the reduction mechanism of delamination phenomenon at the hole exit and elucidate the effects of process parameters on the elimination of delamination in THM. For this purpose, in this work, the hole exit delamination formation in THM was qualitatively compared with that in CHM through kinetic analysis. Then, drilling experiments were conducted on the existing rig to confirm the kinetic analysis by observing the hole exit side at different moments during drilling. Finally, the hole

quality and the thrust force in THM was experimentally compared with those in CHM, in terms of burrs/chippings on hole exits.

3.2 Hole formation and material removal

This difference in the tool attitude between CHM and THM leads to the difference in the hole cross section profiles and the material removal, as shown in Fig. 3.1.

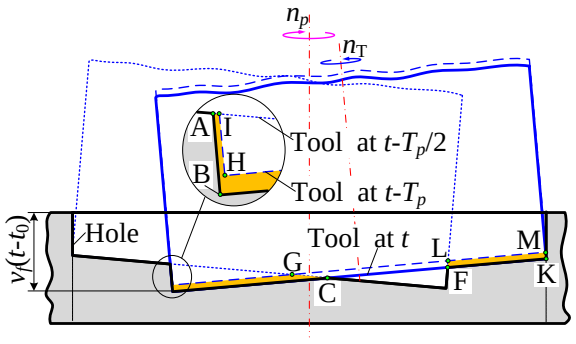

(a) CHM

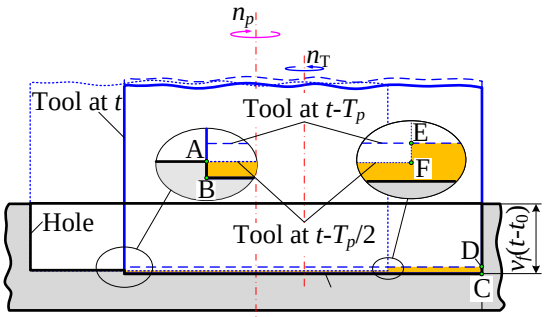

(b) THM

Fig. 3.1 Illustration of the cross sectional profiles of the holes, the tool, and the work-materials removed per tool revolution during CHM and THM

Figs. 3.1 (a) and (b) illustrate the instantaneous cross section profiles of the hole, the tool, and the work-materials removed per tool revolution. These profiles are positioned in a plane that is determined by the tool axis and the hole axis at an arbitrary moment after drilling for time, t, by CHM and THM, respectively. Hereafter, this plane is referred to as the C-C plane for convenience. In addition, in the figures for both CHM and THM, the dashed and dotted lines denote the tool cross sections at the moment t-T_p, i.e., one revolution before the moment, t, and at the moment t-T_p/2, i.e., half a

revolution before the moment, t, respectively. At the moment t, the hole depth reaches $v_f(t-t_0)$ either in CHM or in THM, where t_0 denotes the moment when the drilling starts. It can also be found that the bottom of the hole is roughly flat in CHM, while in THM it is roughly W-shaped, implying that the hole formation process in THM should be much more complicated than that in CHM. Moreover, the brown-shaded areas of the polygon ABCDEF in Fig. 3.1 (a) and the polygon ABCGHI&LFKM in Fig. 3.1 (b) stand for the undeformed cross sections of the work-materials removed per tool revolution in CHM and THM, respectively. The quantitative discussions on the hole formation processes and the variations of the cross section areas of the work-materials removed per tool revolution will be performed in detail in next section.

3.2.1 Kinetic analysis of the hole formation process and material removal behavior

As an essential step towards the development of the THM technique, the hole formation process and the material removal behavior during drilling by the THM technique are kinetically analyzed. The kinetic analysis is also performed on those processes by CHM for comparison.

3.2.1.1 Hole formation process

In CHM, the hole formation process can be divided to three stages based on the material removal behavior. There are four characteristic moments, including the drilling start moment, the two boundary moments between neighbored stages, and the drilling finish moment. Figs. 3.2 (a) – (d) show the cross section profiles of the hole and the tool in the C-C plane at four characteristic moments ($t_0 \sim t_3$), respectively, during the CHM process. At the moment t_0, the tool begins to plunge into the workpiece to begin the hole drilling process. Then, when the tool has motioned for one revolution, the depth of hole reaches h at the moment $t_1 = t_0+T_p$. At this moment, the bottom profile of the hole cross section begins to be shaped like a simple folded line with a drop of $h/2$, and retains this shape until the moment $t_2 = t_0+H/v_f$, when the cutting edges on the end of the tool reach the exit hole for the first time. Finally, one revolution later, at the moment $t_3 = t_2+T_p = t_0+H/v_f+T_p$, the tool end face penetrates the workpiece by h and completes

the hole drilling.

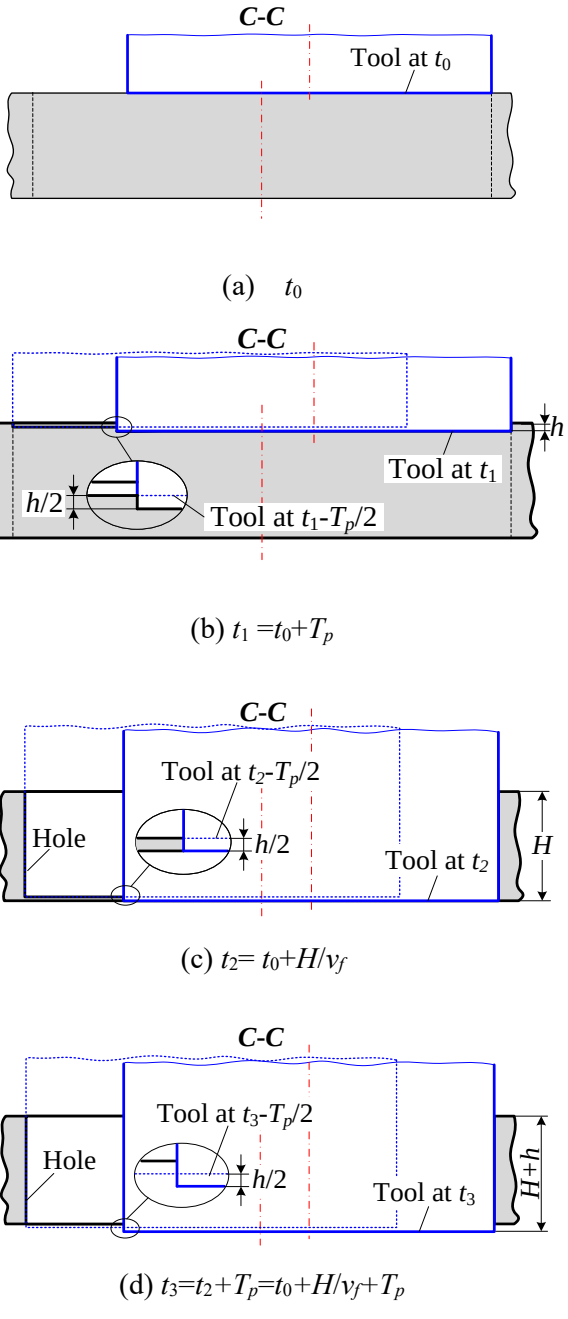

Fig. 3.2 Illustrations of the hole/tool cross sections at characteristic moments in CHM

The hole formation process by THM exhibits a more complicated process than that in CHM due to the tool tilt. In contrast to CHM, the hole formation process in THM should be divided into nine stages, and thus ten characteristic moments exist. Fig. 3.3 shows the cross section profiles of the hole and the tool in the C-C plane at the ten characteristic moments ($t_0 \sim t_9$). At the moment t_0, the lowest end of the cutting edge of the tilted tool first comes into contact with the workpiece at point, P_0. After the tool has

motioned for one revolution, at the moment $t_1 = t_0+T_p$, a circumferential V-groove is formed on the workpiece and its depth reaches h. Then, at the moment t_2, the end face of the tool comes into contact with the workpiece at the hole, i.e., point P_2. From the instantaneous geometrical relationship between the tool and the workpiece at this moment (Fig. 3.3 (c)), the value of t_2 can be determined as $t_2 = t_0+m\tan\theta/v_f+T_p$ where $m = D_T\cos\theta-D_H/2$. As drilling proceeds, the depth of the V-groove increases gradually to form a hole with a simple W-shaped cross section. This continues until the moment t_3, when the end face of tool comes into contact with the edge of the W-shaped hole at point P_3. Similar to the geometrical arrangement shown in Fig. 3.3 (d), the value of t_3 can be obtained as $t_3 = t_0+[n\tan(2\theta)+h]/(2v_f)$ where $n = 2D_T\cos\theta-D_H-h/(2\tan\theta)$. At this moment, the diameter of the hole at its entrance gradually expands until the moment t_4, when the highest end of the cutting edge of the tool reaches the workpiece at point P_4. The hole diameter at its entrance is about to reach the desired one of D_H. It is easy to determine the value of t_4 as $t_4 = t_0+D_T\sin\theta/v_f +T_p$ from the geometrical arrangement shown in Fig. 3.3 (e). t_5 denotes the moment when the lowest end of the cutting edge of the tool comes into contact with the hole exit at point P_5 for the first time. Here, the value of t_5 would be $t_5 = t_0+H/v_f$ (Fig. 3.3 (f)). Next, the tool starts the formation of the hole exit in a manner roughly similar to the hole entrance until the moment $t_6 = t_5+T_p = t_0+H/v_f+T_p$ (Fig. 3.3 (g)). At this moment, the lowest end of the cutting edge of the tool penetrates the workpiece by h, and results in the drop of the conical un-cut work-materials located in the central area of hole (the triangle area in Fig. 3.3 (f)). Thus, a hole with a smaller diameter than the desired one is generated at the hole exit, and its diameter is gradually expanded as the tool continues to feed through. t_7 denotes the moment when the end face of the tool comes into contact with the edge of the smaller hole at point P_7. The value of t_7 can be obtained from the geometrical arrangement in Fig. 3.3 (h) as $t_7 = t_3+H/v_f = t_0+[n\tan(2\theta)+h]/(2v_f)+H/v_f$. Then, at the moment $t_8 = t_0+(D_T\sin\theta+H)/v_f$ (Fig. 4 (i)), the highest end of the cutting edge of the tool comes into contact with the hole exit at point P_8 for the first time. Furthermore, in one revolution of tool at the moment $t_9 = t_8+T_p = t_0+(D_T\sin\theta+H)/v_f+T_p$, the highest end of the cutting edge penetrates the workpiece by h, and the hole diameter at its exit reaches the desired

diameter of D_H. This completes the drilling process (Fig. 3.3 (j)).

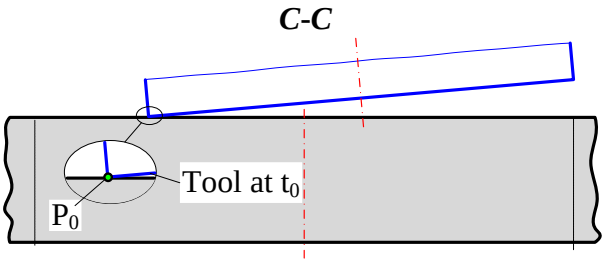

(a) t_0

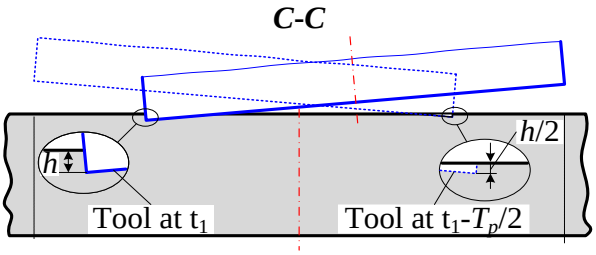

(b) $t_1 = t_0 + T_p$

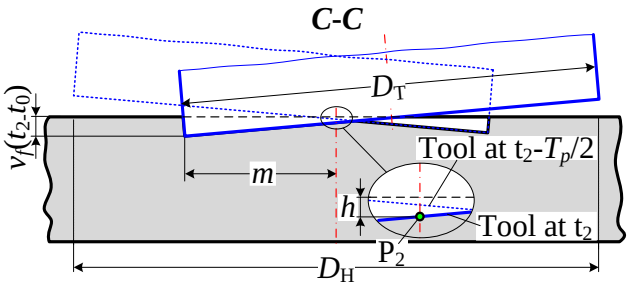

(c) $t_2 = t_0 + m\tan\theta/v_f + T_p$

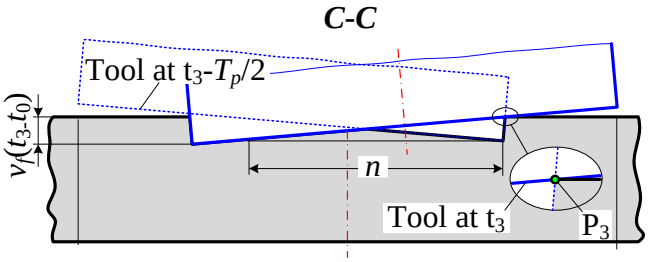

(d) $t_3 = t_0 + [n\tan(2\theta) + h]/(2v_f)$

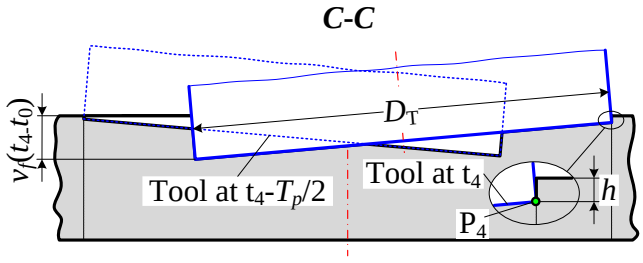

(e) $t_4=t_0+D_T\sin\theta/v_f+T_p$

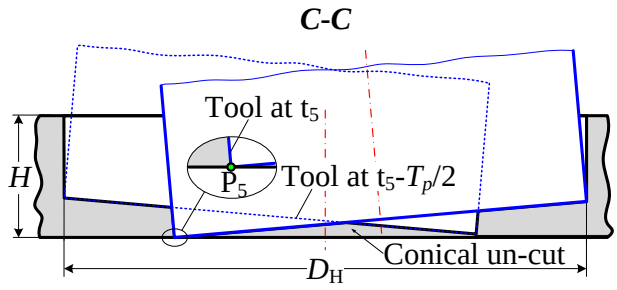

(f) $t_5=t_0+H/v_f$

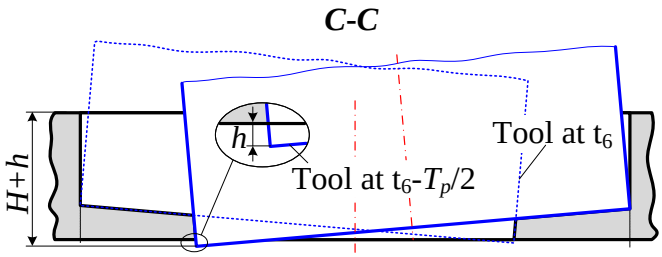

(g) $t_6=t_5+T_p$

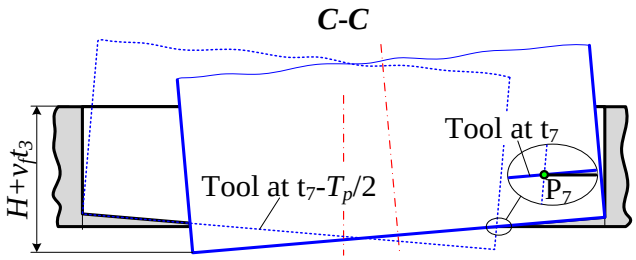

(h) $t_7=t_3+H/v_f$

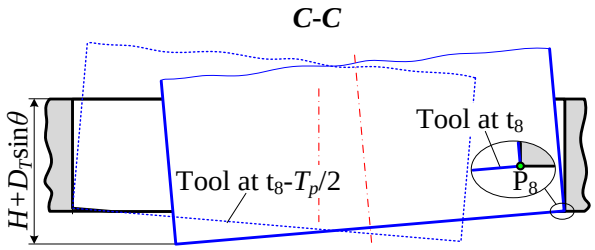

(i) $t_8 = t_0 + (D_T \sin\theta + H)/v_f$

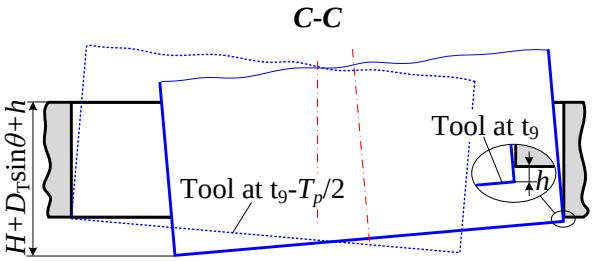

(j) $t_9 = t_8 + T_p$

Fig. 3.3 Illustrations of the hole/tool cross sections at characteristic moments in THM

3.2.1. 2 Material removal behavior during drilling

In order to explain the material removal behavior during drilling, the variation in the undeformed cross section area of the work-materials removed per tool revolution, *s*, was analyzed geometrically.

Initially, the removal behavior of the work material in CHM was analyzed as shown in Fig. 5. In the figure, the brown-shaded areas stand for the cross sectional area, *s,* at arbitrary moments in different stages during the hole drilling process. According to the previous analysis of the hole formation process in section 3.2.1.1, there are three stages in CHM, i.e., stage 1: $t_0 \le t \le t_1$, stage 2: $t_1 < t \le t_2$ and stage 3: $t_2 < t \le t_3$. The *s* at an arbitrary moment in these different stages can be expressed by Eqs. (3.1) - (3.3), respectively, based on the instantaneous geometric relationships between the tool and the workpiece.

Stage 1: $t_0 \le t \le t_1$ (Fig. 3.4 (a))

$$s = s_{ABCDEF} = \frac{D_H v_f (t - t_0)}{2} \tag{3.1}$$

Stage 2: $t_1 \le t \le t_2$ (Fig. 3.4 (b))

$$s = s_{\mathrm{ABCDEF}} = \frac{D_H h}{2} \tag{3.2}$$

Stage 3: $t_2 \le t \le t_3$ (Fig. 3.4 (c))

$$s = s_{\mathrm{AJKDER}} = \frac{D_H v_f (t_3 - t)}{2} \tag{3.3}$$

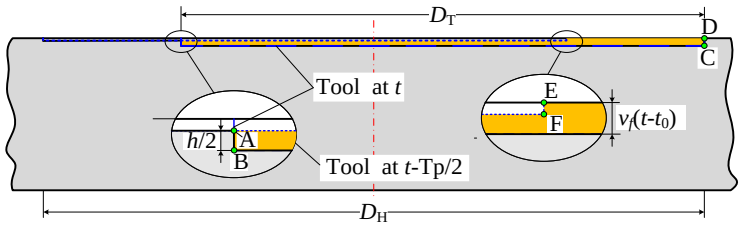

(a) Stage 1: $t_0 \le t \le t_1$

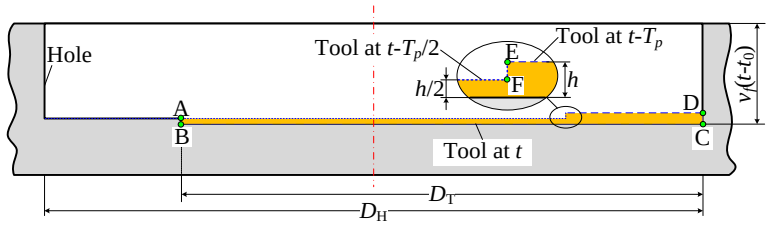

(b) Stage 2: $t_1 < t \le t_2$

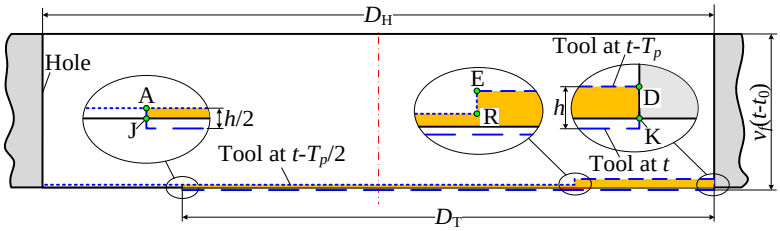

(c) Stage 3: $t_2 < t \le t_3$

Fig. 3.4 Illustrations of the undeformed cross section areas of the work-materials removed per tool revolution at different moments during drilling by CHM.

Next, in contrast to CHM, THM includes nine stages corresponding to ten characteristic moments (see Fig. 3.3). From the respective geometric configurations in Figs. 3.5 (a) - (i), the brown-shaded areas, i.e., the undeformed cross section area of the

work-materials removed per tool revolution, *s*, can be obtained, respectively, as expressed by Eqs. (3.4) - (3.12).

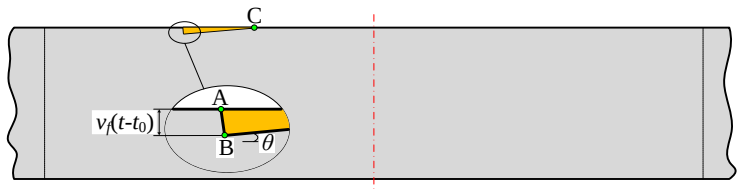

(a) Stage 1: $t_0 \le t \le t_1$

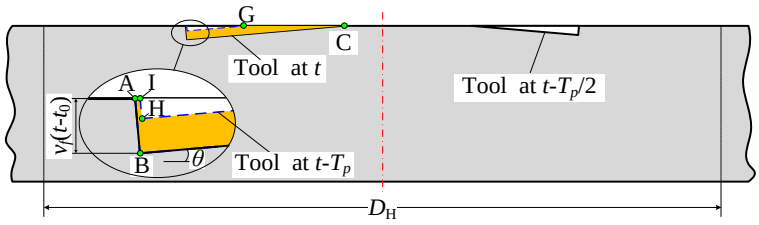

(b) Stage 2: $t_1 < t \le t_2$

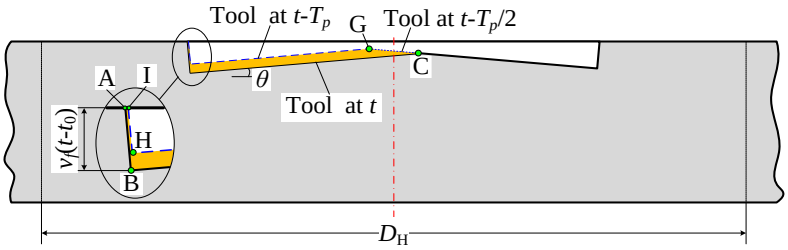

(c) Stage 3: $t_2 < t \le t_3$

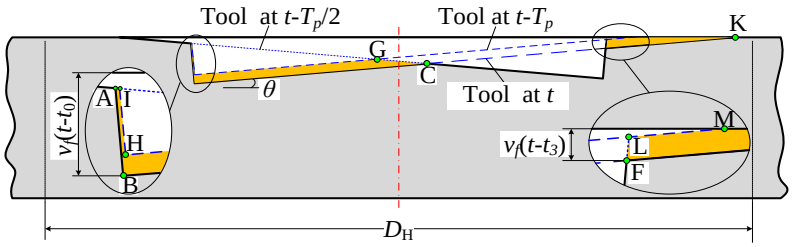

(d) Stage 4: $t_3 < t \le t_4$

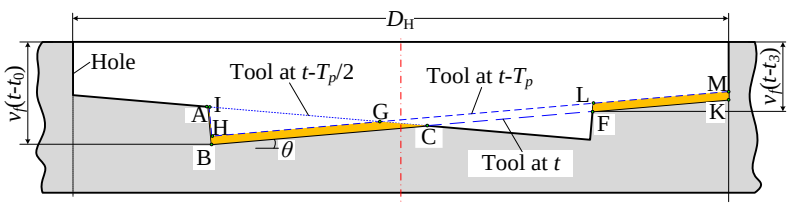

(e) Stage 5: $t_4 < t \le t_5$

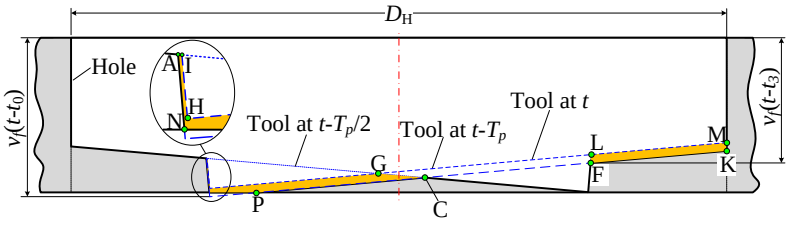

(f) Stage 6: $t_5 < t \le t_6$

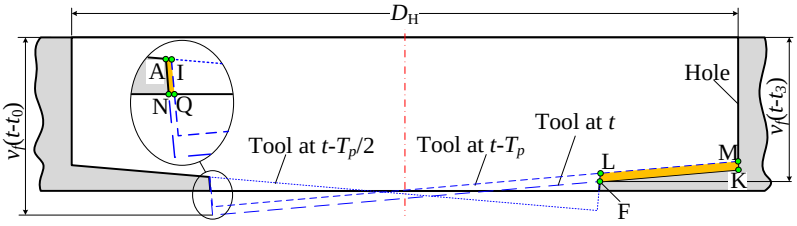

(g) Stage 7: $t_6 < t \le t_7$

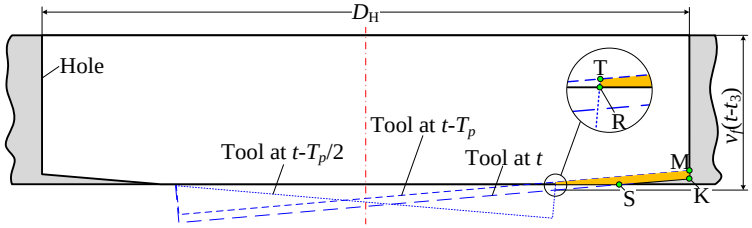

(h) Stage 8: $t_7 < t \le t_8$

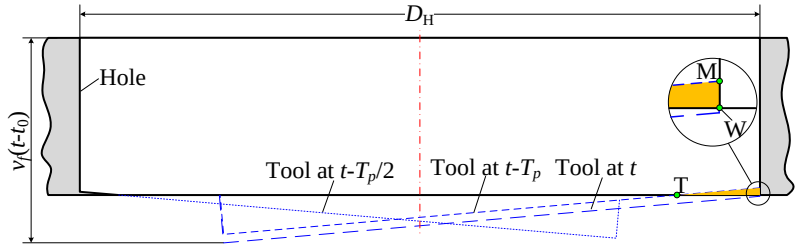

(i) Stage 9: $t_8 < t \le t_9$

Fig. 3.5 Illustrations of the undeformed cross section areas of the work-materials removed per tool revolution at different moments during drilling by CHM

Stage 1: $t_0 \le t \le t_1$ (Fig. 3.5 (a)):

$$s = s_{ABC} = \frac{v_f{}^2 (t - t_0)^2}{\sin(2\theta)} \tag{3.4}$$

Stage 2: $t_1 < t \le t_2$ (Fig. 3.5 (b)):

$$s = s_{\mathrm{ABCGHI}} = \frac{2hv_f\left(t-t_0\right)-h^2}{\sin 2\theta} + \frac{h^3 - h^2 v_f\left(t-t_0\right)}{\tan^2\theta\left(2D_T\cos\theta - D_H\right)} \tag{3.5}$$

Stage 3: $t_2 < t \le t_3$ (Fig. 3.5 (c)):

$$s = s_{\mathrm{ABCGHI}} = h\left(D_T\cos\theta - \frac{D_H}{2}\right) + h\tan\theta\left[v_f\left(t-t_0\right) - \frac{h}{2}\right] \tag{3.6}$$

Stage 4: $t_3 < t \le t_4$ (Fig. 3.5 (d)):

$$s = s_{\mathrm{ABCGHI\&LFKM}} = h\left(D_T\cos\theta - \frac{D_H}{2}\right) + h\tan\theta\left[v_f\left(t_3-t_0\right) - \frac{h}{2}\right] + h\left(t-t_3\right)\left[\frac{2v_f}{\tan(2\theta)} - \frac{h\left(2-\tan^2\theta\right)}{2\tan\theta\left(t_4-t_3\right)}\right] \tag{3.7}$$

Stage 5: $t_4 < t \le t_5$ (Fig. 3.5 (e)):

$$s = s_{\mathrm{ABCGHI\&LFKM}} = \frac{2hD_T\sin\theta}{\tan\left(2\theta\right)} - h\left(D_T\cos\theta - \frac{D_H}{2}\right) + h\tan\theta\left[v_f\left(t_3-t_0\right) - \frac{h}{2}\right] \tag{3.8}$$

Stage 6: $t_5 < t \le t_6$ (Fig. 3.5 (f)):

$$s = s_{\mathrm{ANPCGHI\&LFKM}} = \frac{2hD_T\sin\theta}{\tan\left(2\theta\right)} - h\left(D_T\cos\theta - \frac{D_H}{2}\right) + h\tan\theta\left[v_f\left(t_3-t_0\right) - \frac{h}{2}\right] - \frac{{v_f}^2\left(t-t_5\right)^2}{\sin(2\theta)} \tag{3.9}$$

Stage 7: $t_6 < t \le t_7$ (Fig. 3.5 (g)):

$$s = s_{\mathrm{ANQI\&LFKM}} = h\tan\theta v_f\left(t_7-t\right) + \frac{2hD_T\sin\theta}{\tan\left(2\theta\right)} - 2h\left(D_T\cos\theta - \frac{D_H}{2}\right) \tag{3.10}$$

Stage 8: $t_7 < t \le t_8$ (Fig. 3.5 (h)):

$$s = s_{\mathrm{TRSKM}} = \frac{t - t_8}{t_8 - t_7}\left[\frac{h^2}{2\tan\theta} - \frac{2hD_T\sin\theta}{\tan(2\theta)} + 2h\left(D_T\cos\theta - \frac{D_H}{2}\right)\right] + \frac{h^2}{2\tan\theta} \tag{3.11}$$

Stage 9: $t_8 < t \le t_9$ (Fig. 3.5 (i)):

$$s = s_{\mathrm{TWM}} = \frac{\left[v_f\left(t_9 - t\right)\right]^2}{2\tan\theta} \tag{3.12}$$

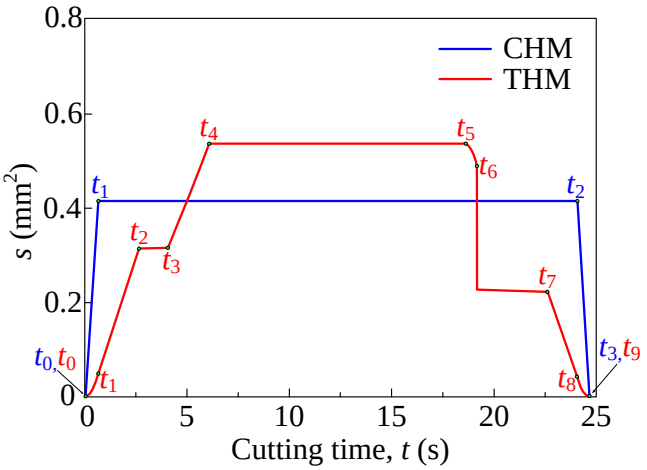

Fig. 3.6 Variations of the s in CHM and THM

As a consequence, the variations of the cross section area during drilling can be obtained quantitatively by using Eqs. (3.1) - (3.3) and Eqs. (3.4) - (3.12), respectively, for CHM and THM. As a typical result obtained, Fig.7 shows the variations of the cross section area in CHM and THM under the process parameters of H = 2.8 mm, D_{T} = 9.5 mm, D_{H} = 12 mm, and θ = 0° for CHM, and 5° for THM. e = 1.25 mm for CHM and 1.27 mm for THM, n_{T} = 2000 min^{-1}, n_p = 101 min^{-1}, v_f = 7 mm/min for CHM and 9.07 mm/min for THM. The eccentricity, e, in THM was set at a different value from that in CHM based on the relationship of $D_{\mathrm{H}} = 2e + D_{\mathrm{T}}\cos\theta$, in order for the hole diameter in THM to be same with that in CHM. In addition, in order for the total time required for completing the hole drilling in THM to be same as that in CHM, the tool feed rate, v_f,

$_{THM,}$ in THM was set at a different value than $v_{f\text{-CHM}}$ in CHM, based on the relationship of $v_{f\text{-THM}} = (1+D_T\sin\theta/H)v_{f\text{-CHM}}$, which is obtained from the geometrical arrangement shown in Fig. 2.1.

It can be seen from the figure that in CHM the cross section area increases sharply from zero at the moment, $t_{0,}$ to a certain value at the moment $t_1 = t_0 + T_p$ in an extremely short period of only one tool revolution. It reaches a steady state under the current process parameters, $t_0 = 0$ s, $T_p = 0.59$ s and the specific value of s is 0.416 mm^2. Then, in the steady stage of $t_1 < t < t_2$, s is kept constant at a specific value. After the moment t_2, s drops rapidly back to zero again at the moment, t_3, in just one revolution. Given that s is directly related to the drilling force, and the increased rate of drilling force was considerably high, strong shock and mechanical damage would be inflicted onto the workpiece at the hole entrance, producing a low quality hole. Similarly at the hole exit, soon before the completion of the hole, the drilling force would remain at a certain value, resulting in easy occurrences of chipping and delamination at the hole exit.

The variation in s in THM reveals that s increases or decreases in a stepwise fashion rather than in a sharp increase or decrease in CHM at the hole entrance or exit. This indicates that in THM, the shock and mechanical damage would not be as strong at the hole entrance and at the hole exit and the drilling force would be quite small. This implies that either at the hole entrance or at the hole exit the hole quality in THM would be significantly better than that in CHM. However, the value of s in the steady stage of $t_4 < t < t_5$ in THM is a little larger than in CHM, meaning that the steady drilling force in THM would be slightly larger than that in CHM.

3.2.1.3 The zero cutting speed point problem

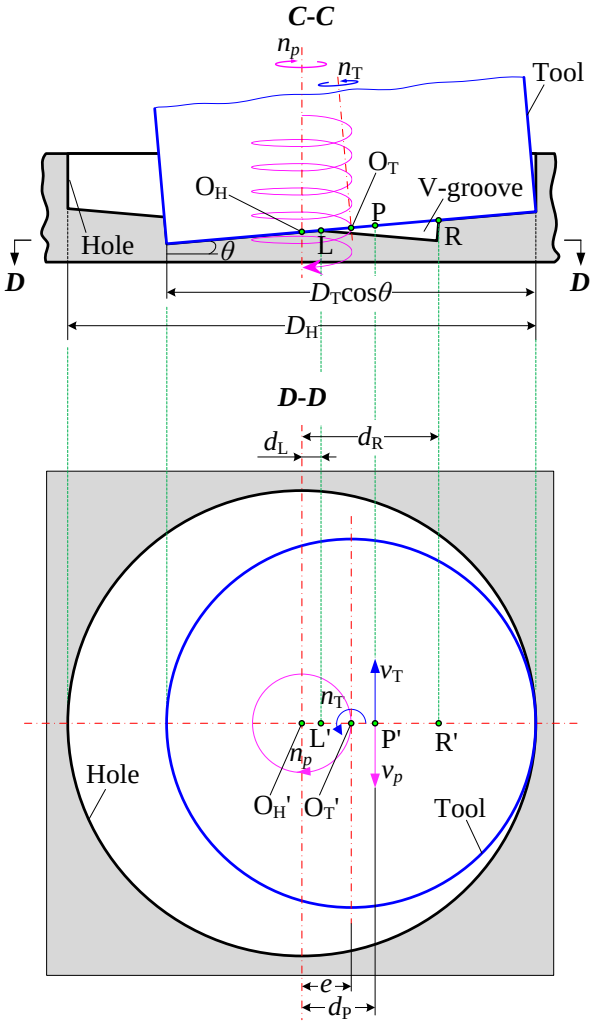

Fig. 3.7 The distribution maps of speed vectors of tool end cutting edges

During hole drilling by CHM (previously shown in Fig. 3.1 (a)) all of the cutting edges on the tool always contact with the work-materials, leading to the occurrence of the zero cutting speed point problem. In order to determine whether this problem also occurs in THM, the speed of an arbitrary point, P, on the end of the cutting edge is kinetically analyzed, as shown in Fig. 3.7. Let point P be in the C-C plane and away from the hole axis by distance, d_P. The speed component of point P in the hole axis would be equal to the tool feed rate, v_f. Its speed components caused by its own rotation at the rotational speed, n_T, and its conical pendulum motion at the revolution speed, n_p, are given by Eqs. (3.13) and (3.14), respectively.

$$v_T = 2\pi(d_P - e)n_T/\cos\theta \tag{3.13}$$

$$v_p = 2\pi d_P n_p \tag{3.14}$$

Usually, as the value of v_f is far smaller than that of v_T and v_p, the resultant speed of point P, v, is predominantly determined by v_T and the v_p, as expressed with Eq. (3.15).

$$v = \begin{cases} 2\pi\left[d_P n_P + n_T\left(d_P - e\right)/\cos\theta\right], & \text{Clockwise tool roration} \\ 2\pi\left[d_P n_P - n_T\left(d_P - e\right)/\cos\theta\right], & \text{Counter - clockwise tool roration} \end{cases} \tag{3.15}$$

Rearranging Eq.(15) yields that the value of v will be zero at $d_P = d_{P\text{-zero}}$ where

$$d_{P\text{-zero}} = \begin{cases} -e\cos\theta/\left(n_T/n_P + \cos\theta\right) + e, & \text{Clockwise tool roration} \\ e\cos\theta/\left(n_T/n_P - \cos\theta\right) + e\ , & \text{Counter - clockwise tool roration} \end{cases} \tag{3.16}$$

This means that the zero cutting speed point problem would also occur also in THM when the cutting edge, located at the position determined by Eq. (3.16), comes into contact with the work-materials. However, it is interesting to discover in Fig. 3.7 that if point P with v = 0 is located between the points L and R, the end of the cutting edge with zero cutting speed does not contact with the work-materials during drilling. This is due to the existence of the V-groove and the zero cutting speed point problem can therefore be avoided.

The points L and R stand for the contact points of the inner and outer sides of the V-groove with the tool end cutting edges, respectively. The point, O_H, is the intersection point between the hole axis and the tool end face. The D-D plane is vertical to the hole axis. The points P', L', R', O_T' and O_H' are the projection of the points P, L, R, O_T, and O_H onto the D-D plane. Thus, from the geometrical arrangement in Fig.8, the distances, d_L, from L' to O_H' and d_R, from R' to O_H', can be determined by Eqs. (3.17) and (3.18), respectively.

$$d_L = \frac{v_f}{4n_p \tan\theta} \tag{3.17}$$

$$d_R = \frac{(D_T\cos\theta - 2e)[1+\tan(2\theta)\tan\theta]}{2} - \frac{v_f \tan(2\theta)}{4n_p} \tag{3.18}$$

Consequently, in order to avoid the zero cutting speed point problem, the value of $d_{\text{P-zero}}$ should meet the following relationship.

$$d_{\text{L}} < d_{\text{P-zero}} < d_{\text{R}} \tag{3.19}$$

For a better understanding of how the zero-cutting speed point problem can be avoided, a single factor analysis was performed on the effects of the parameters of θ, D_T, e and n_T/n_p on the $d_{\text{P-zero}}$, d_{L} and d_{R}, respectively, using Eqs. (3.16), (3.17), and (3.18). This is shown in Figs. 3.8 (a), (b), (c) and (d).

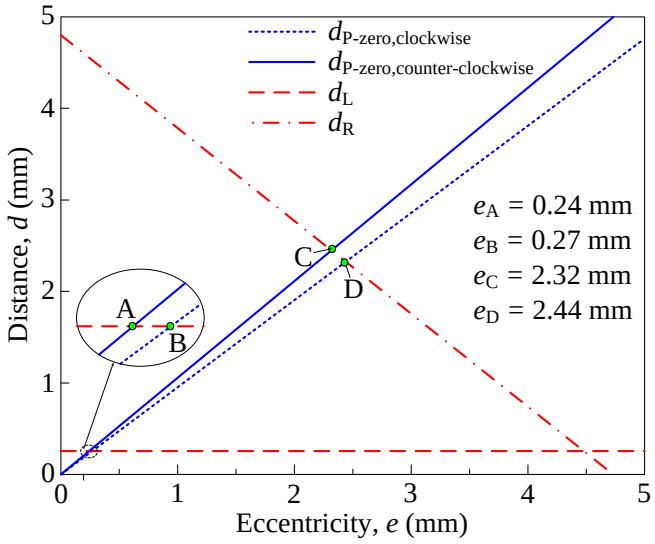

(a) Effect of the eccentricity e

(θ = 5°, D_T=9.5 mm, v_f=9.07 mm·min^{-1}, n_T/n_p =19.8, n_T=2000 min^{-1})

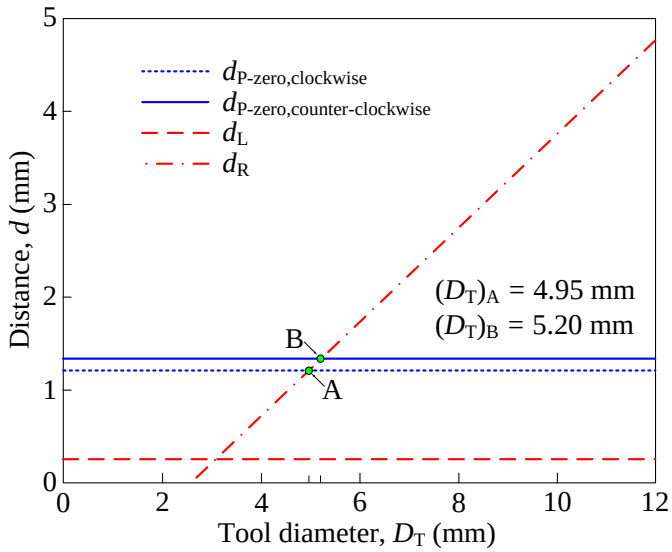

(b) Effect of the tool diameter D_T

(θ = 5°, e = 1.27 mm, v_f=9.07 mm·min^{-1}, n_T/n_p =19.8, n_T=2000 min^{-1})

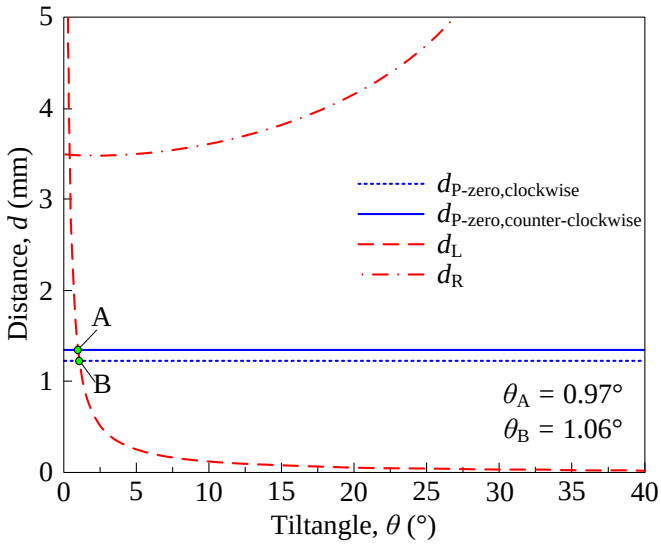

(c) Effect of the tilt angle θ

(e = 1.27 mm, D_T=9.5 mm, v_f=9.07 mm·min^{-1}, n_T/n_p =19.8, n_T =2000 min^{-1})

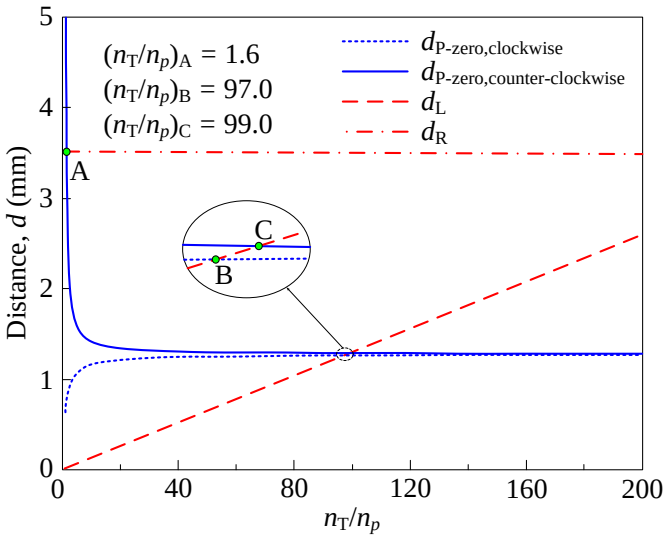

(d) Effect of the rotational speed ratio n_T/n_p

(θ = 5°, e = 1.27 mm, D_T=9.5 mm, v_f=9.07 mm·min^{-1},, n_T =2000 min^{-1})

Fig. 3.8 Effects of the eccentricity, the tool diameter, the tilt angle, and the rotational speed ratio on the $d_{P\text{-zero}}$, d_L and d_R

Initially, it can be determined from the figures that no matter what the values of θ, D_T, e and n_T/n_p are, the effects of the tool rotational direction on the value of $d_{P\text{-zero}}$ are very little. In addition, it was revealed that as long as the eccentricity is in the range of e = 0.27 mm - 2.32 mm under θ = 5°, D_T=9.5 mm, v_f=9.07 mm·min^{-1}, n_T/n_p =19.8, n_T=2000 min^{-1}, the tool diameter is in D_T = 5.20 mm – 12.00 mm under θ = 5°, e = 1.27 mm, v_f=9.07 mm·min^{-1}, n_T/n_p =19.8, n_T =2000 min^{-1}, the tilt angle is in θ = 1.06° - 40° under e = 1.27 mm, D_T=9.5 mm, v_f=9.07 mm·min^{-1}, n_T/n_p =19.8, n_T =2000 min^{-1},and the speed ratio is in n_T/n_p = 1.6 - 99.0 under e = 1.27 mm, D_T=9.5 mm, v_f=9.07 mm·min^{-1}, θ = 5°, n_T =2000 min^{-1}, the value of $d_{P\text{-zero}}$ will meet the requirement determined by Eq. (3.19). Therefore, the zero-cutting speed point problem can be avoided.

3.2.2 Experimental verification

3.2.2.1 Experimental conditions and procedure

In order to verify the kinetic analysis in section 3.2.1, the performance of the THM method was experimentally compared with that of the CHM method in terms of the

hole formation process, the drilling force, the hole quality at the entrance/exit, and the chip removal.

Table 3.1 shows the work-material parameters and experimental conditions. The purpose of the experiments is to validate the previous kinetic analysis and confirm the advantage of the THM method over the CHM method. Thus, the tilt angle was fixed at $\theta = 5°$ for THM, and the rotation speeds of the tool and the rotary worktable were set at $n_T = 2000$ min^{-1} and $n_p = 101$ min^{-1}, respectively. According to the theoretical analysis result shown in Fig. 3.8 (b), the tilt angle should be in $\theta = 1.06°$ - $40°$ in order to avoid the zero cutting speed problem. Consequently, in experiment the tilt angle was set at $\theta = 5°$ further for the simplicity of experiment operation including the alignment of experimental setup. In the determination of the tool rotation speed in experiment, as the cutting speed, i.e., the tool peripheral speed, is usually set at around 60mm·min^{-1} [18] in practical CHM process for CFRP drilling with end mills, the rotation speed of tool (9.5mm in diameter) was thus set at 2000 min^{-1} in this work so that the cutting speed reaches 59.7mm·min^{-1}. Because the stock tool feeds required for completing the hole drilling in CHM and THM are $H + h$ (see Fig.3.2) and $D_T\sin\theta + H + h$ (see Fig. 3.3), respectively; the tool feed rate should be set at different values of $v_f = (H+h)/T$ for CHM and $v_f = (D_T\sin\theta+H+h)/T$ for THM. This is so that the total time, T, required for completing the hole drilling in THM can be same as that of CHM. As the tool, a commercial cemented carbide cross cutting tool (BC4114 by Minitor Co., Ltd., Japan) (Fig. 3.9) of $D_T = 9.5$mm in diameter, which is supposed to be suitable for helical milling process, was employed. The cutting edges on the sides of the tool were helically distributed at 30°. Twelve linear cutting edges on the end of the tool were distributed radially on the tool end face, whose rake and flank angles were 15° and 20°, respectively. Plate-shaped CFRP specimens with dimensions of 80 mm in length, 40 mm in width and 2.8 mm in thickness (T700SC-12K-50C, cross twill weave/epoxy resin by Toray Ltd., Japan) were used as the workpiece. The fiber type and matrix of CFRP are T700SC and epoxy resin, respectively. The laminated structure of CFRP are cross twill weave specifications and 4 sheets stacked in the same direction. The molding method of CFRP is placed in a vacuum bagging and molded under atmospheric pressure. Curing of CFRP

was then carried out at 130°C for 90 min or more. The work-material parameters such as the mechanical properties, the fiber content and the glass transition temperature of CFRP are also exhibited in Table 3.1. Dry drilling operations were carried out without coolant supplying. Finally, in order to meet the requirement given by Eq. (3.19) for avoiding the zero cutting speed point problem in THM, the tool eccentricity was set at e_{THM} = 1.27 mm. The eccentricity in CHM was set at e_{CHM} = 1.25 mm so that the diameter of hole drilled in CHM is the same as that in THM according to the relationships of $D_H = 2e_{CHM}+D_T$ in CHM and $D_H = 2e_{THM}+D_T\cos\theta$.

Table 1 Work-material parameters and experimental conditions

Composite material (T700SC-12K-50C, cross twill weave /epoxy resin)	Fiber: content V_f= 60%, Tensile strength 4900 MPa, Tensile modulus 230 GPa, Strain 2.1%, Density 1.80 g/cm^3
	Tensile strength (0°): R_m= 663 MPa
	Tensile modulus (0°): E= 22 GPa
	Fracture strain (0°): ε_f= 5.25 %
	Tensile strength (90°): R_m= 625 MPa
	Tensile modulus (90°): E= 21.6GPa
	Fracture strain (90°): ε_f= 5.03 %
	Glass transition temperature: Tg= 132.7°C
Tool	Cemented carbide burr tool
	Diameter: D_T=9.5 mm
Cutting conditions	Tool rotational speed, n_T=2000 min^{-1}
	Feed rate: v_f =7 mm·min^{-1}(CHM), 9.07 mm·min^{-1}(THM)
	Workpiece rotational speed, n_p =101 min^{-1}
	Eccentricity, e=1.25 mm (CHM), 1.27 mm (THM)
	Tilting angle, θ=0° (CHM), 5° (THM)
Coolant	Dry cutting

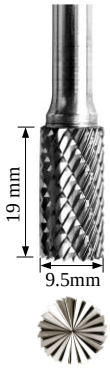

Fig. 3.9 A picture of the tool used

To accomplish the experimental purposes, first, the previous theoretical analysis of the hole formation process was experimentally verified by observing the instantaneous cross sections of hole at several specific moments. In the preparation of the specimen used for the hole cross section observation, the drilling operation was stopped at an appropriate moment during drilling and the specimen was cut in half along the diameter

of the drilled hole. Then, the obtained hole cross section surface was polished and followed by optical observation. This kind of operation was repeated at the different specific moments in the CHM and THM processes. Second, the entrances and exits of the drilled holes were observed and the burr/chipping areas were quantitatively obtained to compare the hole qualities in CHM and THM. Third, SEM observations of tool end face conditions after use in CHM and THM were performed to compare the chip removal behaviors. Moreover, although the direct way to confirm the value of *s* predicted in section 3.2.1 is to collect chips formed during drilling and measure their dimensions, in practice the collection and dimension measurement were difficult. Therefore, in this work the thrust drilling forces along the hole axis during drilling were measured both in CHM and THM using the dynamometer and used for confirming the predicted *s* under the awareness of that there is a linear relationship between the cutting force and the cross section area of chip in drilling process. The obtained results will be presented later in section 3.2.2.2.

3.2.2.2 Experimental results and discussion

Figs. 3.10 and 3.11 show the optical images of the hole cross section at different moments in CHM and THM, respectively. Comparing Figs. 3.10 and 3.11 with Figs. 3.2 and 3.3 revealed that the obtained hole cross section profiles at different specific moments either in CHM or in THM agreed well with the predicted profiles at the corresponding moments. The W-shaped cross sections appeared in THM but never occurred in CHM. Thus, the kinetic analysis results have been confirmed.

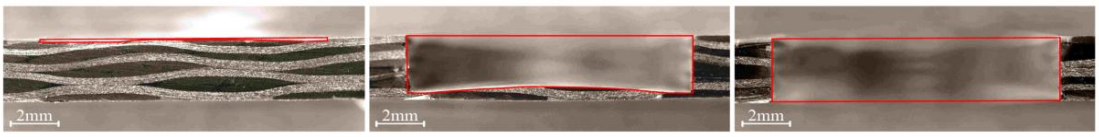

(a) At the moment around t_1 (b) At a moment between t_1 and t_2 (c) At the moment around t_3

Fig. 3.10 Optical images of hole cross sections at four typical moments during drilling by CHM

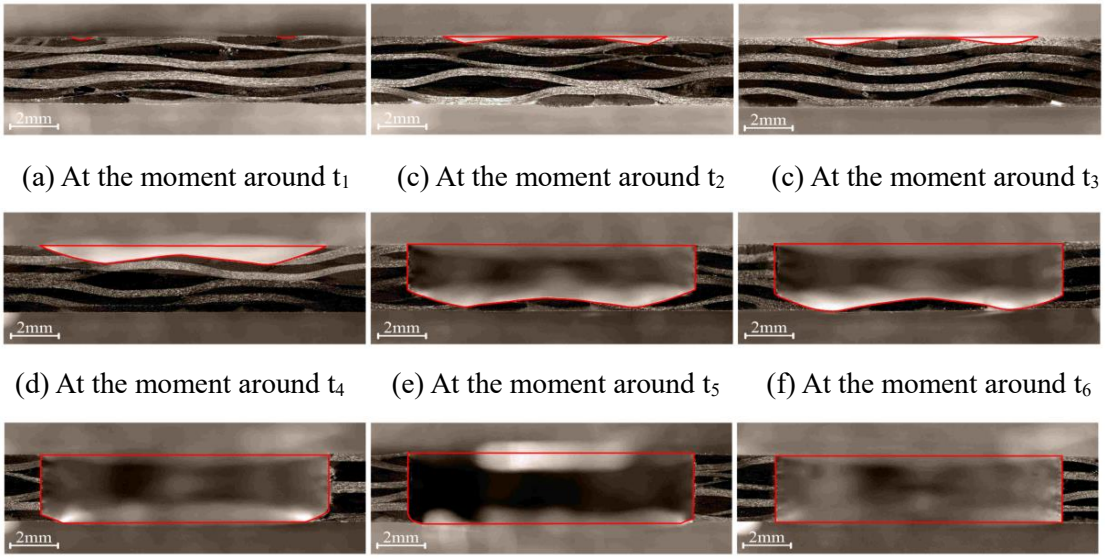

(a) At the moment around t_1 (c) At the moment around t_2 (c) At the moment around t_3

(d) At the moment around t_4 (e) At the moment around t_5 (f) At the moment around t_6

(g) At the moment around t_7 (h) At the moment around t_8 (i) At the moment around t_9

Fig. 3.11 Optical images of hole cross sections at eight typical moments during drilling by THM

Fig.3.12 shows the variations of thrust drilling forces, F_z, measured during drilling in CHM and THM. For confirming the variations of the s during drilling previously predicted in section 3.2.1 (see Fig. 3.6), the averaged thrust drilling forces were also plotted in the same figure to show their variation styles during drilling. It can be seen that the variation style of the thrust drilling force is quite similar to that of the s either in CHM or in THM, indicating that the analytical prediction of s was valid. It is, however, worth noting that the actual average value of force in the steady stage in THM was much smaller than that in CHM; whereas the value of s in the steady stage in THM was predicted to be slightly larger than that in CHM. This is probably attributed to the fact that in actual drilling operation by CHM the chip removal was not smooth and the zero cutting speed point problem existed, leading to the considerable increase in the drilling force. In addition, the heavy and periodic variations can be observed on the actual thrust forces during drilling in both CHM and THM. These phenomena will be further discussed in detail in the future work.

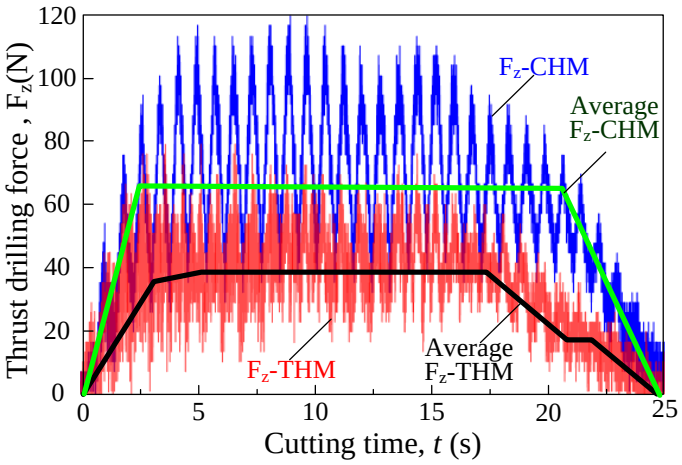

Fig. 3.12 Comparison of variations of *s* and thrust force in both CHM and THM

Finally, the performance of THM in chip removal was compared with that of CHM by observing the conditions of tool end face. Figs. 3.13 (a) - (c) show the SEM images of the tool end face before and after drilling in CHM and THM, respectively. It is evident that chips adhesion on the tool end face occurred either in CHM or in THM. This phenomenon might be due to the fact that the chips form a condensed mass and adhere to the tool cutting edges when the machining temperature exceeds the glass transition temperature of the composite. This issue will be studied in detail in our future works. However, obviously the chips adhesion in CHM was much heavier than that in THM, demonstrating that the chip removal ability of the THM method is much higher than that of the CHM. This in turn contributes to the reduction of drilling force and the improvement of hole quality.

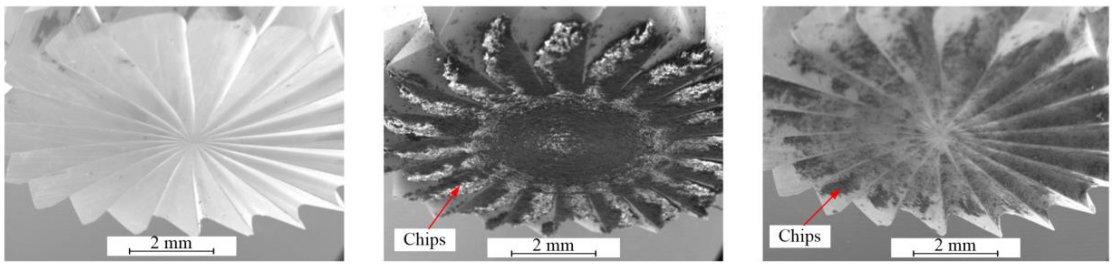

(a) Before drilling (b) After drilling in CHM (c) After drilling in THM

Fig. 3.13 SEM images of tool end face

3. 3 Hole exit formation

3.3.1 The hole exit formation process

As an essential step towards the development of the THM technique, the hole exit formation process in THM is kinetically analyzed. For comparison, the kinetic analysis is also performed for CHM. Figs. 3.14 and 3.15 illustrate the instantaneous cross section profiles of the hole and the tool at different moments. These profiles are positioned in a plane that is determined by the tool axis and the hole axis at an arbitrary moment after drilling for time, t. Hereafter, this plane is referred to as the C-C plane for convenience. In addition, in all the figures, the dotted lines denote the tool cross sections at the moment t-T_p, i.e., one revolution before the moment, t.

Figs. 3.14 (a) and (b) show the cross section profiles of the hole and the tool in the C-C plane at two characteristic moments, t_0 and t_1, respectively, during the CHM process. At the moment t_0-T_p, the cutting edges on the tool end reach the hole bottom-ply for the first time. Then, the entire end of the tool is cut out the workpiece suddenly as the tool continues to feed through. Around the moment t_0, the tool pushes aside the material and tears the fibers, leading to the frequent occurrence of hole exit delamination owing to the fact that the thrust cutting force, F_z, is beyond the combination strength between layers. At the moment t_1, the tool end face penetrates the workpiece and completes the hole drilling, but burrs are formed on the hole exit because of the delamination. Consequently, the tool feed rate should be enough small so that the thrust force is restrained at an enough low level. This in turn leads to a low drilling efficiency.

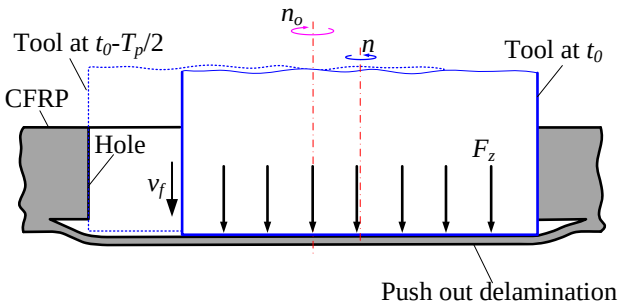

(a) t_0

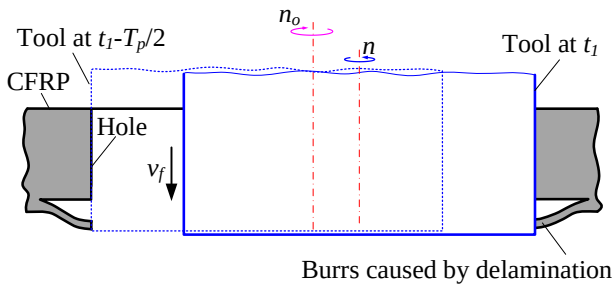

(b) t_1

Fig. 3.14 Illustrations of the hole/tool cross sections at characteristic moments in CHM

The hole exit formation process in THM exhibits a more complicated process than that in CHM due to the tool tilt. The hole exit formation process can be composed of a primary-stage (from t_0 to t_1) and a secondary-stage (from t_1 to t_3) in THM as shown in Fig. 3.15. At the moment t_0, the lowest cutting edge on the tool end comes into contact with the hole bottom-ply for the first time. Next, the tool starts to form the hole exit and the lowest cutting edge penetrates the workpiece after one revolution. It results in the drop of the conical un-cut work-materials located in the hole central area (the triangle area in Fig. 3.15 (a)) at the moment t_1 (see Fig. 3.15 (b)), thus leading to the generation of a hole with a diameter of D_P which is smaller than the desired one D_b. Similar to CHM, the tool pushes aside the material and tears the fiber, leading to the frequent occurrence of hole exit delamination on the smaller hole exit due to the thrust cutting force. Then, the diameter gradually expanded as the tool continues to feed through until the moment t_2 (see Fig. 3.15 (c)) when the highest cutting edge reaches the hole exit for the first time. As the process further progresses one revolution to the moment t_3, the un-cut material with triangle cross section profile is gradually cut off and the hole with the desired diameter of D_b is eventually formed. It can be figured out from the hole exit formation process in THM that in the secondary stage (t_1 – t_3), the delamination previously generated in the primary stage could be eliminated. Although there is still a risk that new delamination would occur in the secondary stage, as revealed previously in the final period of t_2 – t_3, the material removal rate is considerably small and the thrust cutting force is low enough to prevent the occurrence of delamination. In particular, it can be found from Fig. 3.15 (d) that the beveling of hole exit is performed

with side cutting edge of the tool. Shortly, in THM the delamination formed in primary-stage may be removed in secondary-stage and the exit quality could be further improved by the beveling effect.

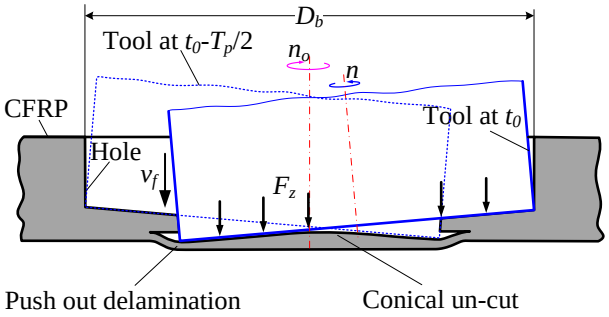

(a) t_0

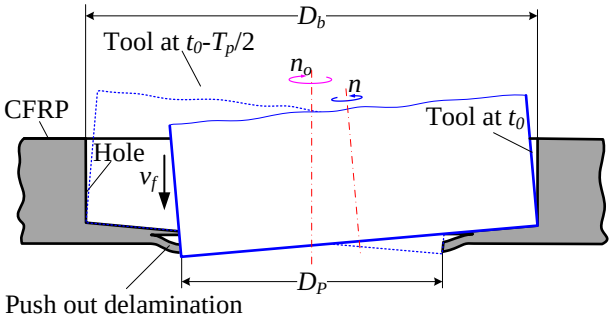

(b) t_1

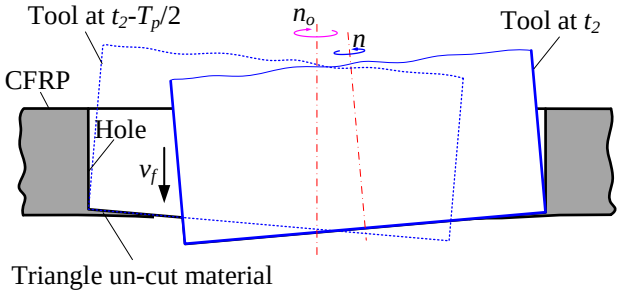

(c) t_2

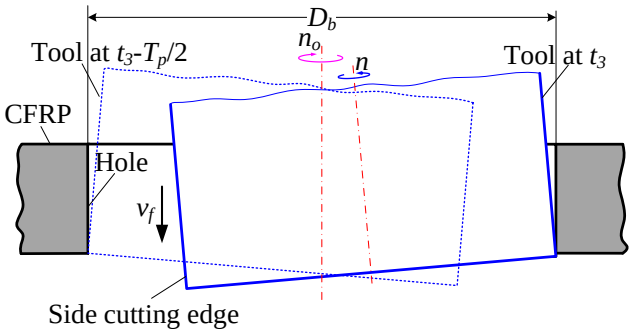

(d) t_3

Fig. 3.15 Illustrations of the hole/tool cross sections at characteristic moments in THM

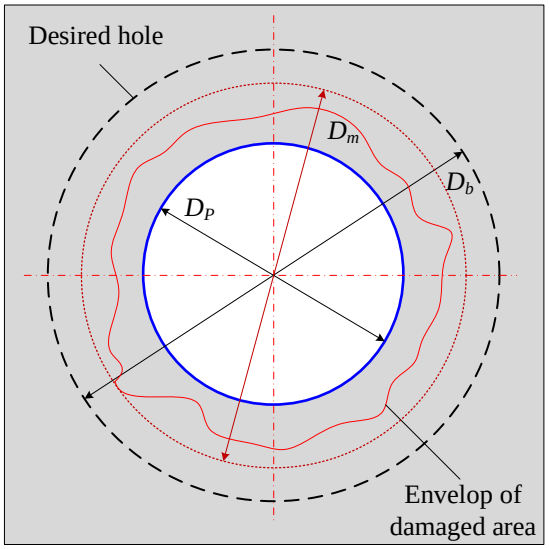

Fig. 3.16 Illustration of hole exit side at moment t_1 during the hole exit formation process by THM

However, it is still unclear that in THM the delamination formed in the primary stage can be or not eliminated in the secondary stage and how the setup parameters, i.e., tilt angle, eccentricity and tool diameter, affect the elimination of delamination. Hereafter, the related discussion is carried out.

Fig. 3.16 shows the Illustration of hole exit side at moment t_1 during the hole exit formation process by THM. At the moment t_1, a hole with a diameter of D_P, has just been generated and the value of D_p can be expressed in Eq. (3.19). The eccentricity, e, is the distance from the tool end face center to the hole axis. The diameter of the desired

hole, D_b, is determined as in Eq. (3.20). If D_m is the outlet diameter of the damaged zone with delamination, a delamination factor F_d can be introduced as in Eq. (3.21).

$$D_P = 2D_t \cos\theta - D_b \tag{3.19}$$

$$D_b = D_t \cos\theta + 2e \tag{3.20}$$

$$F_d = D_m / D_P \tag{3.21}$$

Combining Eqs. (3.19), (3.20) and (3.21), one gets

$$D_m = F_d(D_t \cos\theta - 2e) \tag{3.22}$$

In order for the damaged zone generated in the primary stage to be removed in secondary-stage, the value of D_m should be smaller than the desired diameter of hole, D_b as following.

$$D_m < D_b \tag{3.23}$$

For determining the process parameters which meet the relationship of Eq. (5), a single factor analysis was performed on the effects of the parameters F_d, D_t, θ and e on the D_P, D_m and D_b, respectively, using Eqs. (3.19) – (3.23), and the results are as shown in Fig. 3.17.

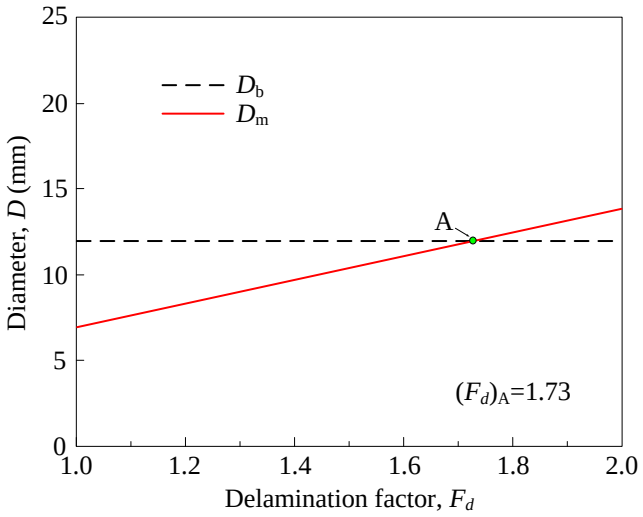

(a) Effect of the delamination factor F_d (θ = 5 °, e = 1.27 mm, D_t = 9.5 mm)

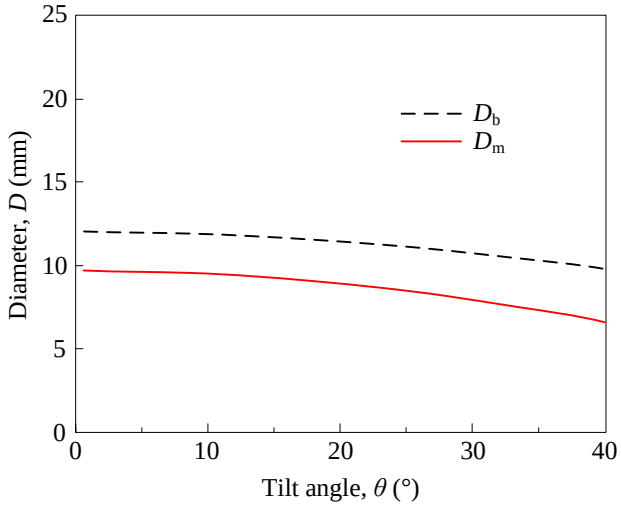

(b) Effect of the tilt angle θ ($\theta \neq 0$) (F_d = 1.4, e = 1.27 mm, D_t = 9.5 mm)

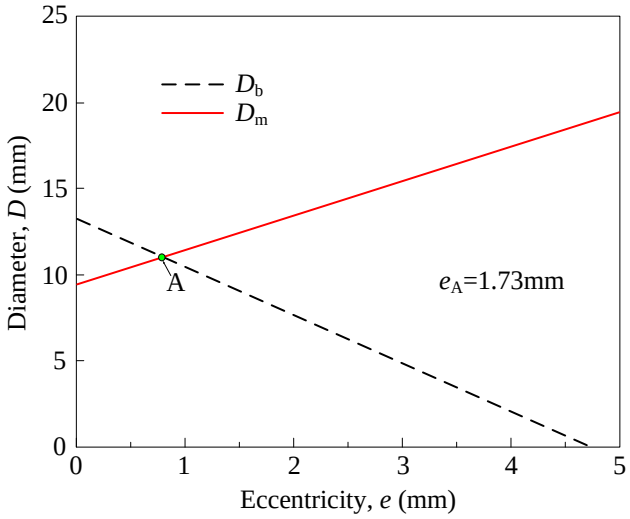

(c) Effect of the eccentricity e (F_d = 1.4, θ = 5 °, D_t = 9.5 mm)

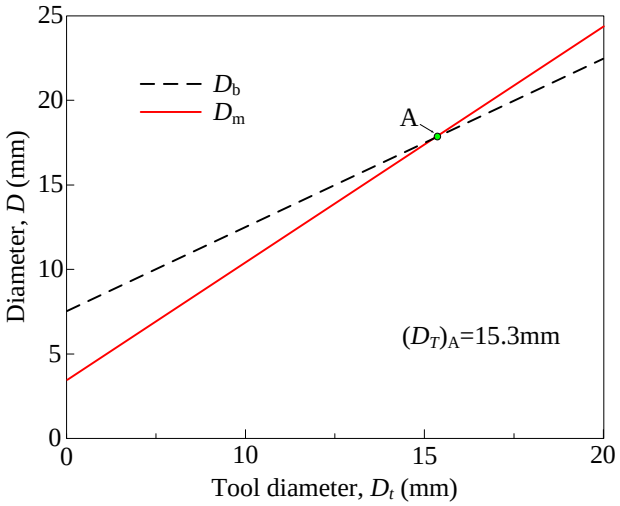

(d) Effect of the tool diameter D_t (F_d =1.4, θ = 5°, e = 1.27 mm)

Fig. 3.17 Effects of the delamination factor, the tilt angle, the tool diameter and the eccentricity on the D_m and D_b

It was revealed that as long as the delamination factoris in the range of F_d = 1 – 1.73 under θ = 5°, e = 1.27 mm, D_t = 9.5 mm, the tilt angle is in the range of 0° to 40° but unequal to 0° under F_d = 1.4, e = 1.27 mm, D_t = 9.5 mm, the eccentricity is in 0 – 1.73 mm under F_d = 1.4, θ = 5°, D_t = 9.5 mm, the tool diameter is in 0 – 15.3 mm under F_d =1.4, θ = 5°, e = 1.27 mm, the value of D_m will meet the requirement determined by Eq. (3.17). Therefore, in THM the delamination formed in primary-stage can be removed in secondary-stage once the process parameters are setup appropriately.

3.2.2 Experimental results and discussion

Figs. 3.18 and 3.19 show the optical images of hole exit side at several specific moments during the hole exit formation process by CHM and THM, respectively. The meaning of the specific moment is the same as the kinetic analysis in section 3.2.1. In CHM, the moment t_x is in the period of $t_0 - t_1$. Evidently, a significant quantity of uncut fibers occurred in CHM which located in the hole exit edge at the moment around t_0 and t_x (see Figs. 3.18 (a) and (b)). The tool pushes aside the material and tears the fiber as the tool continues to feed through, leading to the frequent occurrence of hole exit delamination on the hole exit at the drilling finish moment, t_1 (see Fig. 3.18 (c)).

In contrast to CHM where the uncut fibers the hole exit edge, many uncut fibers occurred in THM which located in the hole exit central area at the moment around t_0 (see Fig. 3.19 (a)). Next, a hole with a diameter of D_P was observed in the hole exit central area which is smaller than the desired one D_b (see Fig. 3.19 (b)). Similar to CHM, the hole exit delamination occurred at the smaller hole exit. The outlet diameter of the damaged zone with delamination is D_m (see Fig. 3.19 (b)). The delamination factor, F_d, was calculated by Eq. (3.21) and the value of F_d was 1.22. It can meet the relationship of Eq. (3.23) according to the single factor analysis of Fig. 3.15 (a). Burrs and chippings in THM were rarely found at exit of the hole at the drilling finish moment, t_3 (see Fig. 3.19 (c)). The result means that the delamination formed in primary-stage was removed in secondary-stage.

The above-mentioned results demonstrate that the obtained hole exit side at several specific moments either in CHM or in THM agreed well with the predicted analysis at

the corresponding moments. The kinetic analysis results have been confirmed.

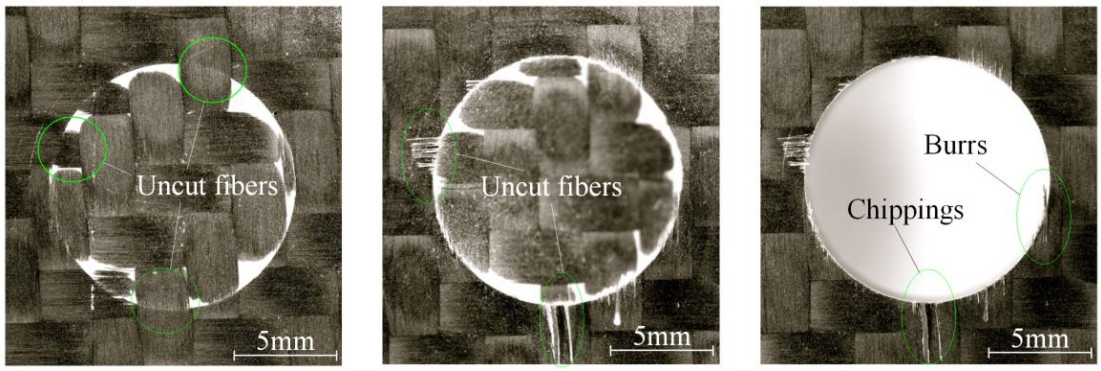

(a) At the moment around t_0 (b) At the moment around t_x (c) At the moment around t_1

Fig. 3.18 Optical images of hole exit side at several specific moments during the hole exit formation process by CHM

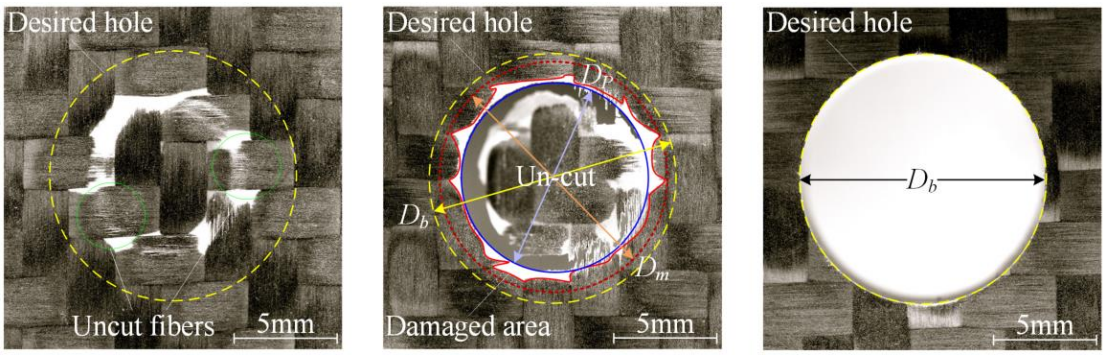

(a) At the moment around t_0 (b) At the moment around t_1 (c) At the moment around t_3

Fig. 3.19 Optical images of hole exit side at several specific moments during the hole exit formation process by THM

3.4 Summary

As a step toward the development of the tilted helical milling (THM) technique, the hole formation processes in THM and conventional helical milling (CHM) were kinetically analyzed. The undeformed cross-sectional areas of work-materials removed per tool revolution in THM were theoretically compared with that in CHM, followed by the discussion on the zero-cutting speed point problem. Then, experiments were performed to confirm the theoretical analysis in terms of the variations of the drilled hole cross section profile, the drilling forces, and the chip removal. Finally, its advantages over the conventional helical milling (CHM) is abstracted through the

kinetic comparison of the hole exit delamination. Then, drilling experiments were conducted to confirm the kinetic analysis by observing the hole exit side at different moments during drilling. The obtained results can be summarized as follows:

(1) During THM drilling, the cross section of the bottom of the hole is W-shaped and a circumferential V-groove exists between the tool end face and the hole bottom. This is beneficial to timely chip removal and drilling force reduction/cutting heat dissipation. This is a unique advantage of THM over CHM and has been experimentally verified through the observation of chips adhered on the tool end face and the measurement of drilling force.

(2) In CHM, the undeformed cross section area of the work-materials removed per tool revolution, s, initially increases rapidly and then drops quickly at the end, implying the drilling force would increase and decrease rapidly. This leads to a strong shock force and damage on the workpiece, which eventually lowers the quality of the hole. In contrast, in THM, s increases or decreases in a stepwise fashion, which implies that the shock force and damage would be weaker, therefore, higher quality holes could be obtained by THM. These predictions have been confirmed by experimentally investigating the quality of the drilled hole at the entrance/exit.

(3) In CHM, the zero-cutting speed point problem always exists, but in THM it can be avoided as long as the tool tilt angle, the tool eccentricity, and the ratio of tool rotation speed to tool revolution speed have been set at their respective appropriate values.

(4) The measured thrust drilling force in THM was approximately half of that in CHM, which disagrees with the predicted results on the s where the value of s in THM is slightly larger than that in CHM. This is probably attributed to the fact that compared with CHM in actual operation of THM the chip removal was much smoother and the zero-cutting point problem was avoided.

(5) In THM the hole exit formation process can be composed of a primary-stage (a hole with a smaller diameter than the desired one is generated at the hole exit) and a secondary-stage (the diameter gradually expanded until its exit reaches the desired diameter) which never occur in CHM.

(6) In CHM, the tool pushes aside the material at the hole exit, leading to the frequent occurrence of hole exit delamination. In THM the delamination formed in primary-stage can be removed in secondary-stage cutting.

(7) The measured thrust drilling force in THM was approximately half of that in CHM.

(8) The advantage that the delamination formed during primary-stage cutting may be removed in secondary-stage cutting can be achieved as long as the tool diameter, the tool tilt angle and the tool eccentricity have been set at their respective appropriate values during THM.

References

[1] Tanaka H, Ohta K, Takizawa R, Yanagi K (2012) Experimental Study on Tilted Planetary Motion Drilling for CFRP. Procedia CIRP 1:443–448.

[2] Ohta K, Tanaka H, Takizawa R (2012) Development of Tilted Planetary Drilling System. Procedia CIRP 1:681–682.

[3] Muhammad, A.; Songmei, Y.; Muhammad, Z.K.; Chong, Z.; Qi, W. (2017) Development of cutting force prediction model for carbon fiber reinforced polymers based on rotary ultrasonic slot milling. *Machining Science and Technology*, DOI 10.1080/10910344.2017.1365895.

[4] Xu, W.X.; Zhang, L.C. (2016) Mechanics of fibre deformation and fracture in vibration-assisted cutting of unidirectional fibre-reinforced polymer composites. *International Journal of Machine Tools and Manufacture*, 103: 40–52.

[5] Dharan, C.K.H.; Won, M.S. (2000) Machining parameters for an intelligent machining system for composite laminates. *International Journal of Machine Tools and Manufacture*, 40 (3): 415–426.

[6] Tsao, C.C.; Hocheng, H. (2005) Effects of exit back-up on delamination in drilling composite materials using a saw drill and a core drill. *International Journal of Machine Tools and Manufacture*, 45: 1261–1270.

[7] Koenig, W.; Wulf, C.; Grass, P.; Willerscheid, H. (1985) Machining of fiber reinforced plastics. *CIRP Annals*, 34 (2): 538–548.

[8] Hocheng, H.; Dharan, C.K.H. (1990) Delamination during drilling in composite laminates. *Transactions of the ASME, Journal of Engineering for Industry*, 112: 236–239.

[9] Jain, S.; Yang, D.C.H. (1993) Effects of feedrate and chisel edge on delamination in composite drilling. *Transactions of the ASME, Journal of Engineering for Industry*, 115: 398–405.

[10] Jain, S.; Yang, D.C.H. (1994) Delamination-free drilling of composite laminates. *Transactions of the ASME, Journal of Engineering for Industry*, 116: 475–481.

[11] Tsao, C.C.; Hocheng, H. (2003) Comprehensive analysis of delamination in drilling of composite materials with various drill bits. *Journal of Materials Processing Technology*, 140: 335–339.

[12] Tsao, C.C.; Hocheng, H. (2001) Analysis of delamination in drilling Composite materials using step drill. *Proceedings 18th National Conference on Mechanical Engineering*, 4: 895–900.

[13] Tsao, C.C.; Hocheng, H. (2003) Analysis of delamination in drilling composite materials using core drill. *Australasian Journal of Mechanical Engineering*, 1 (1): 49–53.

[14] Won, M.S.; Dharan, C.K.H. (2002) Chisel edge and pilot hole effects in drilling composite laminates, *Transactions of the ASME, Journal of Manufacturing Science and Engineering*, 124: 242–247.

[15] Tsao, C.C. (2006) The effect of pilot hole on delamination when core drill drilling composite materials. *International Journal of Machine Tools and Manufacture*, 46: 1653–1661.

[16] Pereira, R.B.D.; Brandao, L.C; Paivab, A.P; Ferreira, J.R.; Davim, J.P. (2017) A review of helical milling process. *International Journal of Machine Tools and Manufacture*, 120: 27-48.

[17] Wang, H.Y.; Qin, X.D.; Li, H.; Tan, Y.Q. (2016) A comparative study on helical milling of CFRP/Ti stacks and its individual layers. *The International Journal of Advanced Manufacturing Technology*, 86(5): 1973–1983.

[18] Li, Z.Q.; Liu, Q.; Ming, X.Z.; Wang, X.; Dong, Y.F. (2014) Cutting force prediction and analytical solution of regenerative chatter stability for helical milling operation. *The International Journal of Advanced Manufacturing Technology*, 73(1): 433–442.

[19] Wang, H.Y.; Qin, X.D. (2016) A mechanistic model for cutting force in helical milling of carbon fiber-reinforced polymers. *The International Journal of Advanced Manufacturing Technology*, 82(9): 1485–1494.

[20] Li, Z.L.; Ding, Y.; Zhu, L.M. (2017) Accurate cutting force prediction of helical milling operations considering the cutting tool runout effect. *The International Journal of Advanced Manufacturing Technology*, 92: 4133–4144.

[21] Deitert, L. (2011) Orbital drilling. *SAE Technical Paper*, DOI 10.4271/2011-01-2533.

[22] Denkena, B.; Boehnke, D.; Dege, J.H. (2008) Helical milling of CFRP-titanium layer compounds. *CIRP Journal of Manufacturing Science and Technology*, 1(2): 64–69.

[23] Liu, J.; Chen, G.; Ji, C.H. (2014) An investigation of workpiece temperature variation of helical milling for carbon fiber reinforced plastics (CFRP). *International Journal of Machine Tools and Manufacture*, 86: 89–103.

[24] Lindqvist, R.; Eriksson, I.; Wolf, M. (2011) Orbital drilling of sandwich constructions for space applications. *Sae Technical Papers*, DOI 10.4271/2001-01-2571.

[25] Wu, Y.B.; Wang, Q.; Nomura, M. (2016) Proposal of tilt helical milling method for hole creation of carbon fiber reinforced plastic (CFRP). *Advanced Materials Research*, 1136: 190-195.

[26] Wang, Q.; Wu, Y.B.; Bitou, T.; Nomura, M.; Fujii, T. (2017) Proposal of a tilted helical milling technique for high quality hole drilling of CFRP: Kinetic analysis of hole formation and material removal. *The International Journal of Advanced Manufacturing Technology*, DOI 10.1007/s00170-017-1106-3.

[27] Muhammad, A.; Songmei, Y.; Muhammad, Z.K.; Chong, Z.; Qi, W. (2017) Development of cutting force prediction model for carbon fiber reinforced polymers based on rotary ultrasonic slot milling. Machining Science and Technology, DOI 10.1080/10910344.2017.1365895.

[28] Xu, W.X.; Zhang, L.C. (2016) Mechanics of fibre deformation and fracture in vibration-assisted cutting of unidirectional fibre-reinforced polymer composites. International Journal of Machine Tools and Manufacture, 103: 40–52.

[29] Dharan, C.K.H.; Won, M.S. (2000) Machining parameters for an intelligent machining system for composite laminates. International Journal of Machine Tools and Manufacture, 40 (3): 415–426.

[30] Tsao, C.C.; Hocheng, H. (2005) Effects of exit back-up on delamination in drilling composite materials using a saw drill and a core drill. International Journal of Machine Tools and Manufacture, 45: 1261–1270.

[31] Koenig, W.; Wulf, C.; Grass, P.; Willerscheid, H. (1985) Machining of fiber reinforced plastics. CIRP Annals, 34 (2): 538–548.

[32] Hocheng, H.; Dharan, C.K.H. (1990) Delamination during drilling in composite laminates. Transactions of the ASME, Journal of Engineering for Industry, 112: 236–239.

[33] Jain, S.; Yang, D.C.H. (1993) Effects of feedrate and chisel edge on delamination in composite drilling. Transactions of the ASME, Journal of Engineering for Industry, 115: 398–405.

[34] Jain, S.; Yang, D.C.H. (1994) Delamination-free drilling of composite laminates. Transactions of the ASME, Journal of Engineering for Industry, 116: 475–481.

[35] Tsao, C.C.; Hocheng, H. (2003) Comprehensive analysis of delamination in drilling of composite materials with various drill bits. Journal of Materials Processing Technology, 140: 335–339.

[36] Tsao, C.C.; Hocheng, H. (2001) Analysis of delamination in drilling Composite materials using step drill. Proceedings 18th National Conference on Mechanical Engineering, 4: 895–900.

[37] Tsao, C.C.; Hocheng, H. (2003) Analysis of delamination in drilling composite materials using core drill. Australasian Journal of Mechanical Engineering, 1 (1): 49–53.

[38] Won, M.S.; Dharan, C.K.H. (2002) Chisel edge and pilot hole effects in drilling composite laminates, Transactions of the ASME, Journal of Manufacturing Science and Engineering, 124: 242–247.

[39] Tsao, C.C. (2006) The effect of pilot hole on delamination when core drill drilling composite materials. International Journal of Machine Tools and Manufacture, 46: 1653–1661.

[40] Pereira, R.B.D.; Brandao, L.C; Paivab, A.P; Ferreira, J.R.; Davim, J.P. (2017) A review of helical milling process. International Journal of Machine Tools and Manufacture, 120: 27-48.

[41] Wang, H.Y.; Qin, X.D.; Li, H.; Tan, Y.Q. (2016) A comparative study on helical milling of CFRP/Ti stacks and its individual layers. The International Journal of Advanced Manufacturing Technology, 86(5): 1973–1983.

[42] Li, Z.Q.; Liu, Q.; Ming, X.Z.; Wang, X.; Dong, Y.F. (2014) Cutting force prediction and analytical solution of regenerative chatter stability for helical milling operation. The International Journal of Advanced Manufacturing Technology, 73(1): 433–442.

[43] Wang, H.Y.; Qin, X.D. (2016) A mechanistic model for cutting force in helical milling of carbon fiber-reinforced polymers. The International Journal of Advanced Manufacturing Technology, 82(9): 1485–1494.

[44] Li, Z.L.; Ding, Y.; Zhu, L.M. (2017) Accurate cutting force prediction of helical milling operations considering the cutter runout effect. The International Journal of Advanced Manufacturing Technology, 92: 4133–4144.

[45] Deitert, L. (2011) Orbital drilling. SAE Technical Paper, DOI 10.4271/2011-01-2533.

[46] Denkena, B.; Boehnke, D.; Dege, J.H. (2008) Helical milling of CFRP-titanium layer compounds. CIRP Journal of Manufacturing Science and Technology, 1(2): 64–69.

[47] Liu, J.; Chen, G.; Ji, C.H. (2014) An investigation of workpiece temperature variation of helical milling for carbon fiber reinforced plastics (CFRP). International Journal of Machine Tools and Manufacture, 86: 89–103.

[48] Lindqvist, R.; Eriksson, I.; Wolf, M. (2011) Orbital drilling of sandwich constructions for space applications. Sae Technical Papers, DOI 10.4271/2001-01-2571.

[49] Wu, Y.B.; Wang, Q.; Nomura, M. (2016) Proposal of tilt helical milling method for hole creation of carbon fiber reinforced plastic (CFRP). Advanced Materials Research, 1136: 190-195.

[50] Wang, Q.; Wu, Y.B.; Bitou, T.; Nomura, M.; Fujii, T. (2017) Proposal of a tilted helical milling technique for high quality hole drilling of CFRP: Kinetic analysis of hole formation and material removal. The International Journal of Advanced Manufacturing Technology, DOI 10.1007/s00170-017-1106-3.

Chapter IV
Cutting Force and Temperature in Tilted Helical Milling process

4.1 Introduction

Due to heterogeneity, anisotropy and fiber reinforcement, CFRP is difficult to process [1, 2]. To improve the cutting efficiency and quality of CFRP during drilling, many recent studies have focused on the relationship between machining parameters and hole quality. Pecat [3] studied the effect of cutting parameters on the surface integrity of CFRP. The result is a different cutting mechanism for different fiber orientations. Hintze [4] studied the stratification problem when milling one-way CFRP. They report that the main power supply will cause initial damage to the laminate, which may cause the fiber to deflect without being cut. Chibane [5] used damage and vibration analysis to obtain the best grinding conditions for carbon/epoxy composites. Yashiro [6] uses the tool - workpiece thermocouple method to measure the cutting temperature during the CFRP cutting process. It was found that as the cutting speed became higher, the cutting temperature in the CFRP immediately below the cutting point became lower. Azmi [7] studied the influence of cutting parameters on different cutting performance of GFRP milling and found that the feed rate plays a leading role in affecting surface roughness. Phadnis [8] studied the effects of drilling parameters on thrust force and torque through experiments and numerical studies. It can be concluded that low feed rates (<150 mm • min^{-1}) and high cutting speeds (>600 rpm) are preferred for drilling CFRP. Madhavan [9] concluded that as the orientation angle of the fiber increases, the cutting force increases until the cutting force drops below 65° at a large feed of 90° and the feed is low. Sasahara [10] reported that the internal coolant supply cutting temperature during CFRP grinding was significantly lower than that of CFRP matrix epoxy. Haddad [11] studied the effects of tool geometry and cutting conditions on surface defects and dust generated during CFRP milling. These defects have been observed to occur

primarily due to cutting conditions and tool geometry. Zegna [12] analyzed the cutting forces, induced the interaction between cutting damage and CFRP composite processing parameters, and pointed out that the increase in fiber orientation and depth of cut resulted in increased cutting forces and the resulting damage.

At present, a lot of researches have been done on the relationship between hole quality, cutting force and tool wear. However, few studies have focused on the interaction of cutting forces and cutting temperatures in CFRP milling.

If the cutting temperature exceeds the glass transition temperature of CFRP, degradation of the resin may reduce its strength [13]. In order to measure temperature changes during CFRP cutting, it is important to capture the dynamic response of the temperature measurement system. Conventional metal cutting [14] typically uses the "tool-workpiece thermocouple method" in which the thermal EMF between the tool material and the workpiece material is measured.

The processing of composite materials is basically based on the theory of brittle fracture mechanics [15]. Cutting force is the most direct parameter to evaluate the cutting process [16]. When estimating the cutting force, modeling is critical to assessing the accuracy of the model, followed by determining the cutting force coefficient, which is a particularly prominent factor. Budak [17] developed a general method for modeling using data extracted from orthogonal cutting experiments. Wan and Zhang [18] used a most practical method to compare cutting force modeling in detail. Recently, Kalla [19] established CFRP general milling cutting force modeling, considering the influence of fiber orientation on the model, and using Artificial Neural Network (ANN) method to determine the cutting coefficient. Karpat [20] simulates the milling force of a one-way CFRP in which the radial and tangential cutting force coefficients are calculated from the fiber cutting angle. In this study, least squares fitting, and other optimization algorithms were used, and relatively accurate cutting force coefficients were obtained to establish an accurate force model [16, 19, 20]. Since CFRP is very nonlinear and non-uniform compared to metals, the effect of fiber orientation on cutting forces cannot be ignored.

Cutting temperature and cutting force are the main factors affecting the surface

quality of carbon fiber reinforced polymer (CFRP). In order to accurately predict the cutting force in CFRP spiral milling, according to the cutting principle of spiral milling, a mechanical cutting force model considering fiber cutting angle is established. Based on the experimental data, the one-way CFRP-based mean method was used to identify the cutting force coefficient and fitted by the response surface method (RSM). The results show that the newly established cutting force coefficient force model can improve the cutting force precision, so that the cutting force in the spiral milling of carbon fiber reinforced polymer can be accurately estimated. In addition, since it is difficult to capture the dynamic response of the temperature measurement system, little research has been done on the cutting temperature. When the temperature exceeds the glass transition temperature of the resin matrix, degradation of the resin occurs on the processed surface or surface layer. In this study, an infrared camera and thermocouple were used to measure the temperature at the entrance to the hole and the position inside the hole. Then, the manufacturing tool - the workpiece thermocouple temperature measuring device was designed and calibrated. The hole cutting temperature is measured to establish the relationship between the cutting parameters and the cutting temperature and cutting force.

4.2 Cutting force modeling analysis

4.2.1 Mechanistic cutting force model

Chip separation during CFRP cutting is a failure rather than a plastic deformation, which should be based on the theory of fracture mechanics. At present, many of the analytical prediction models for composite processing are empirical models or use the same shear plane theory as metals [11]. Among the different predictive modeling techniques used, the mechanical modeling approach is the most robust, simple and effective.

The overall motion of the tool is relatively complex during THM machining. It is important to establish an accurate cutting force model in CFRP spiral milling. The infinite cutting forces (tangential, radial and axial) during spiral milling are shown in

Fig. 4.1, where the tangential force (F_t) points in the opposite direction of the cutting and the radial force (F_r) acts on the cutting center. The axial force (F_a) along the z_b axis.

Considering the kinematics of the tool during the spiral milling process, two coordinate systems are established: the tool coordinate system [$x_t y_t z_t O_t$] and the workpiece coordinate system [$x_b y_b z_b O_b$], as shown in Fig. 4.1. the O_b point is the origin of the workpiece coordinate system, and O_t is the origin of the tool coordinate system.

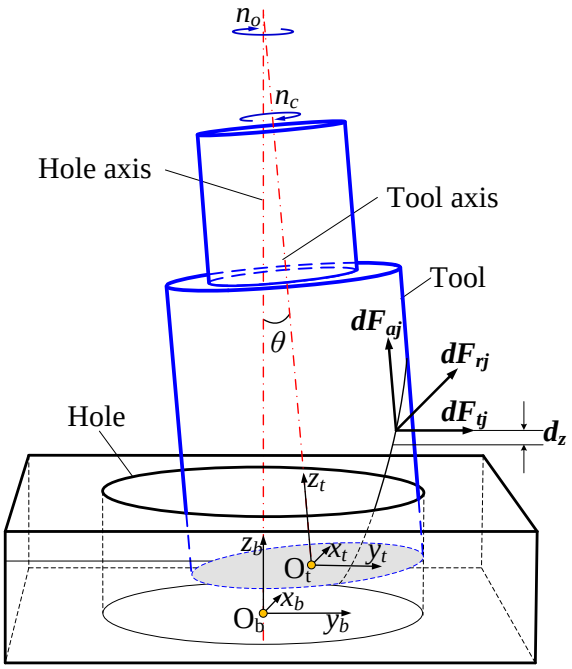

Fig. 4.1 Schematic illustrations of tilted helical milling

In general milling, the cutting force consists of shear force and friction. In view of the brittleness of the carbon fiber composite, powdery chips can be obtained during the cutting process. The chips can be removed at any time during the cutting process and the friction generated during the cutting process is negligible. Therefore, the tangential force acting on the inclined cutting edge of the groove j during the spiral milling process, the radial force and the axial force are given by

In the general milling process, the cutting force consists of cutting force and friction. Considering the brittleness of carbon fiber composites, powdery cuttings can be obtained during the cutting process. The cuttings can be removed at any time during the cutting process, and the frictional forces generated during the cutting process are negligible. Therefore, the tangential, radial and axial forces acting on the inclined

cutting edge of flute j during spiral milling are given by

$$\begin{cases} \mathrm{d}F_{tj}(\varphi,z) = K_{tc}h_j(\varphi,z)\mathrm{d}z + K_{te}\mathrm{d}z \\ \mathrm{d}F_{rj}(\varphi,z) = K_{rc}h_j(\varphi,z)\mathrm{d}z + K_{re}\mathrm{d}z \\ \mathrm{d}F_{aj}(\varphi,z) = K_{ac}h_j(\varphi,z)\mathrm{d}z + K_{ae}\mathrm{d}z \end{cases} \quad (i=1,2...,N;\ j=1,2...,M) \tag{4.1}$$

where K_{tc}, K_{rc}, and K_{ac} are cutting force coefficients aroused by the shearing at the shear zone in tangential, radial, and axial directions caused by side edges, respectively; K_{te}, K_{re}, and K_{ae} are Cutting force coefficients due to rubbing or plowing at the cutting edge; and d_z is the thickness of each element. Instantaneous uncut chip thickness is given by

$$h_j(\varphi,z) = f_t \sin\varphi_j(t) \quad (t=0,1,2,3) \tag{4.2}$$

where f_t represents the tangential feed rate per tooth of the tool center and h_j is the chip thickness of tooth j. Assume that the tool cuts into the workpiece at the angle φ_{st} and cuts out with φ_{ex}, and the angle φ will change from φ_{st} to φ_{ex}.

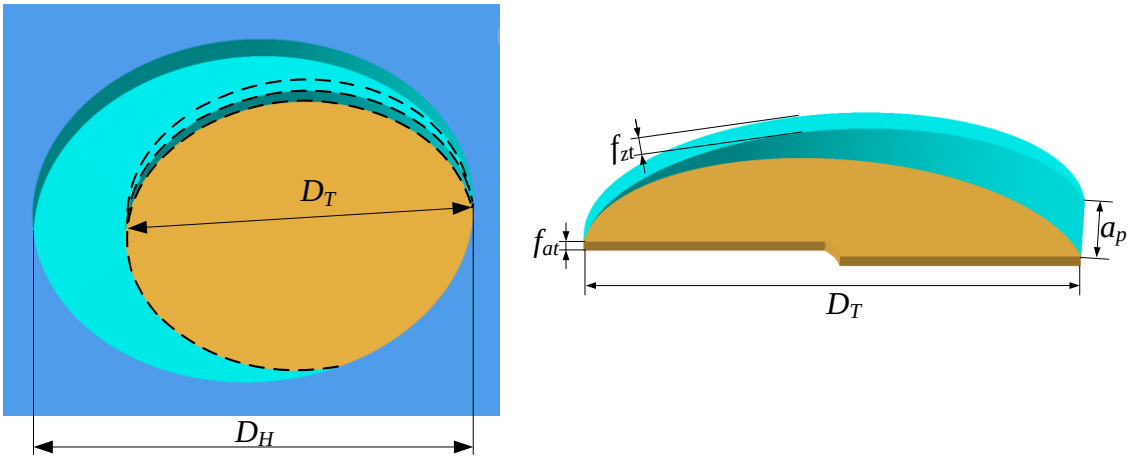

(a) CHM

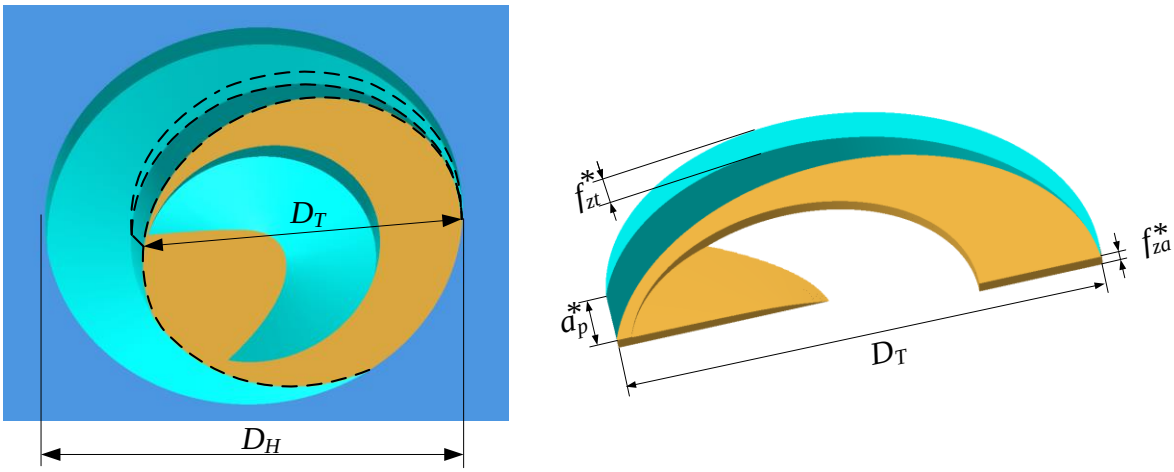

(b) THM

Fig.4.2 Undefromed chip of CHM and THM

As shown in Fig. 4.2, the tool is in the cutting area, and the two angles must be followed condition as

$$\varphi_{st} \le \varphi_j \le \varphi_{ex}, \quad \left(0 \le \varphi_j \le 2\pi\right) \tag{4.3}$$

Due to tool revolution and rotation during helical milling

$$\varphi_j(t) = \varphi_1(t) + (j-1)\cdot 2\pi/N - 2z\tan\beta/D_c \tag{4.4}$$

Due to the influence of the spiral trajectory, the three-dimensional basic cutting force of the side cutting edge in the tool coordinate system $x_tO_ty_t$ needs to be converted into the relationship between the coordinates in the $x_tO_ty_t$ plane and the movement path of the tool according to the revolution and rotation of the tool. Receive the cutting force in the work coordinate system $[x_by_bz_bO_b]$ as follows

$$\begin{bmatrix} dF_{x_b} \\ dF_{y_b} \\ dF_{z_b} \end{bmatrix} = \boldsymbol{R_0R_1R_2R_3R_4} \begin{bmatrix} dF_{tj} \\ dF_{rj} \\ dF_{aj} \end{bmatrix} \tag{4.5}$$

$$\mathbf{R_0} = \begin{bmatrix} \cos\varphi_{i,j,k} & -\sin\varphi_{i,j,k} & 0 \\ \sin\varphi_{i,j,k} & \cos\varphi_{i,j,k} & 0 \\ 0 & 0 & 1 \end{bmatrix} \tag{4.6}$$

$$\mathbf{R_1} = \begin{bmatrix} \cos\gamma & \sin\gamma & 0 \\ -\sin\gamma & \cos\gamma & 0 \\ 0 & 0 & 1 \end{bmatrix} \tag{4.7}$$

$$\mathbf{R_2}=\begin{bmatrix}\cos(-\beta) & \sin(-\beta) & 0\\ -\sin(-\beta) & \cos(-\beta) & 0\\ 0 & 0 & 1\end{bmatrix} \tag{4.8}$$

$$\mathbf{R_3}=\begin{bmatrix}\cos(\theta) & 0 & -\sin(\theta)\\ 0 & 1 & 0\\ \sin(\theta) & 0 & \cos(\theta)\end{bmatrix} \tag{4.9}$$

$$\mathbf{R_4}=\begin{bmatrix}\cos(\beta) & \sin(\beta) & 0\\ -\sin(\beta) & \cos(\beta) & 0\\ 0 & 0 & 1\end{bmatrix} \tag{4.10}$$

Milling of Helical Milling the cutting conditions of the cutting teeth during the cutting cycle can be divided into three phases. In stage I, the cutters did not cut into the workpiece in both machining modes. The micro-element cutting edge was in the idle state. Afterwards, the cutter gradually cut into the workpiece in the phase II range. The axial cutting depth was also gradually increased and the tool was rotated. The maximum value is reached when the lag angle φ_q is exceeded. However, in the conventional helical-blade milling, the cutting teeth are usually fed only in the circumferential direction, so the axial cutting depth of the unformed chips is constant. When the tool is turned into the phase III range, the micro-element cutting edges on the cutting teeth will be all Involved in cutting, and the spiral tool in a cutting cycle, the tool feeds in the tangential direction while also axial feed, so the screw hole tool side edge of the uncut chip axial cutting depth and tool rotation linearly change relationship. After the tool tip cuts the workpiece, the micro-elements of the helical milling tool no longer participate in the cutting.

From the above analysis, it can be seen that when the tool rotates to phase III in the screw hole, only part of the micro-element cutting edge is involved in the cutting. Therefore, when calculating the combined force of the cutting edges of a single tooth, the upper and lower limits of participation in the numerical integration are z_2 and z_1, respectively, ie, the maximum number of effective microelements involved in cutting.

Considering the change in fiber orientation caused by the revolution of the tool, the cutting force change function M(α), where α is the instantaneous fiber cutting angle (the relative angle between the fiber orientation and the cutting direction. The numerical integration and summation of the cutting forces of all the microelement cutting edges

participating in the cutting on the side cutting tool teeth of the cutting tool can obtain the three milling forces x_b, y_b and z_b of the side cutting edge when the cutting tool is at the position of the i-th rotation angle.

$$\begin{cases} \mathrm{F}_{x_b}(\varphi,\beta,\theta)=\mathrm{M}(\alpha)\sum_{i=1}^{N} g(\varphi_i)\left[m_{1,1}(\varphi_j,\beta,\theta)(K_{tc}h_i+K_{te})z+m_{1,1}(\varphi_j,\beta,\theta)(K_{rc}h_i+K_{re})z+m_{1,1}(\varphi_j,\beta,\theta)(K_{ac}h_i+K_{ae})z \right]_{z_1}^{z_2} \\ \mathrm{F}_{y_b}(\varphi,\beta,\theta)=\mathrm{M}(\alpha)\sum_{i=1}^{N} g(\varphi_i)\left[m_{1,1}(\varphi_j,\beta,\theta)(K_{tc}h_i+K_{te})z+m_{1,1}(\varphi_j,\beta,\theta)(K_{rc}h_i+K_{re})z+m_{1,1}(\varphi_j,\beta,\theta)(K_{ac}h_i+K_{ae})z \right]_{z_1}^{z_2} \\ \mathrm{F}_{z_b}(\varphi,\beta,\theta)=\mathrm{M}(\alpha)\sum_{i=1}^{N} g(\varphi_i)\left[m_{1,1}(\varphi_j,\beta,\theta)(K_{tc}h_i+K_{te})z+m_{1,1}(\varphi_j,\beta,\theta)(K_{rc}h_i+K_{re})z+m_{1,1}(\varphi_j,\beta,\theta)(K_{ac}h_i+K_{ae})z \right]_{z_1}^{z_2} \end{cases} \tag{4.11}$$

Since the helical milling process is a combination of drilling and milling, the thrust force is caused by the side edges and the end edge. The edge of the knife edge plays a key role in the axial feed; it is assumed that the F_{ba} is the cutting force generated by the leading edge, which is much larger than the thrust cutting force caused by the side edge of the tool. According to THM kinematics, it is assumed that the axial chip thickness and the bottom edge width are fixed values. Taking into account the influence of the tool inclination angle θ and the part caused by the edge of the tool can be expressed as:

$$F_{ba}=K_{fc}s_a\frac{D_t}{2}+K_{ft}\theta\frac{D_t}{2}+K_{fe}\frac{D_t}{2} \tag{4.12}$$

where K_{fc} is cutting force coefficient aroused by the shearing at the shear zone in tangential, radial, and axial directions caused by side edges, respectively; K_{ft} is correction coefficient by tilt angle θ; K_{fe} is Cutting force coefficient due to rubbing or plowing at the cutting edge; and D_t is the diameter of cutting tool. The thrust force F_z is given by

$$\begin{aligned} &\mathrm{F}_z(\varphi,\beta,\theta)= \\ &\mathrm{M}(\alpha)\sum_{i=1}^{N} g(\varphi_i)\left[m_{3,1}(\varphi_j,\beta,\theta)(K_{tc}h_i+K_{te})z+m_{3,2}(\varphi_j,\beta,\theta)(K_{rc}h_i+K_{re})z+m_{3,3}(\varphi_j,\beta,\theta)(K_{ac}h_i+K_{ae})z \right]_{z_1}^{z_2} \\ &+\left(K_{fc}s_a+K_{ft}\theta+K_{fe}\right)\frac{D_t}{2} \end{aligned} \tag{4.13}$$

The cutting force coefficient in the full factor experiment is calculated by the single

factor mean force method [17]. Table 4.1 lists the determined cutting force coefficients.

Table 4.1 Cutting force coefficients

K_{tc}	K_{rc}	K_{ac}	K_{te}	K_{re}	K_{ae}	K_{fc}	K_{ft}	K_{fe}
4085.96	3762.13	1018.14	7.38	5.58	29.7	8264.19	-1.421	15.579

The effect of fiber orientation on cutting force was fitted based on experimental results. The thrust force model substituted by the cutting force coefficient determined under different cutting parameters using the average cutting force method and the data fitting method. Fitting the thrust force of CHM and THM gives the result as shown in Fig. 4.3. It can be seen that the fitting value of the thrust model perfectly simulates and captures the change of the thrust force, and the fitting error is small.

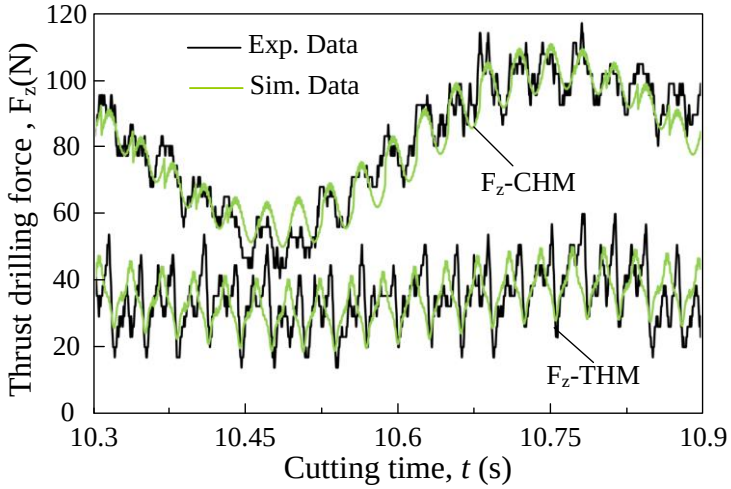

Fig. 4.3 Simulated thrust force using improved model versus original model: spindle speed of 2000 rpm, total cutting time of 24.6s, tool revolution speed of 101 rpm, tilt angle of 0° in CHM and 5° in THM, hole diameter of 12 mm

4.3 Temperature measuring system

4.3.1 Temperature at the entrance side of hole

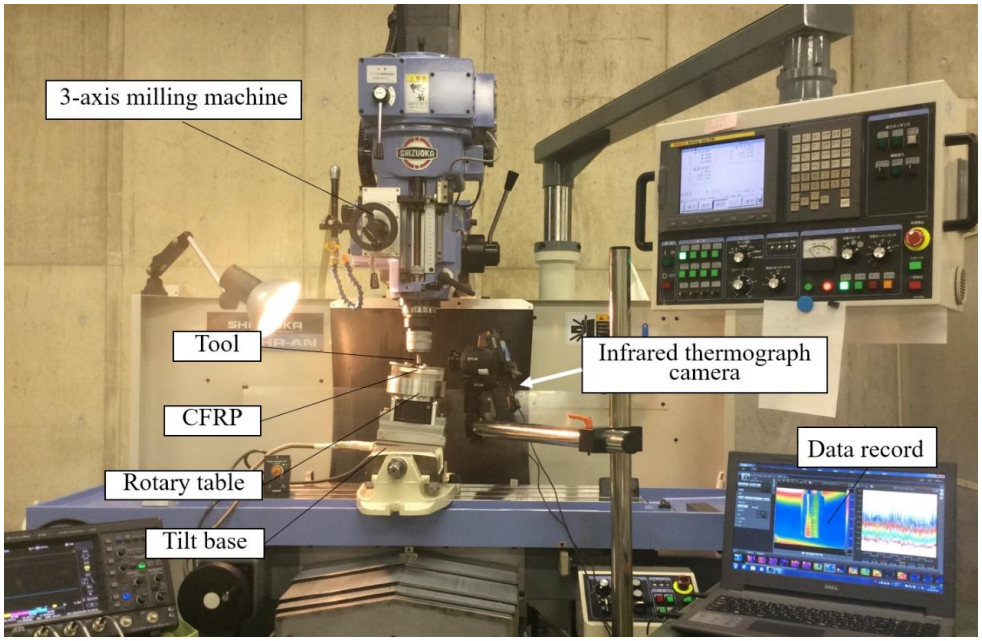

Fig. 4.4 Temperature measurement by infrared thermograph camera

First, the thermal imager was used to measure the cutting temperature variations of the CHM and THM entrances, respectively, and compared. The temperature measuring device is shown in Fig. 4.4. The temperature distribution at some point in the measurement process is shown in Fig. 4.5.

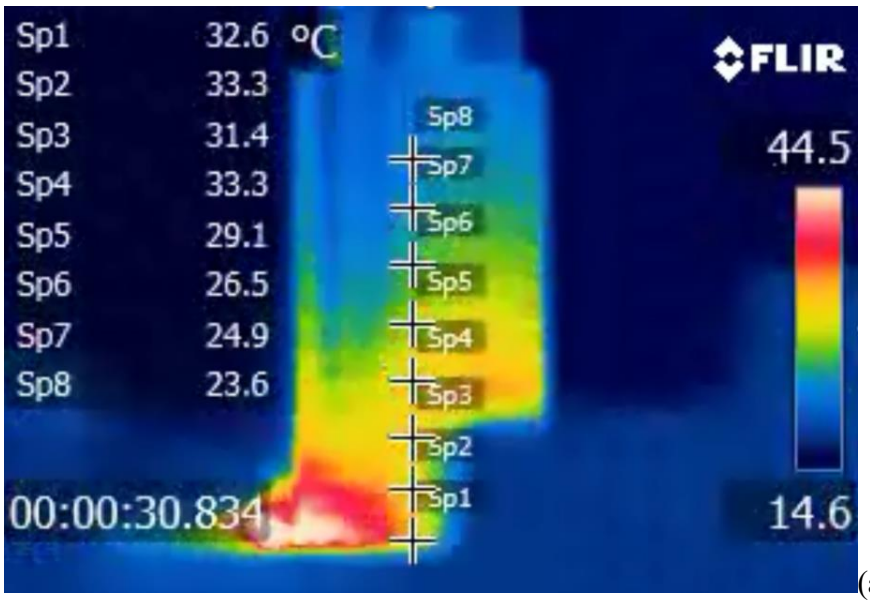

(a) CHM

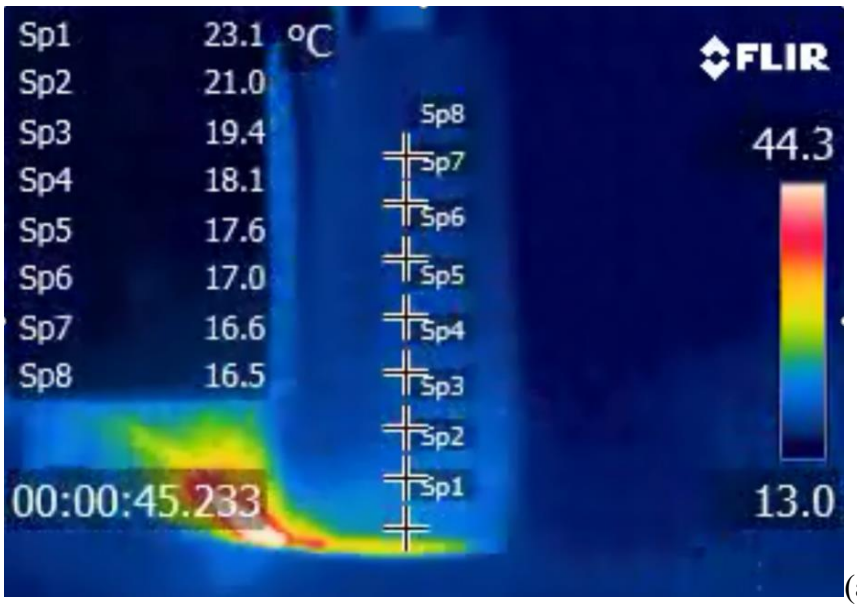

(a) THM

Fig. 4.5 The temperature distribution at some point in the measurement process: spindle speed of 2000 rpm, total cutting time of 24.6s, tool revolution speed of 101 rpm, tilt angle of 0° in CHM and 5° in THM, hole diameter of 12 mm.

As can be seen from Fig. 4.5, the surface temperature of the CHM tool is significantly higher than the THM during the inlet machining process. During the inlet process, the maximum temperatures of CHM and THM are 65°C and 53°C, respectively. This shows that in the THM inlet process, the heat dissipation capability is better than CHM.

4.3.2 Temperature at the hole surface

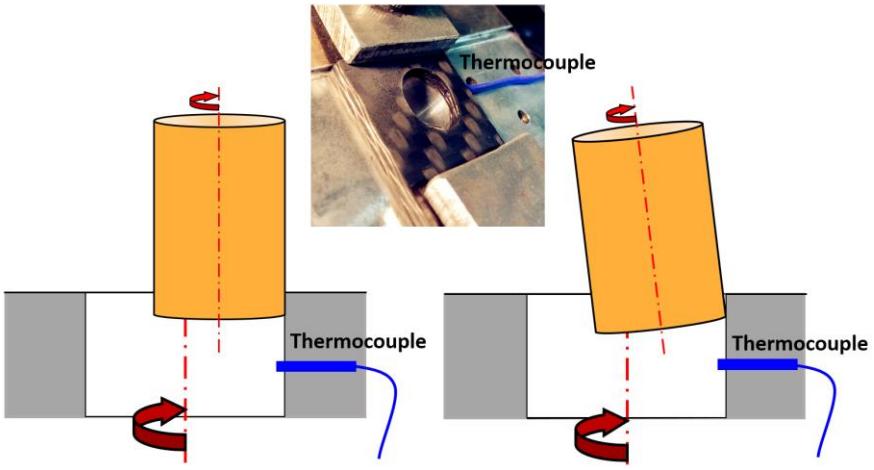

Fig. 4.6 Temperature measurement by K-type thermocouple

In order to obtain the internal processing temperature of the hole, measuring with a K-type thermocouple is the most common method. As shown in Fig. 4.6, the thermocouple is embedded in the workpiece before the hole is machined. When the tool is machining a hole, it will be in contact with the thermocouple and a short section of thermocouple material may be cut off. For ease of comparison, the relative positions of the holes buried in CHM and THM remain the same. The measurement results are shown in Fig. 4.7.

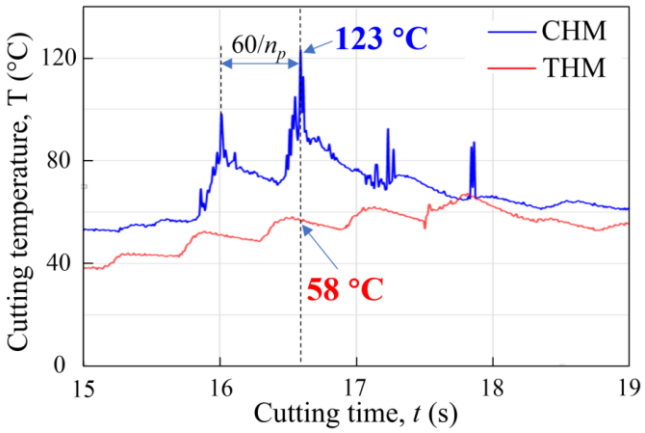

Fig. 4.7 The temperature distribution at some point at the hole surface: spindle speed of 2000 rpm, total cutting time of 24.6s, tool revolution speed of 101 rpm, tilt angle of 0° in CHM and 5° in THM, hole diameter of 12 mm.

As can be seen from Fig. 4.7, the temperature in CHM is much higher than THM, the highest temperature in CHM is 123°C, and the THM temperature in the same position is 58°C.

4.3.3 Temperature at the cutting point during the drilling process

The data fluctuation period in Fig. 4.7 is just one cycle of tool rotation. This indicates that the tool has been in contact with the thermocouple once after one revolution. This measurement method has some drawbacks. For example, the measured temperature is the temperature at which the tool cuts the CFRP material and the thermocouple material. In addition, due to the anisotropy of CFRP, the cutting simulation analysis of section 4.2.2 shows that the magnitude of cutting force fluctuates

greatly with the frequency of revolution of the tool. Therefore, in order to accurately obtain the cutting temperature change and the maximum cutting temperature in the CFRP cutting process. The real-time measurement of the changing temperature in the cutting process is required. The Tool-workpiece thermocouple temperature measurement can meet this demand. Therefore, this work designed and manufactured a tool-workpiece thermocouple temperature measuring device as shown in Fig. 4.8.

Fig. 4.8 (a) shows the schematic of the temperature measurement. The surrounding insulating material is thin Constantan embedded in CFRP parts. When the insulating material is opened, a hot junction is generated. Based on the Seebeck effect, thermo-electromotive force is generated at the same time. The output voltage signal is amplified and sent to the data acquisition device. Finally, the temperature during the milling process can be recorded by data acquisition/analysis software.

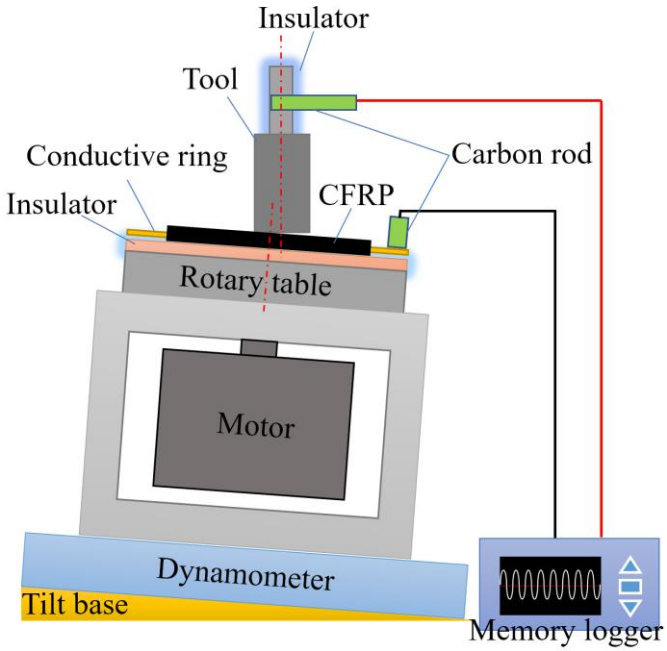

(a) Illustration

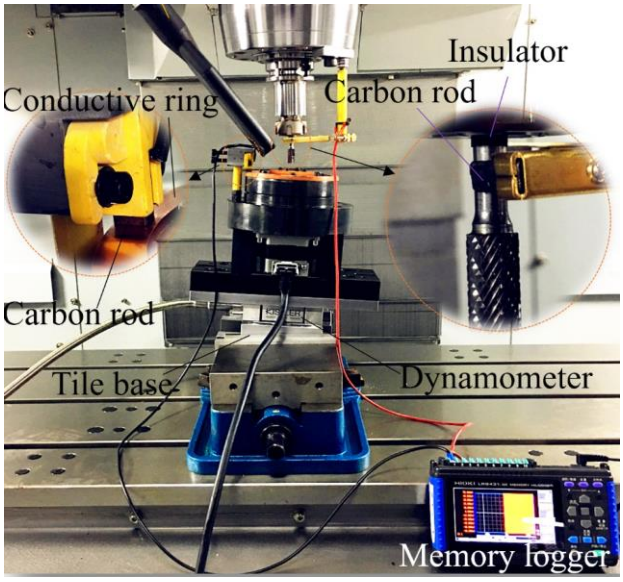

(b) A picture

Fig. 4.8 Tool-workpiece thermocouple temperature system

Due to the tool-workpiece non-standard thermocouple, the correspondence between the thermo-electromotive force and the temperature must be in the tool-workpiece thermocouple. Therefore, as shown in Fig. 4.9, the CFRP and the tool are placed together in a heating table for heating. A K-type thermocouple is placed on the tool and the CFRP contact area to measure the temperature change. The tool and CFRP are connected to the loop circuit and the data recorder is used to collect the thermo-electromotive force changes in the CFRP and tool loops. Use the thermo-electromotive force change corresponding to the temperature data to draw as Fig. 4.10.

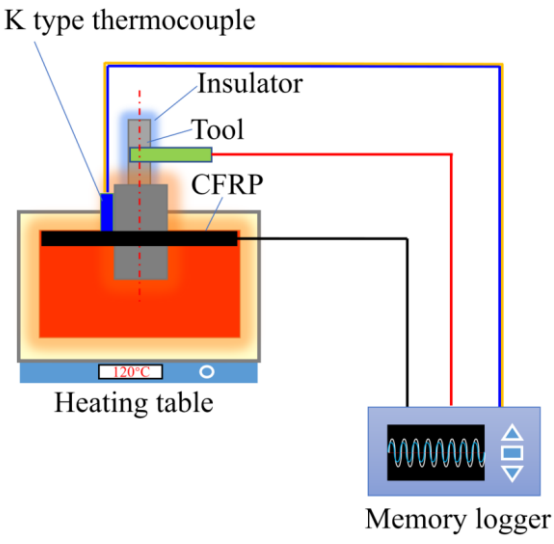

Fig. 4.9 Calibration method of tool-workpiece thermocouple

Fig. 4.10 shows the relationship between thermo-electromotive force and temperature for a calibrated tool-workpiece thermocouple. It can be approximated by a linear fitting and expressed by the following Eq. (4.2).

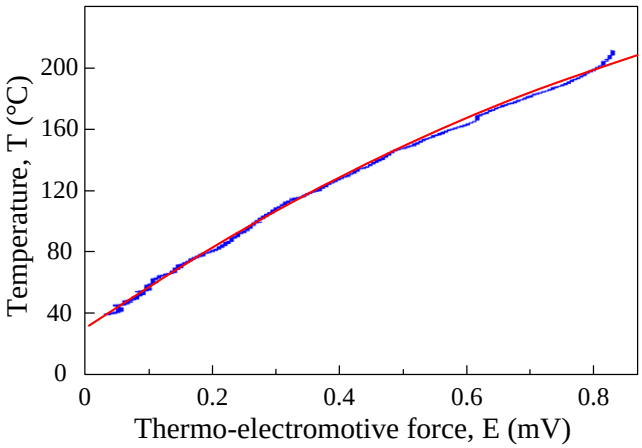

Fig. 4.10 Calibration of tool-workpiece thermocouple

$$T = -73.91E^2 + 233.2E + 31.2 \quad (4.2)$$

The tool-workpiece thermocouple method was used to measure the cutting temperature during CHM and THM processing, respectively, and the obtained data is shown in Figure 4.11. During the machining process, the cutting temperatures for CHM and THM were 117°C and 72°C, respectively, at a time comparable to the thermocouple measurement position in section 4.3.2. This is similar to the temperature measured by the thermocouple in section 4.3.2. In addition, as can be seen from the figure, similar to the axial cutting force data, the cutting temperature in the cutting process fluctuates greatly with the frequency of the tool revolution, the CHM fluctuation amplitude is approximately 40°C, and the THM fluctuation amplitude is approximately 20. °C.

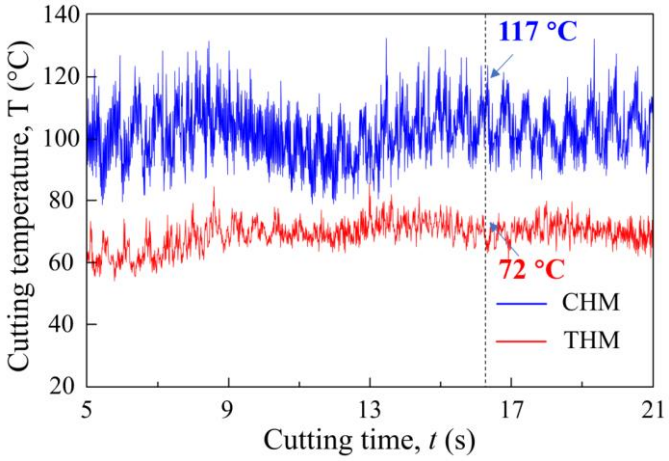

Fig. 4.11 The cutting temperature in the CHM and THM processes: spindle speed of 2000 rpm, total cutting time of 24.6s, tool revolution speed of 101 rpm, tilt angle of 0° in CHM and 5° in THM, hole diameter of 12 mm.

4.3.4 Glass transition temperature

The glass transition is the transition between rubber and glass states. When the temperature exceeds the thermal weight of the carbon fiber composite, degradation of the resin occurs. It may cause defects and reduce the strength of the workpiece. On the dilatometer basis, Tg is at the turning point of the thermal expansion curve. In this study, Tg was measured using the Dynamic Mechanical Analysis method. The measurement setup is shown in Fig. 4.12(a) and the measured data is shown in Fig. 4.12(b). Finally, the TG obtained by carbon fiber is 132.6°C.

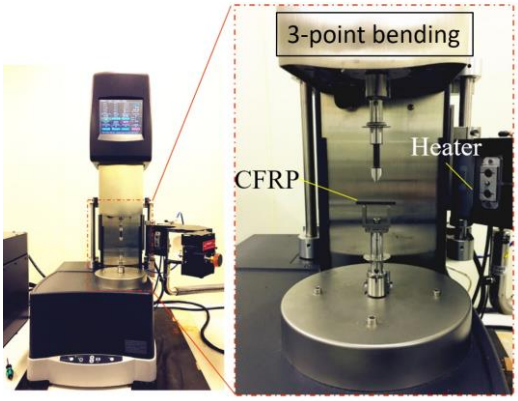

(a) Dynamic Mechanical Analysis (DMA)

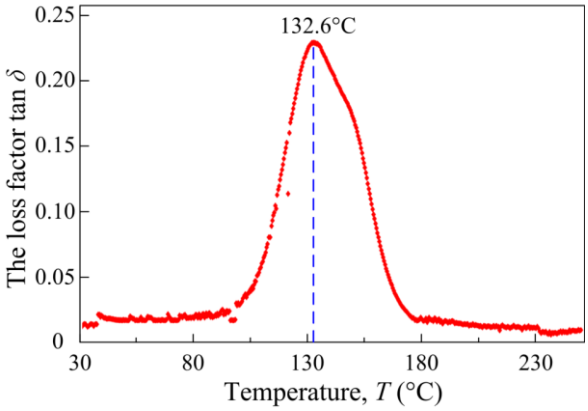

(b) Glass transition temperature

Fig. 4.12 Glass transition temperature measurement

4.4 Influence factors of cutting force and temperature

When the cutting temperature exceeds the glass transition temperature (Tg), the matrix cannot provide sufficient support for the fiber and the composite material has poor processing quality. Therefore, it is significant to study the influence of different processing parameters on the cutting force and cutting temperature to select the optimal parameters. Fig. 4.13 shows the influence of tilt angle θ, cutting speed v_c, axial feed speed v_f, and eccentricity e on thrust force and cutting temperature, respectively. Among them, the thrust force and the cutting temperature decrease rapidly with increasing inclination angle (see Fig. 4.13 (a)). The influence of cutting speed on the thrust force and cutting temperature of CHM and THM is similar, the thrust force slowly decreases with increasing axial feed speed, and the cutting temperature increases slowly with increasing cutting speed (see Fig. 4.13 (a)). The axial feed speed has little effect on the cutting temperature and the axial cutting force in the THM, but in the CHM, the thrust force and the cutting temperature increase rapidly as the axial feed speed increases. In addition, eccentricity has little effect on the thrust force and cutting temperature of CHM and THM. The results show that the tilt angle is a key parameter that affects the thrust force and cutting temperature. High cutting speed can obtain lower thrust force but higher cutting temperature. The feed rate in the CHM is a key parameter affecting the thrust force and cutting temperature, and then the influence in the THM is smaller, which means that THM is more suitable for high efficiency machining than CHM. In

addition, in CHM and THM, eccentricity has less influence on thrust force and cutting temperature. The above results can be used as a reference for future optimal parameter selection.

$$s=H+D_t\sin\theta+v_f/n_o \tag{4.3}$$

$$T_o=s/v_f \tag{4.4}$$

$$v_c=\pi n_T D_t \tag{4.5}$$

$$D_H=2e+D_t\cos\theta \tag{4.6}$$

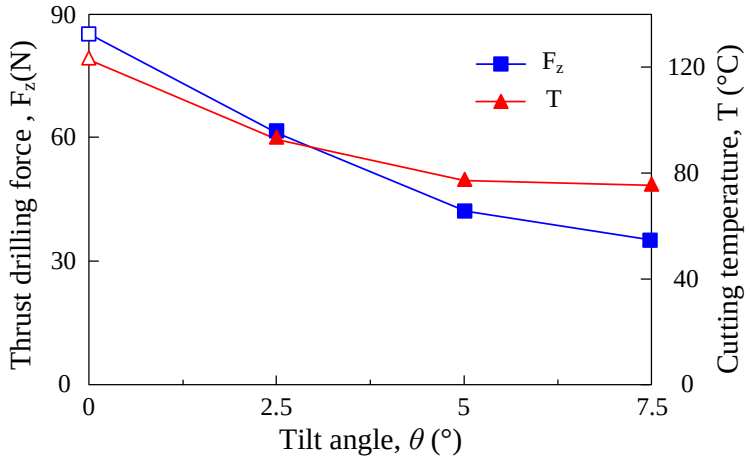

(a) Effect of θ on F_z and T: spindle speed of 2000 rpm, total cutting time of 24.6s, tool revolution speed of 101 rpm, hole diameter of 12 mm.

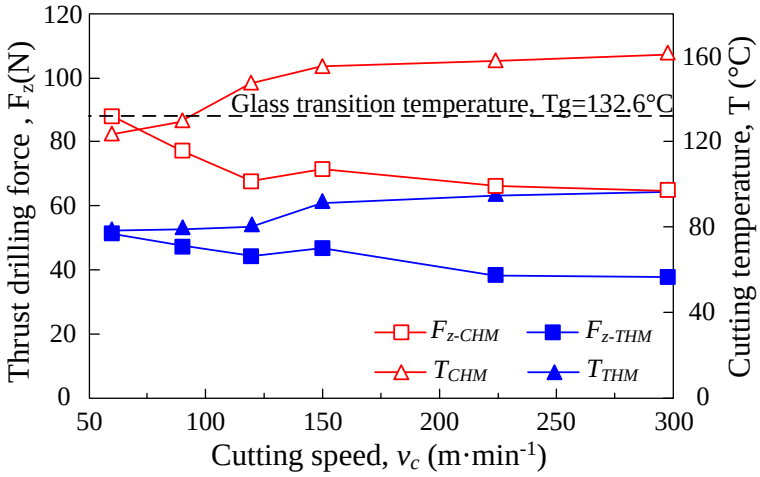

(b) Effect of v_c on F_z and T: total cutting time of 24.6s, tool revolution speed of 101 rpm, tilt

angle of 0° in CHM and 5° in THM, hole diameter of 12 mm.

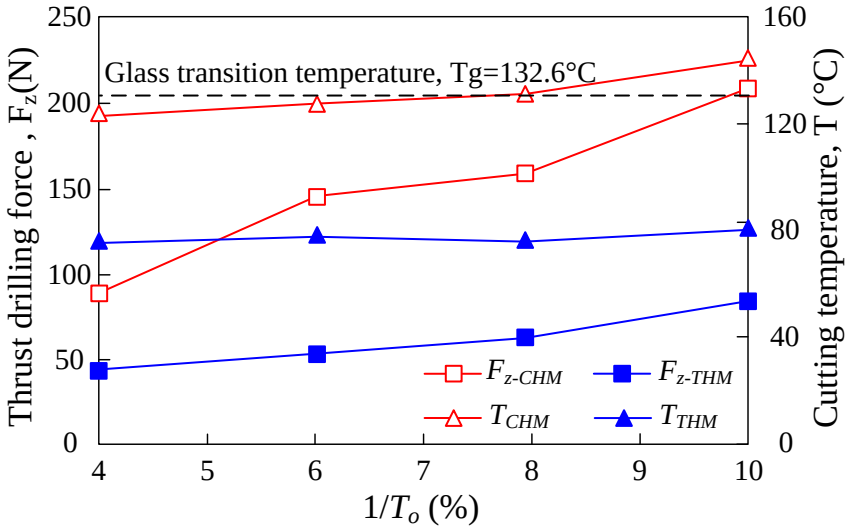

(c) Effect of axial feed speed v_f on F_z and T: spindle speed of 2000 rpm, tool revolution speed of 101 rpm, tilt angle of 0° in CHM and 5° in THM, hole diameter of 12 mm. $s=H+D_t\sin\theta+v_f/n_o$, $T_o=s/v_f$

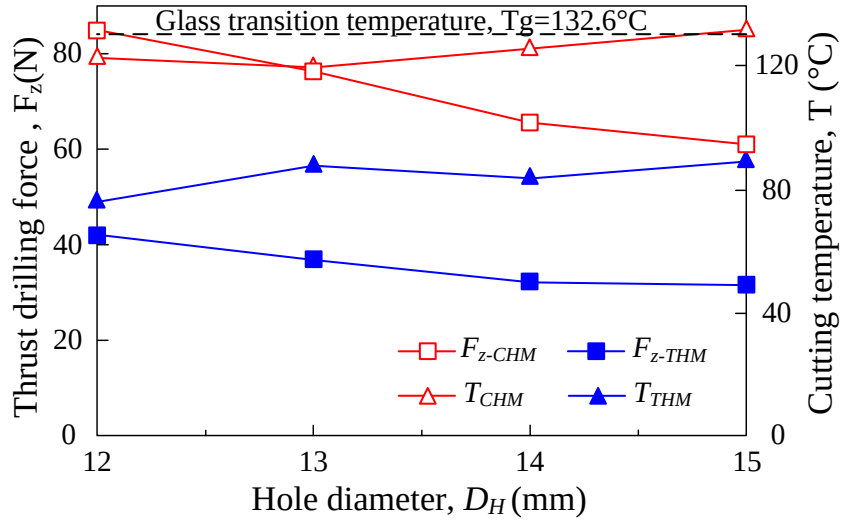

(d) Effect of eccentricity e on F_z and T: spindle speed of 2000 rpm, total cutting time of 24.6s, tilt angle of 0° in CHM and 5° in THM, tool revolution speed of 101 rpm.

$$D_H=2e+D_t\cos\theta$$

Fig. 4.13 The influence of tilt angle θ, cutting speed v_c, axial feed speed v_f, and eccentricity e on thrust force and cutting temperature

4.5 Summary

Both cutting force and cutting temperature can produce a significant effect on the CFRP processing quality. Therefore, this paper established a mechanical model about the cutting force of THM to study the factors performing on the cutting force. A string of plans was adopted to measure the cutting temperature during THM processing, and the effects of cutting force and cutting temperature were analyzed in different machining conditions. Some conclusions can be drawn as following:

(1) The fitting value of the Mechanistic cutting force model perfectly simulates and captures the change of the thrust force, and the fitting error is small.

(2) Compared with Conventional Helical Milling (CHM), Thrust force in Tilted Helical Milling (THM) is reduced by ~ 50% and cutting temperature is reduced by ~ 45%.

(3) The tilt angle is a key parameter that affects thrust force and cutting temperature.

(4) The axial feed speed in CHM is a key parameter affecting thrust force and cutting temperature, but then the influence in THM is smaller. Its means that THM can be applied to higher efficiency drilling.

References

[1] Silva D, Pamies Teixeira J, Machado C (2014) Methodology analysis for evaluation of drilling-induced damage in composites. Int J Adv Manuf Technol 71(9–12):1919–1928. doi:10.1007/s00170-014-5616-y.

[2] Qi Z, Zhang K, Cheng H, Wang D, Meng Q (2015) Microscopic mechanism based force prediction in orthogonal cutting of unidirectional CFRP. Int J Adv Manuf Technol :1–11. doi:10.1007/s00170-015-6895-7.

[3] Pecat O, Rentsch R, Brinksmeier E (2012) Influence of milling process parameters on the surface integrity of CFRP. Procedia CIRP 1:466–470.

[4] Hintze W, Hartmann D (2013) Modeling of delamination during milling of unidirectional CFRP. Procedia CIRP 8:444–449.

[5] Chibane H, Morandeau A, Serra R, Bouchou A, Leroy R (2013) Optimal milling conditions for carbon/epoxy composite material using damage and vibration analysis. Int J Adv Manuf Technol 68(5–8):1111–1121.

[6] Yashiro T, Ogawa T, Sasahara H (2013) Temperature measurement of cutting tool and machined surface layer in milling of CFRP. Int J Mach Tools Manuf 70:63–69.

[7] Azmi AI, Lin RJT, Bhattacharyya D (2013) Machinability study of glass fibre-reinforced polymer composites during end milling. Int J Adv Manuf Technol 64(1–4):247–261.

[8] Phadnis VA, Makhdum F, Roy A, Silberschmidt VV (2013) Drilling in carbon/epoxy composites: experimental investigations and finite element implementation. Compos A: Appl Sci Manuf 47:41–51.

[9] Madhavan V, Lipczynski G, Lane B, Whitenton E (2014) Fiber orientation angle effects in machining of unidirectional CFRP laminated composites. J Manuf Process (0).

[10] Sasahara H, Kikuma T, Koyasu R, Yao Y (2014) Surface grinding of carbon fiber reinforced plastic (CFRP) with an internal coolant supplied through grinding wheel. Precis Eng 38(4):775–782.

[11] Haddad M, Zitoune R, Eyma F, Castanie B (2014) Study of the surface defects and dust generated during trimming of CFRP: influence of tool geometry,

machining parameters and cutting speed range. Compos A: Appl Sci Manuf 66:142–154.

[12] Zenia S, Ben Ayed L, Nouari M, Delamézière A (2014) Numerical analysis of the interaction between the cutting forces, induced cutting damage, and machining parameters of CFRP composites. Int J Adv Manuf Technol :1–16.

[13] Chatterjee A (2009) Thermal degradation analysis of thermoset resins. J Appl Polym Sci 114(3):1417–1425.

[14] Sun Y, Sun J, Li J, Xiong Q (2014) An experimental investigation of the influence of cutting parameters on cutting temperature in milling Ti6Al4V by applying semi-artificial thermocouple. Int J Adv Manuf Technol 70(5–8):765–773.

[15] Lazar MB, Xirouchakis P (2013) Mechanical load distribution along the main cutting edges in drilling. J Mater Process Tech 213(2):245–260

[16] Wang HY, Qin XD, Li H, Ren CZ (2013) Analysis of cutting forces in helical milling of carbon fiber-reinforced plastic. P I Mech Eng B-J Eng 227(1):62–74

[17] Budak E, Altintas Y, Armarego EJA (1996) Prediction of milling force coefficients from orthogonal cutting data. J Manuf Sci E-T ASME 118:216–224

[18] Wan M, Zhang WH, Qin GH, Tan G (2007) Efficient calibration of instantaneous cutting force coefficients and runout parameters for general end mills. Int J Mach Tool Manuf 47:1767–1776.

[19] Kalla D, Ahmad JS, Twomey J (2010) Prediction of cutting forces in helical end milling fiber reinforced polymers. Int J Mach Tool Manuf 50:882–891

[20] Karpat Y, Bahtiyar O, Deger B (2012) Mechanistic force modeling for milling of unidirectional carbon fiber reinforced polymer laminates. Int J Mach Tool Manuf 56:79–93

Chapter V
Hole edge/surface finish of Tilted Helical Milling

5.1 Introduction

Carbon fiber reinforced plastic (CFRP) is widely used in aerospace, defense industry and other fields because of its high specific strength, high specific modulus and good corrosion resistance [1-2]. With the continuous development of aviation, aerospace and military equipment technology, the requirement for the CFRP components is becoming increasingly stringent. Depending upon application, a large number of holes are often created on the CFRP components in order to match with other components [3-4]. The accuracy and surface finish of holes in CFRP structural components are the most critical factors affecting their service performance, reliability and service life [5]. However, CFRP is a multiphase structure composed of carbon fiber and matrix, with non-uniform, anisotropic, high hardness characteristics, so conventional drilling operation is prone to creating entrance split, exit delamination, and poor hole surface finish. The assembly accuracy and the load bearing capacity of the joint as well as the fatigue life of CFRP structure can be greatly influenced by these damages, even disable the components in some serious cases [6-7].

In order to find a CFRP drilling technology featured by low cost, high quality, and high efficiency, many researchers have studied the CFRP cutting mechanism through experiments and simulations. At present, the conventional helical milling (CHM) has become an alternative method for conventional drilling and has been widely used in CFRP processing [8-9]. In CHM, the cutting tool performs a helical feed motion which is different from drilling holes, the material near the center of the hole is removed by cutting instead of being squeezed, and generating low thrust forces [10]. Adjusting the helical diameter of tool path can obtain holes with different diameters by using only one cutting tool [11-12], and it can also possibly calibrate the hole size and geometric

errors caused by tool wear by a slight change in the helical diameter [13]. Besides, the diameter of the cutting tool in CHM is smaller than that of the hole, so there is a gap between the tool and the hole wall. This gap is conducive to the timely discharge of chips and reducing cutting temperature [9-10]. Therefore, CHM does have many advantages over conventional drilling methods in terms of hole drilling accuracy, costs and efficiency. However, there still exist several shortcomings in CHM. At the exit side of the hole, an abrupt cutting force from bottom cutting edge of the tool pushes material to the hole exit, causing frequent formation of delamination at the hole exit. Moreover, the chisel edge issue in CHM, i.e., the existence of zero cutting speed point, not only exacerbates tool wear, but also causes the delamination at the edges of CFRP holes. In addition, a large amount of fiber bending and fiber-matrix debinding may happen in the CHM, which induces a large number of burrs and poor hole surface finish [14].

An improved CHM method, namely tilted helical milling (THM), was proposed by authors in previous works [15-16]. In THM, the problems of the hole exit side and the zero-cutting speed point are partially overcome since cutting tool axis is always tilted against the hole with the tilt angle, θ, due to conical pendulum motion [16]. In addition, the scraggly hole surface can be mitigated in THM owing to a downward cutting force component along the hole axis acting on the fibers during cutting process, which makes the fiber easily fracture. The fiber cutting process gets steady and gives rise to a smooth surface of holes. In this article, the formation of hole damage is analyzed theoretically and experimentally so that the THM drilling mechanism can be clarified. The principle of THM is briefly introduced in comparison with CHM. The fiber fracture behavior was theoretically analyzed in the hole drilling at different θ. Drilling experiments were also carried out verify theoretical analysis.

5.2 Appearance of hole edge

Appearance of hole edge. The observations of the hole entrances and exits obtained in CHM and THM were conducted and typical results are as shown in Fig. 15 and Fig. 16, respectively. Evidently, in CHM, a significant quantity of burrs and chippings occurred. In contrast, burrs and chippings in THM were rarely found at both the entrance and exit

of the hole. These results indicate that the hole quality in THM was considerably better than that in CHM, owing to the small thrust drilling force, especially the gradual increase and decrease in the thrust drilling force at the hole entrance and exit in THM, rather than the large force and sharp increase and decrease in force in CHM.

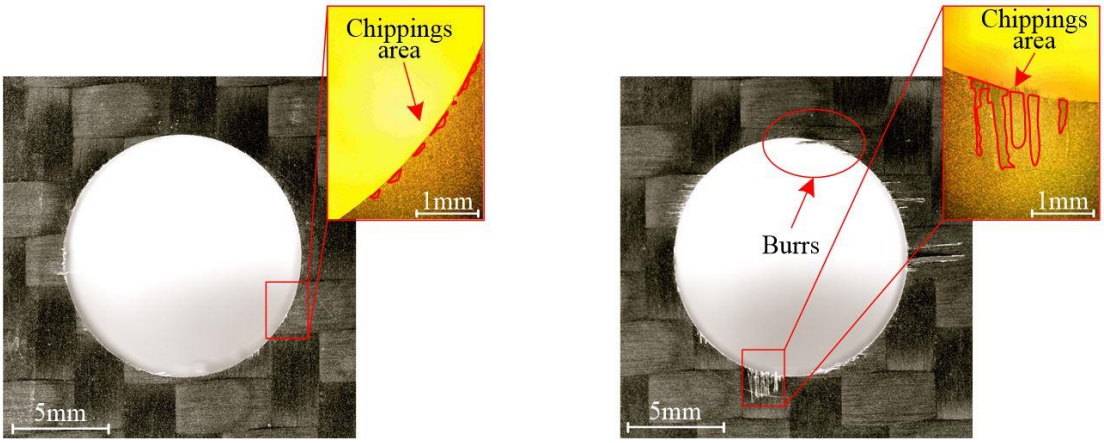

(a) Entrance side (b) Exit side

Fig. 5.1 Optical images of entrance (a) and exit (b) sides of a typical hole obtained by CHM

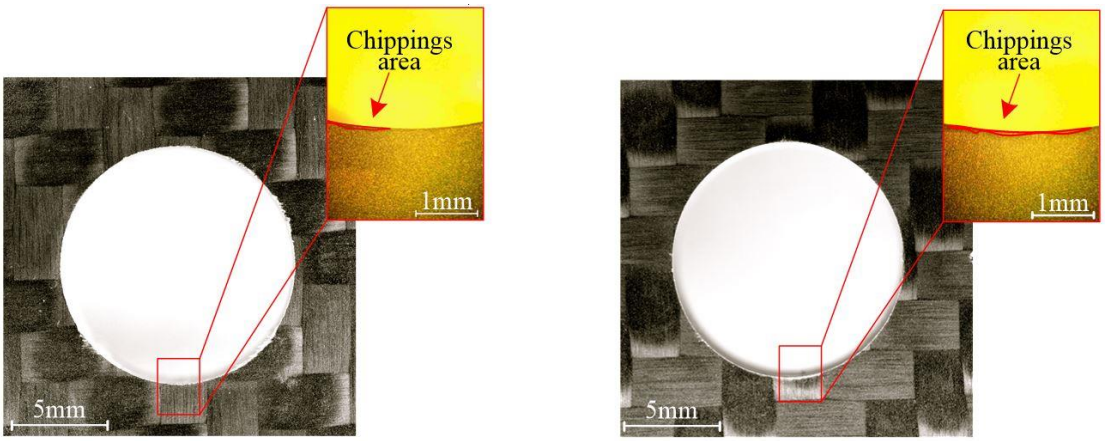

(a) Entrance side (b) Exit side

Fig. 5.2 Optical images of (a) entrance and (b) exit sides of a typical hole obtained by THM

Due to the brittleness of the composite and poor interlayer adhesion, various damages may occur during the drilling process. The degree of burr, spalling and delamination of appearance of hole edge represents the drilling quality. For evaluating the hole quality, the evaluation methods for these three defects are as follows:

Burrs factor. After drilling the CFRP, many of the fibers may not be cut and still join the surface of the hole. These residual fibers are called burrs. They are usually parallel to the fiber direction. Burr damage can affect the assembly accuracy of the composite. Therefore, the degree of influence of the burr damage of the hole outlet on the quality of the hole can be expressed by the burr damage factor F_b:

$$F_b = \frac{\sum_{i=1}^{n} A_{bi}}{A_h} \tag{1}$$

where $\sum_{i=1}^{n} A_{bi}$ is the accumulation of the burr area, the A_h is hole area (see Fig.5.3(a)).

Chippings factor. The calculation of the area of the tear area can be used to evaluate the degree of damage at the edge of the hole, the Chipping factor F_c was introduced which is defined as in Eq. (2).

$$F_c = \frac{\sum_{i=1}^{n} A_{ci}}{A_h} \tag{2}$$

where $\sum_{i=1}^{n} A_{ci}$ is the accumulation of the chippings area (see Fig.5.3(b)).

Delamination. the delamination factor F_d was introduced which is defined as in Eq.(3).

$$F_d = \frac{D_m^2 - D_h^2}{D_h^2} \tag{3}$$

where D_m is the maximum diameter of the damaged zone and D_h is the ideal diameter of the hole (Fig.5.3(c))

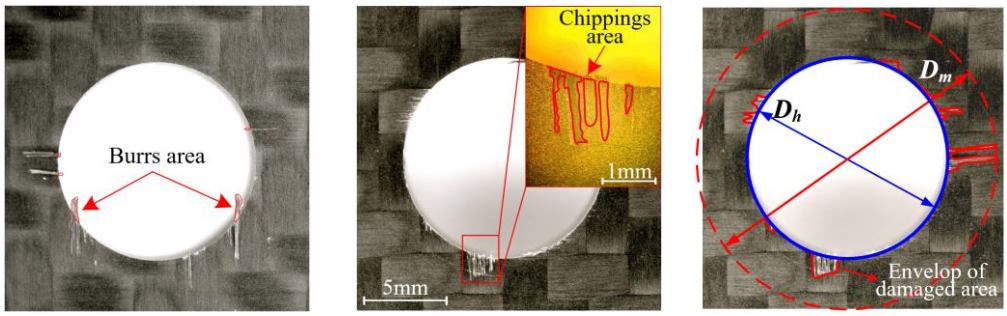

(a) Burrs area (b) Chippings area (c) Delamination

Fig. 5.3 Schematic of hole damage factor

For comprehensively characterize the hole quality, damages of burr, spalling and delamination are considered as a unity. The comparing factor relates the different damages. By setting the influence coefficient, the three factors are combined into one factor, the damage factor of hole edge F_h:

$$F_h = k_b F_b + k_c F_c + k_d F_d \tag{4}$$

where k_b, k_c, and k_d are the influence coefficients of F_b, F_c and F_d, respectively. According to the degree of influence of each defect on the quality of the hole edge, the value of k_b, k_c, and k_d are set to 1, 1.5 and 2.5, respectively [17].

Fig. 5.4 shows the influence of different tool geometry and number of blade on hole quality. The result is that the hole quality of the flat endmill tool is better than that of the ball endmill tool, and the more number of blade, the better the hole quality. Therefore, the flat endmill tool (see Fig.3.9) is used to study the influence of different processing parameters on the damage factor of hole edge F_h to select the optimal parameters. Fig. 5.5 shows the influence of tilt angle θ, cutting speed v_c, axial feed speed v_f, and eccentricity e on thrust force and cutting temperature, respectively. At a tilt angle of 5.0°, the F_h of hole exit side was reduced by 29.5% compared to the CHM values (measured at a tilt angle of 0°). This reduction may be attributable to the small thrust force and the tool attitude. At different tilt angles (θ=2.5°, 5.0°, 7.5°) in THM, the F_h was nearly in the same level (Fig. 5.4 (a)). In addition, in THM at θ = 5°, the F_h was reduced by 18.2% to 29.5% compared to that in CHM (θ = 0°) at different cutting speeds (Fig. 5.4 (b)), whilst the F_a keeps almost unchanged at different v_c in THM. The results show that the THM ($\theta > 0°$) is effective in reducing hole damage.

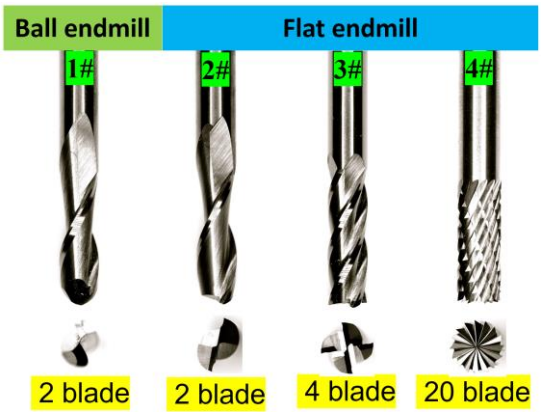

(a) Picture of the cutting tool

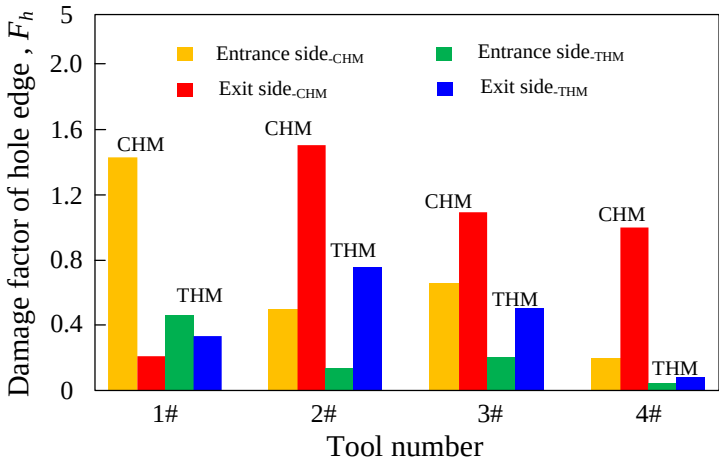

(b) Effect of tool geometry and number of blade on F_h: tool materials of cemented carbide, tool diameter 6mm, total cutting time of 24.6s, tool revolution speed of 101 rpm, tilt angle of 0° in CHM and 5° in THM, hole diameter of 8 mm.

Fig.5.4 Influence of different tool geometry and number of blade on hole quality

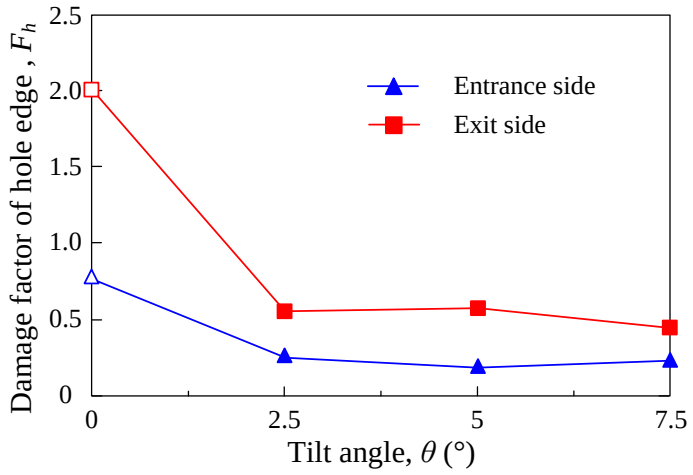

(a) Effect of θ on F_h: spindle speed of 2000 rpm, total cutting time of 24.6s, tool revolution speed of 101 rpm, hole diameter of 12 mm.

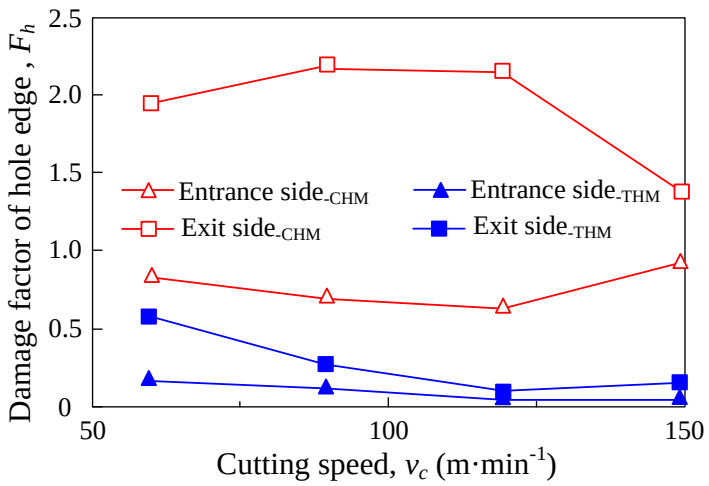

(b) Effect of v_c on F_z and T: total cutting time of 24.6s, tool revolution speed of 101 rpm, tilt angle of 0° in CHM and 5° in THM, hole diameter of 12 mm.

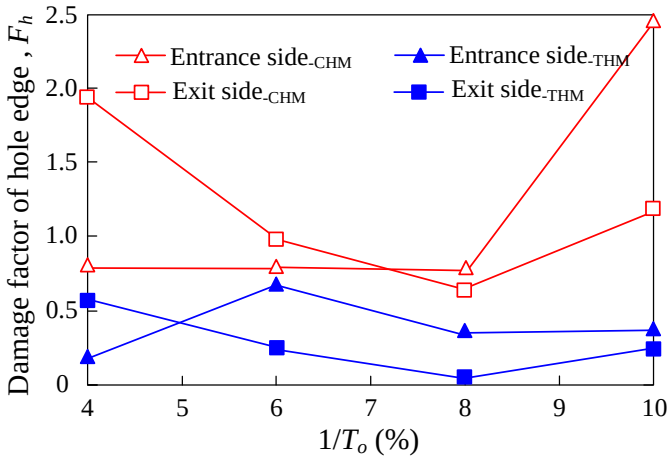

(c) Effect of axial feed speed v_f on F_z and T: spindle speed of 2000 rpm, tool revolution speed of 101 rpm, tilt angle of 0° in CHM and 5° in THM, hole diameter of 12 mm.

$s=H+D_t\sin\theta+v_f/n_o$, $T_o=s/v_f$

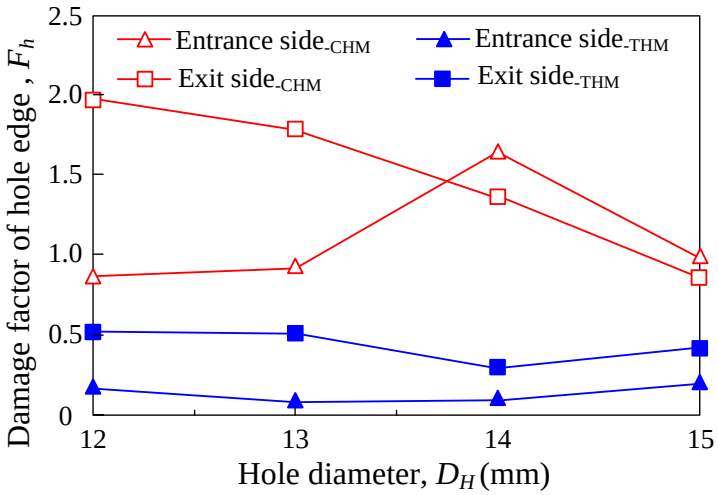

(d) Effect of eccentricity e on F_z and T: spindle speed of 2000 rpm, total cutting time of 24.6s, tilt angle of 0° in CHM and 5° in THM, tool revolution speed of 101 rpm.

$$D_H = 2e + D_t \cos\theta$$

Fig. 5.5 The influence of tilt angle θ, cutting speed v_c, axial feed speed v_f, and eccentricity e on the damage factor of hole edge F_h

5.3 Hole surface finish

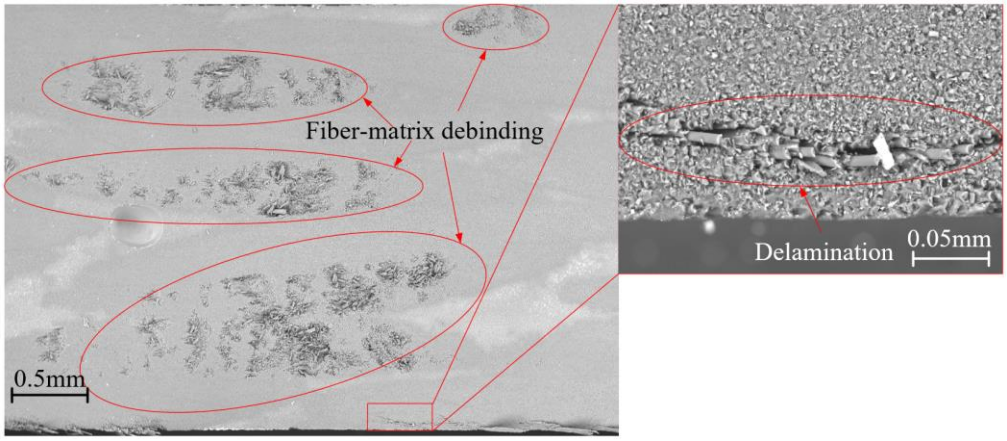

(a) CHM

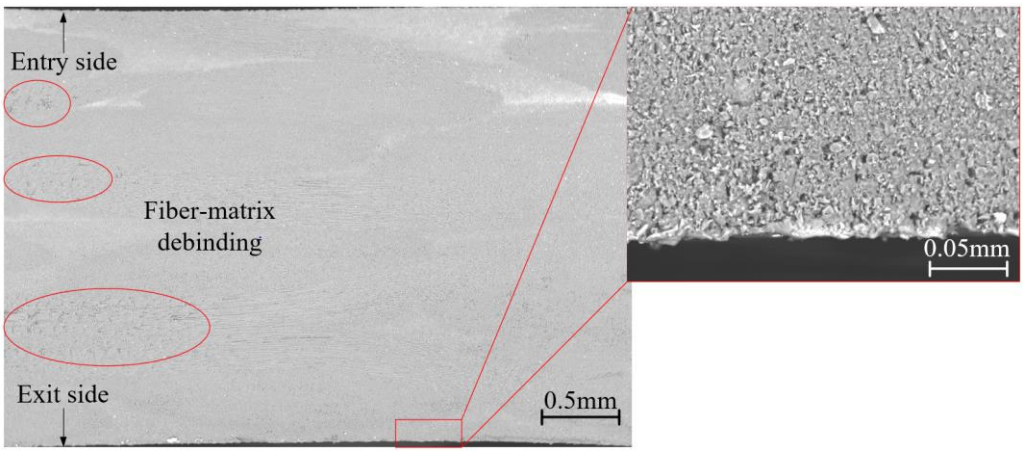

(b) THM

Fig. 5.6 The photos of hole surface topography of CHM (a) and THM (b) by SEM

The damage on hole surface was investigated by SEM observation. Fig. 5.6 show images of a typical hole wall by CHM and THM. Evidently, in CHM, a significant quantity of surface defects occurred. In contrast, surface defects in THM were rarely

found at hole surface. These results indicate that the hole surface quality in THM was considerably better than that in CHM.

Also, the form accuracy of the holes by CHM and THM were investigated by measuring the longitudinal profile of holes along the direction parallel to the hole axis. Fig.5.7 shows the measured profiles of holes obtained by CHM and THM. It is obvious that in CHM the profile fluctuated strongly, implying that significant damages took place on the hole wall. In contrast, in THM little fluctuation can be observed on the profile, demonstrating that the hole has a good straightness and integrity.

In addition, the surface roughness of the holes walls were investigated and the results are as shown in Fig. 5.8. It can be seen that although the step feed affects the surface roughness Ra either in CHM or in THM, the Ra values in THM were smaller than those in CHM greatly.

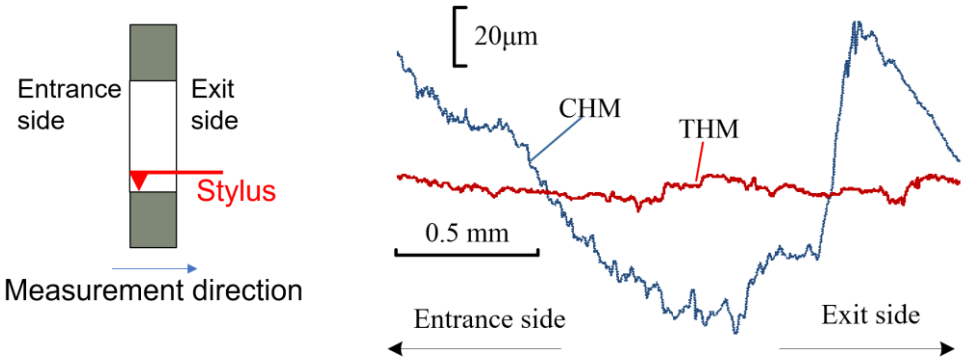

Fig. 5.8 Surface profile of the inner holes

The workpiece selected in this paper is CFRP and the two directions are distributed as shown in Fig. 5.9. The distribution of the inner wall of the hole is measured at eight positions as shown in the direction along the axis of the hole. The distribution of the angle between the cutting direction of the tool and the angle of the fiber in the eight positions is shown in Table 5.1. Therefore, as shown in Fig. 5.10. It can be seen from the figure that the surface roughness of the 1, 3, 5, and 7 positions is the lowest at different inclination angles. The 2, 4, 6, and 8 positions have the largest surface roughness. In other words, the surface is the roughest when the angle α of the fiber direction is 45°/135°.

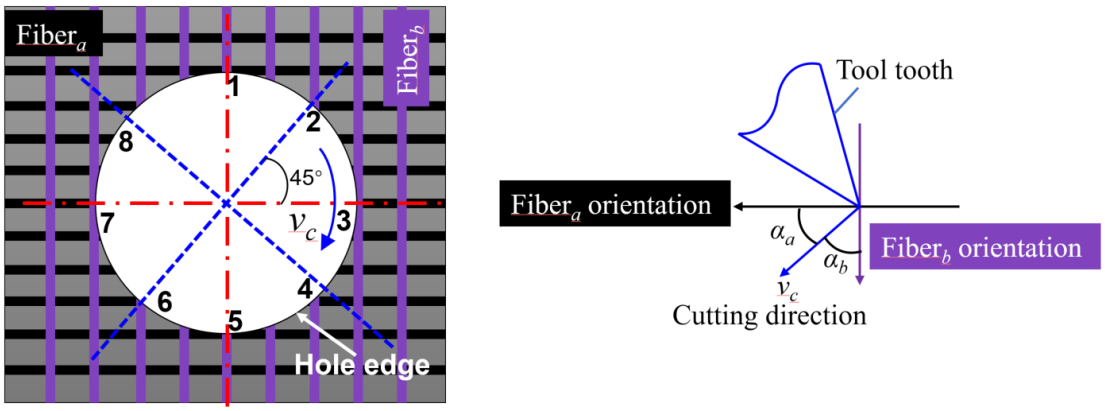

Fig. 5.9 Fiber distribution direction

Tab. 5.1 The angle α corresponding to the measurement position

Position	1	2	3	4	5	6	7	8
α_a	0°	45°	90°	135°	180°	45°	90°	135°
α_b	90°	135°	180°	45°	90°	135°	180°	45°

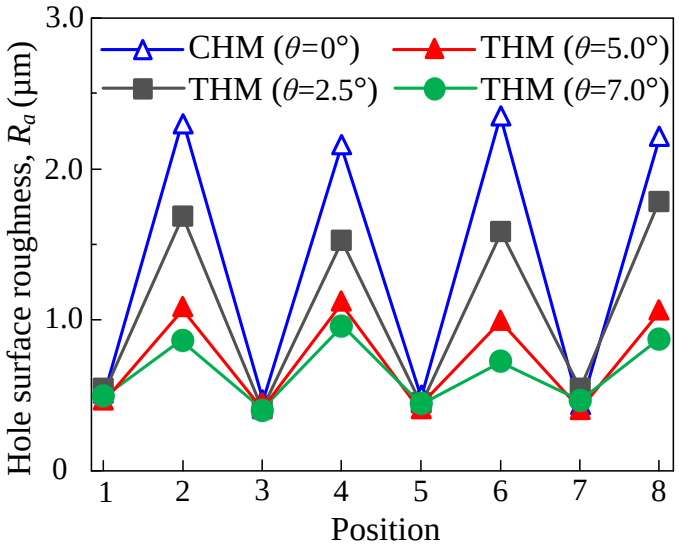

Fig. 5.10 Effect of α on hole surface roughness

During the hole making process of the composite material, the fiber can be cut at an angle of 0°-180° per revolution of the tool. Since the chip formation process of CFRP is a complicated process in which resin matrix destruction and carbon fiber fracture are intertwined, in order to simplify the CFRP chip formation process, the angle θ between

the fiber direction and the cutting direction can be 0°, 45°, 90° and 135°. Four typical paving structures are analyzed for orthogonal cutting process. The CFRP orthogonal cutting processing mechanism is shown in Fig.5.11. When the angle is 0°, the chips formed are mainly separated by layers; when the angle is 0° to 90°, the fibers are cut to form chips; when the angle is 90° to 180°, the bending and shearing interaction of the fibers causes the CFRP machined surface to assume a zigzag morphology. Studies of the various stages of the chip formation process can reveal the mechanism of chip formation and contribute to the study of the hole surface finish.

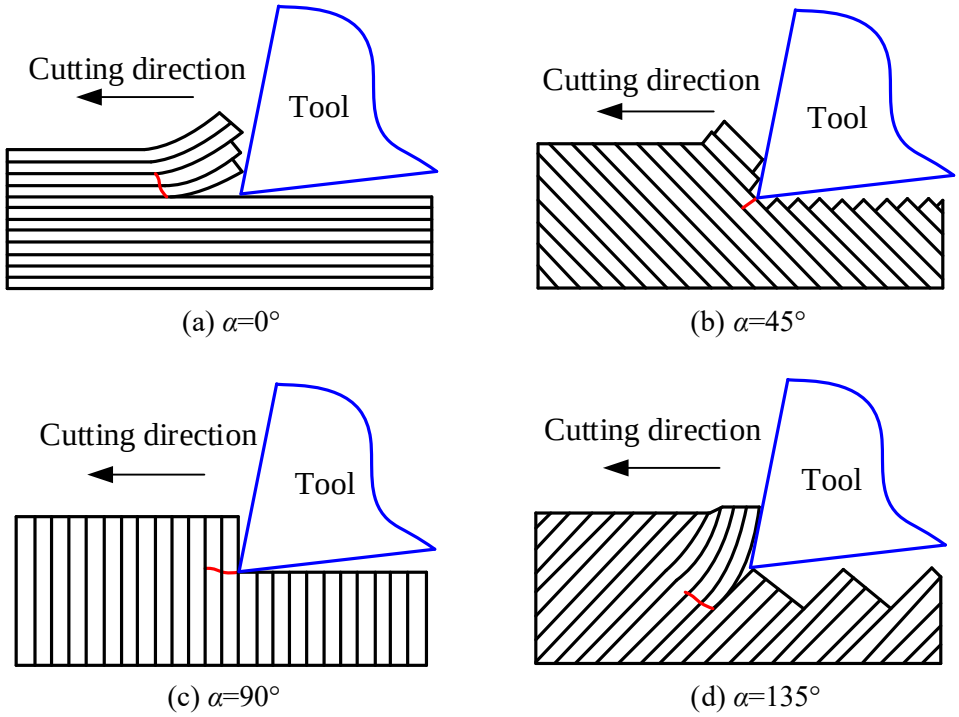

(a) α=0° (b) α=45°

(c) α=90° (d) α=135°

Fig.5.11 Cutting mechanisms in orthogonal machining of CFRP

Figure 5.12 and 5.13 are obtained by observing the inner wall of the hole by SEM. It can be seen from the figure that the angle α of the fiber direction is 0°, 45°, 90°, and the surface is smooth. When α is 135°, the surface quality is the worst at this time.

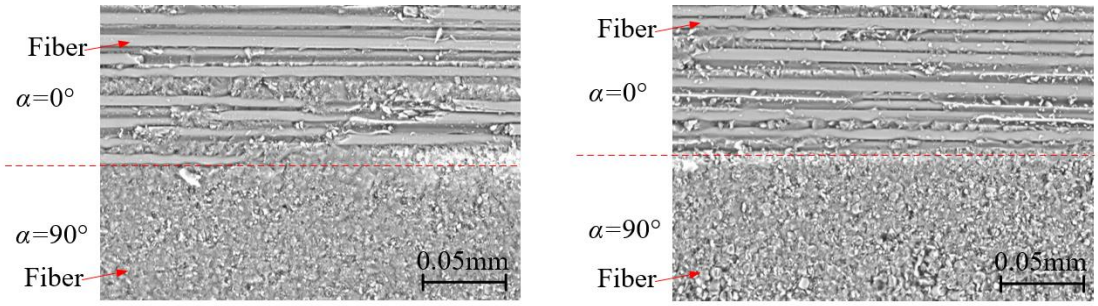

(a) CHM (b)THM

Fig. 5.12 The photos of hole surface topography of CHM (a) and THM (b) by SEM

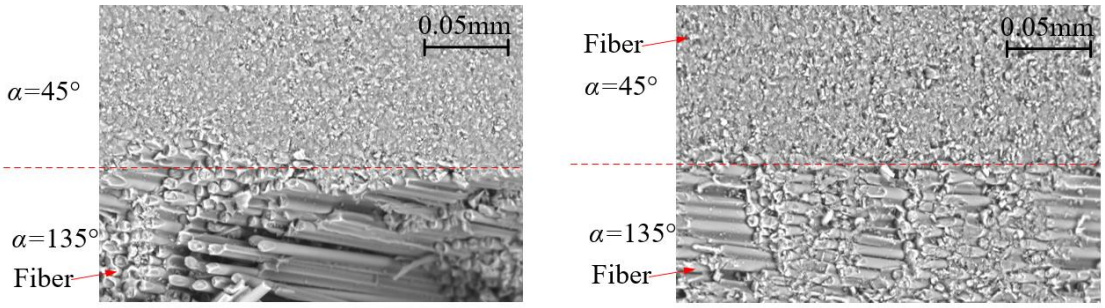

(a) CHM (b)THM

Fig. 5.13 The photos of hole surface topography of CHM (a) and THM (b) by SEM

In order to study the above problems, unidirectional CFRP was selected for CHM and THM as the processing object. The research content is as follows:

Qualitative CT-scans

Micro-computer tomography (CT) scans (Inspe Xio SMX-225 CT FPD HR, Shimadzu Co., Ltd. Japan) have been executed to analyze qualitatively the structure of the finished holes. During the experiment, a plate detector, which ran at 200 kV tube voltage, was used to measure the hole entrances. Further, an industrial micro-CT system was used at 225 kV accelerating voltage and 4μm resolution ratio to scan the holes by CHM and THM. The scanning data was visualized using software (VGStudio MAX 3.0).

Figs. 5.14 (a) and (b) show the CT-scan results of the holes obtained by CHM (θ = 0°) and THM (θ = 5°), respectively. It is clear that there are many chippings at hole entrance in CHM while chipping is rarely found at the entrance of hole in THM. The tearing of hole entrance in THM has been restrained. In CHM, the hole surface is rather rough at $90° < \alpha < 180°$. In contrast, the hole surface is smooth for all α in THM.

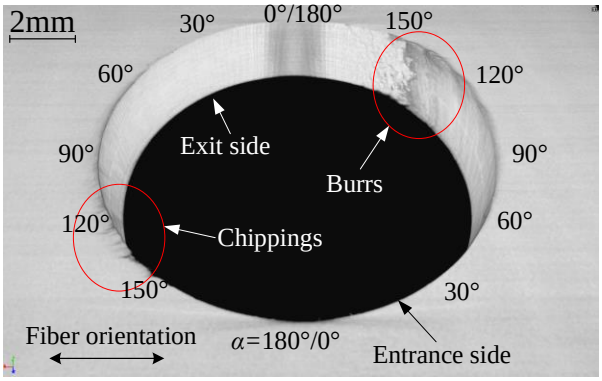

(a) CHM (θ = 0°)

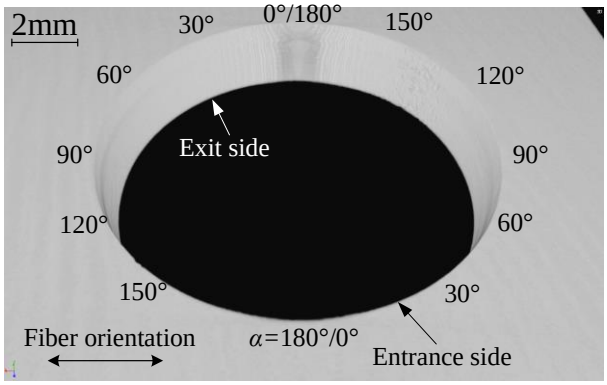

(b) THM (θ = 5°)

Fig. 5.14 3D CT-scans of the holes by means of CHM and THM

Hole accuracy

Fig. 5.15 shows the fitting mode of a typical hole surface obtained by CHM (θ = 0°) and THM (θ = 5°). Void pixels of the fitting mode represent the defects of hole wall where the fit deviation is $\geqslant$0.11 mm or $\leqslant$ -0.11 mm. Evidently, a large number of defects are be found in CHM finished hole while there are few in THM finished hole. The diameters of fitting modes in CHM and THM are 11.93 mm and 12.02 mm, respectively. The ideal diameter of the hole is 12.00 mm in this work. The accuracy error of hole size in THM is 71.3% smaller than that of CHM. The burrs on the hole surface created by CHM are considered to the cause.

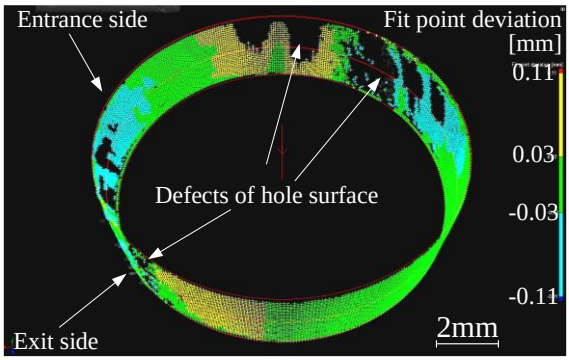

(a) CHM (θ = 0°)

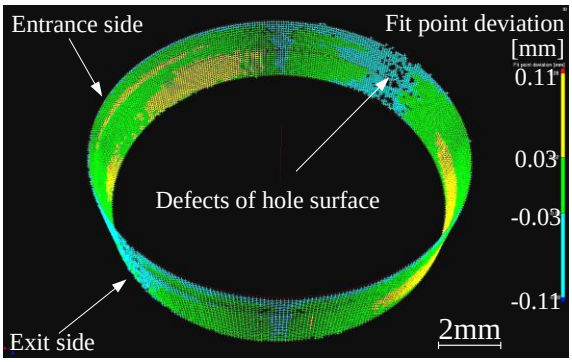

(b) THM (θ = 5°)

Fig.5.15 Fitting mode of the hole surface of a typical hole obtained by CHM and THM

Delamination

The hole cross sections of a hole obtained by CHM (θ = 0°) and THM (θ = 5°) are also imaged with optical microscope (Fig. 5.16). The delamination is found at both entrance and exit surface of holes finished by CHM, which is in stark contrast to hole finished by THM by which no delamination is observed. The quality of finished hole by THM is considerably better than CHM, which is attributed to two-stage formation of exit holes in THM: in the primary-stage an exit hole of smaller diameter than the desired one is generated and the diameter of the hole gradually expands until the desired diameter is reached in secondary-stage [16].

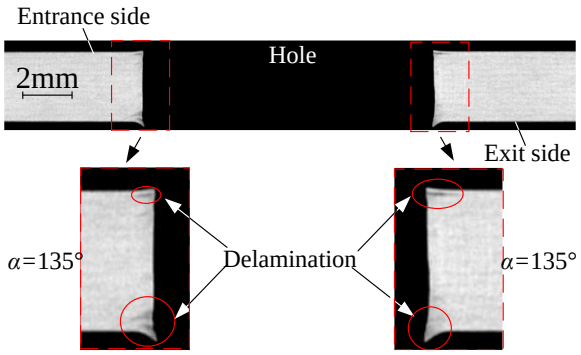

(a) CHM (θ = 0°)

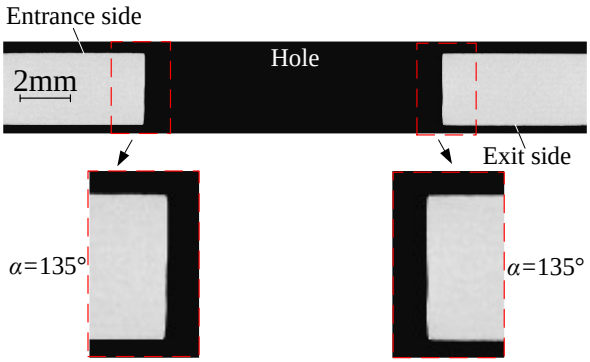

(b) THM (θ = 5°)

Fig.5.16 Optical images of hole cross sections of a typical hole obtained by CHM and THM

Hole surface finish

Hole surface topography of CHM (θ = 0°) and THM (θ = 5°) by CT-scans (unrolling the hole surfaces) and SEM (the hole surface at 90°<α<180°) are presented in Figs. 5.17 & 5.18. In CHM, at 90°<α<180°, rugged surface can be observed and most defects are located around α= 135°. But in THM, drilled hole surface is smooth for all α.

Figs. 5.17 (b) and 5.18 (b) are the SEM images of the hole surface at 120°<α<150°. One can see that there is severe fiber bending and fiber-matrix debinding in CHM whilst it is not the case for THM. From the images, the longest burrs by CHM and THM measure 0.204mm and 0.031 mm, respectively. The length of THM burr is 85% shorter than CHM and the quantity of the burrs by THM is much smaller.

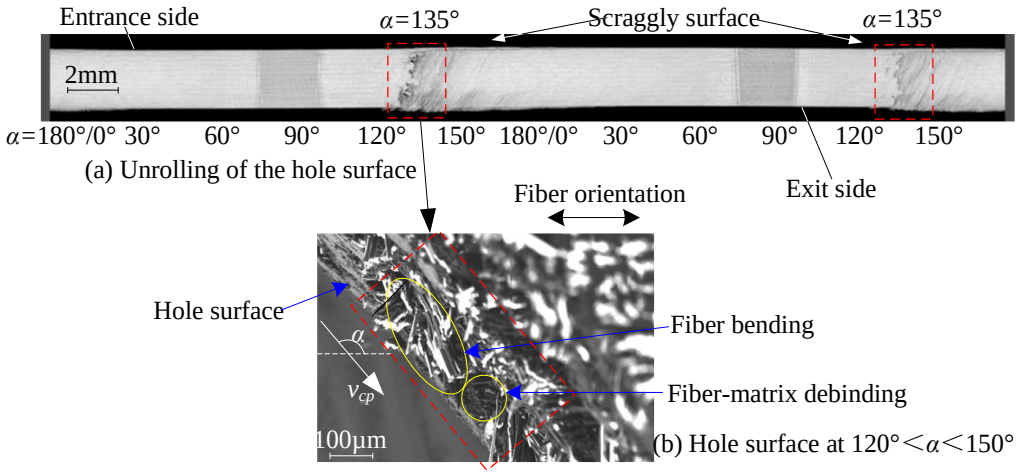

Fig.5.17 The photos of hole surface topography of CHM by CT-scans (a) as well as SEM (b)

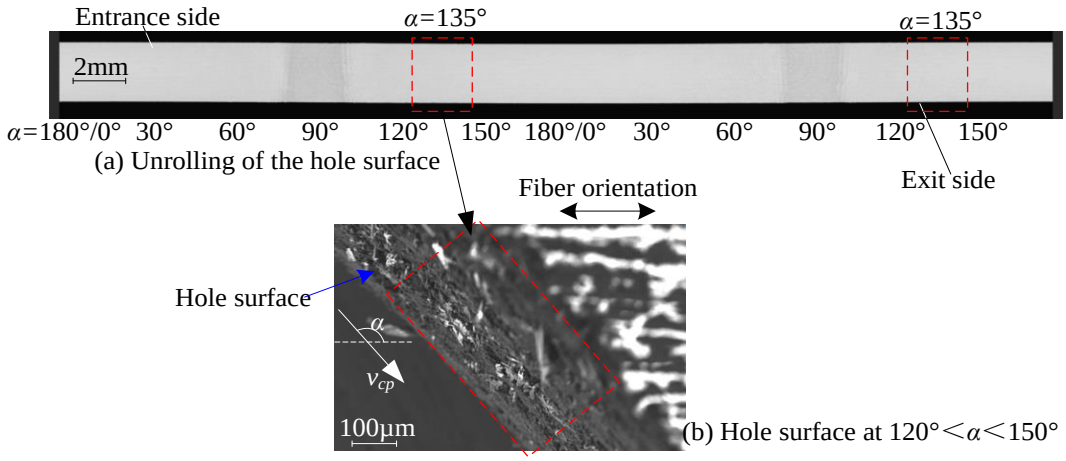

Fig.5.18 The photos of hole surface topography of THM by CT-scans (a) as well as SEM (b)

The quality of finished hole surface was also evaluated with a contact-type surface profiler. The measurements were taken at four positions on inner surface of holes finished by CHM (θ = 0°) and THM (θ= 2.5°, 5.0°, 7.5°), namely at α = 180°/0°, 45°, 90° and 135° respectively. The stylus of the profiler was dragged 2 mm long along axial direction of the hole for all measurements. It was repeated five times for each position. The effect of α on R_a at different tilt angles θ is in Fig. 5.19. α has a significant effect on the R_a and at different tilt angles θ, namely under different conditions of CHM and THM, R_a changes with respect to α in a similar trend. In addition, there exists a critical value of α = 90°. In the range of 0° $\leqslant$ α $\leqslant$ 90°, R_a keeps almost unchanged for CHM (θ = 0°) and THM (θ = 2.5°, 5.0°, 7.5°). The value of R_a ranges from 0.55 μm to 0.83

μm, 0.55 μm to 0.82 μm, 0.53 μm to 0.81 μm, and 0.52 μm to 0.79 μm, respectively. Once α is in excess of the critical value 90°, R_a increases sharply. When CHM ($\theta = 0°$) and α = 135°, the value of R_a is even greater than the measurement range of 6.3μm, which is caused by a large amount of fiber bending and fiber-matrix debinding when α = 135°. Meanwhile, when α = 135°, the value of R_a is significantly affected by θ. As θ increases from 0° to 7.5°, R_a decreases from that more than 6.3 μm to 1.07 μm. This shows that THM ($\theta > 0°$) is effective in reducing fiber bending and fiber-matrix debinding when $\alpha = 135°$; the larger the angle θ, the more significant the reduction. The above results also indicate better uniformity of hole surface roughness in THM, which will benefit fitting accuracy of the holes and operational lifetime of workpiece.

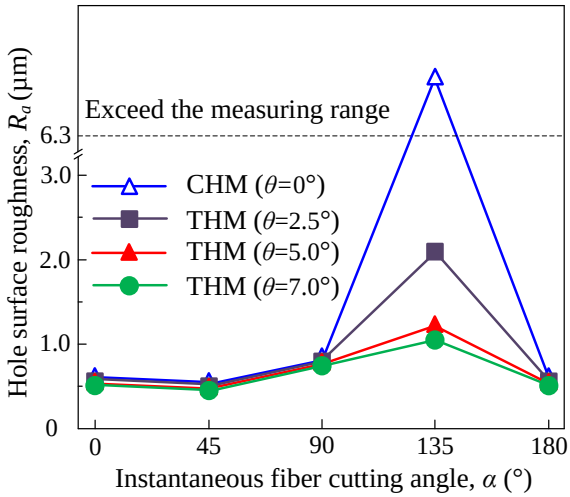

Fig.5.19 The effect of α on R_a at different tilt angles θ

Theoretical analysis of the above experimental results as follow:

Fiber fracture behavior

Fig. 5.20 (a) illustrates the hole drilling of CFRP in the THM and the close-up of cutting area is in Fig. 5.20 (b). For the sake of simplicity, the unidirectional CFRP is chosen as the material of workpiece. Two coordinate systems $[x_by_bz_bO_b]$ and $[x_ty_tz_tO_t]$ are set up. The $[x_by_bz_bO_b]$ with origin of O_b is for workpiece and $[x_ty_tz_tO_t]$ with origin of O_t for tool. O_b and O_t are the centers of the hole and tool, respectively. In the $[x_by_bz_bO_b]$

coordinate, x_b is parallel to the direction of fiber in the unidirectional CFRP and z_b is along the axis of hole and the end face of hole lies in the plane of $x_bO_by_b$. On the other hand, z_t is in the direction of tool axis in the coordinate of $[x_ty_tz_tO_t]$ and the end face of tool is in the $x_tO_ty_t$ plane. The workpiece coordinate system $[x_by_bz_bO_b]$ is stationary while the $[x_ty_tz_tO_t]$ is fixed onto the cutting tool and can rotate with cutting tool. From THM kinematical analysis, the angle θ is the z_t with respect to z_b. Q is located on the perimeter of the tool end face. Assuming that Q is on the x_t of the coordinate $[x_ty_tz_tO_t]$ and in contact with the inner surface of the hole at time instant t_0, the Q will rotate with respect to its axis at an angle of β after Δt and reach to P and the $[x_ty_tz_tO_t]$ will be $[x_t'\ y_t'\ z_tO_t]$ (Fig. 5.20 (b)). β can be written as the Eq. (5.1). The shadowed QTMP (Fig. 5.20 (b)) is the area that is cut away during the time interval Δt. P is in the plane of $x_b'\ O_b'\ y_b'$ which is parallel to $x_bO_by_b$. v_c is designated the linear speed of P. The v_c is a linear velocity of P which can be decomposed into the linear rotation velocity of tool, v_t, and linear revolution velocity of tool, v_o, in the helical milling process. As v_t, i.e., the cutting speed, is usually greater than 20 times the v_o in practical helical milling of CFRP drilling with end mills [8-9, 17], $v_c \approx v_t$. Therefore, the influence of revolution velocity v_o of tool is not taken into consideration here. In this case, v_{cp} and v_{ca} are the projections of v_c in plane $x_b'\ O_b'\ y_b'$ and the axis of the hole, respectively. The revolution speed of the tool is discarded since the revolution rate is far lower than the rotation rate of the tool. Likewise, the force F_{cp} and F_{cp} are the components of force F_c in the directions of v_{cp} and v_{ca}. F_c can be expressed with Eq. (5.2), the same direction as v_c. Specifically, F_c can be formulated as Eq. (5.3) in the coordinate $[x_by_bz_bO_b]$. Accordingly, F_{cp} and $F_{\tau a}$ are listed out in Eqs.(5.4)&(5.5).

$$\beta = 60 n_c \Delta t \tag{5.1}$$

$$\overrightarrow{F_c} = \left(0, -\left|\overrightarrow{F_c}\right|, 0\right) \tag{5.2}$$

$$\begin{bmatrix} x_{bF_c} \\ y_{bF_c} \\ z_{bF_c} \end{bmatrix} = \begin{bmatrix} \cos\theta & 0 & -\sin\theta \\ 0 & 1 & 0 \\ \sin\theta & 0 & \cos\theta \end{bmatrix} \begin{bmatrix} \cos\beta & -\sin\beta & 0 \\ \sin\beta & \cos\beta & 0 \\ 0 & 0 & 1 \end{bmatrix} \times \begin{bmatrix} 0 \\ -\left|\overrightarrow{F_c}\right| \\ 0 \end{bmatrix} \tag{5.3}$$

$$\overrightarrow{F_{cp}}=\left(x_{bF_c},y_{bF_c},0\right) \tag{5.4}$$

$$\overrightarrow{F_{\tau a}}=\left(0,0,z_{bF_c}\right) \tag{5.5}$$

Combining Eqs. (5.2) - (5.5), the relations between these three forces is written as follows

$$F_{cp}=F_c\sqrt{\sin^2\theta\cos^2\beta+\cos^2\theta} \tag{5.6}$$

$$F_{\tau a}=F_c\sin\theta\sin\beta \tag{5.7}$$

Figs. 5.21 and 5.22 shown are top view of fiber cutting by helical milling on the $x_b{}'$ $O_b{}'$ $y_b{}'$ plane. The points Q′ and $O_t{}'$ are the projection of the points Q and O_t onto the $x_b{}'$ $O_b{}'$ $y_b{}'$ plane. The angle β' is the projection of the angle β onto the $x_b{}'$ $O_b{}'$ $y_b{}'$ plane. The dashed line in the figure shows the projection of the position of the previous rotation cycle of the tool on the $x_b{}'$ $O_b{}'$ $y_b{}'$ plane. At the point P, bottom cutting edge contacts the fiber to be cut away. The polygon Q′ UVP area represents the material removal area by the cutting edge rotating from Q′ to P. The force exerted onto the fiber was analyzed. The cutting force F_{cp} parallel to cutting direction can be decomposed to the tensile force $F_{\sigma p}$ along the fiber axis direction and the shear force $F_{\tau p}$ perpendicular to the fiber axis. The relations between them are shown in Eqs. (5.8) and (5.9).

$$F_{\sigma p}=F_{cp}\cos\alpha \tag{5.8}$$

$$F_{\tau p}=F_{cp}\sin\alpha \tag{5.9}$$

Where α is the instantaneous fiber cutting angle (the relative angle between the fiber orientation and the cutting direction, see Figs. 5.21 & 5.22). Figs. 5.21 and 5.22 illustrate the THM process on $x_b{}'$ $O_b{}'$ $y_b{}'$ plane at $0°\leqslant\alpha\leqslant 90°$ and $90° < \alpha < 180°$, respectively.

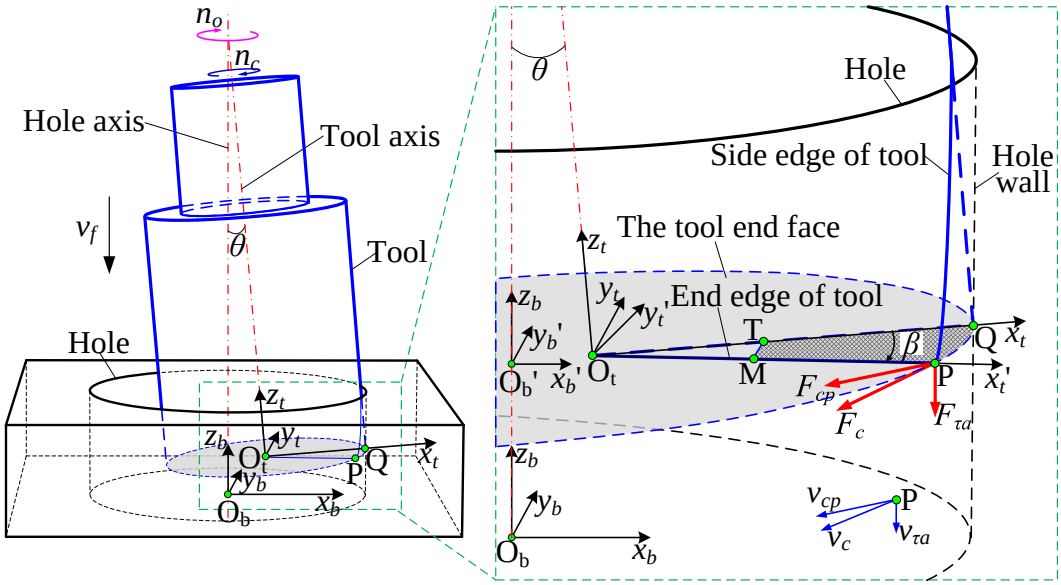

(a) The hole drilling of CFRP (b) Partial enlarged detail

Fig. 5.20 Schematic illustrations of tilted helical milling

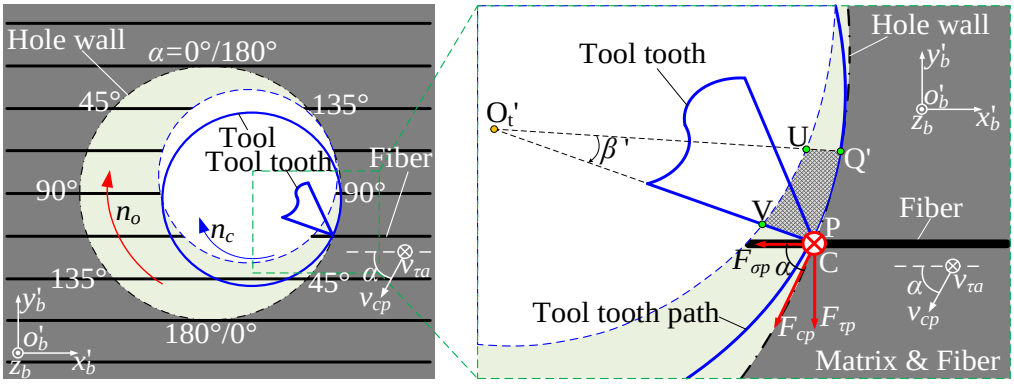

(a) THM process on x_b' O_b' y_b' plane (b) Close-up of cutting area

Fig. 5.21 Schematic of THM process on x_b' O_b' y_b' plane at $0° \leqslant \alpha \leqslant 90°$

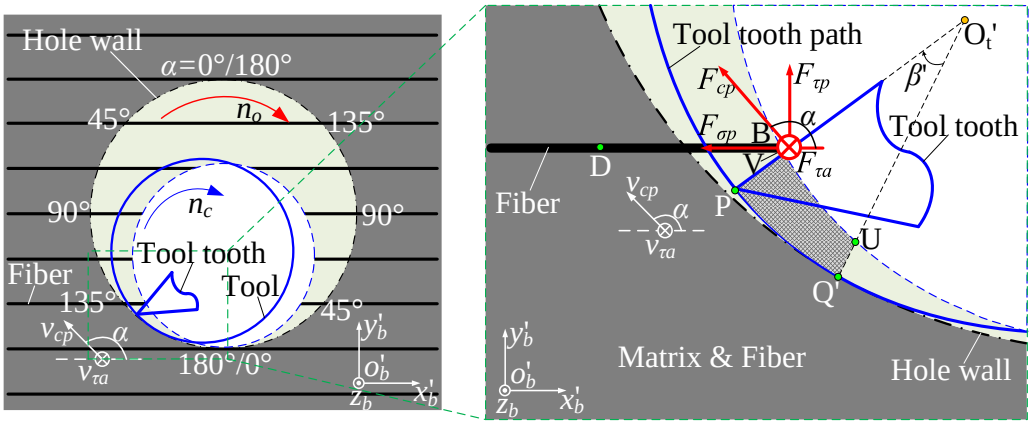

(a) THM process on x_b' O_b' y_b' plane (b) Close-up of cutting area

Fig. 5.22 Schematic of THM process on x_b' O_b' y_b' plane at $90° < \alpha < 180°$

In the THM, the tool rotates with its axis and concurrently revolves on the hole axis. The cutting direction keeps changing continuously and periodically with tool revolving. It is known that the instantaneous fiber cutting angle α has a great impact on the cutting modes of the fiber [13-14, 18-20], which is discussed in detail as follows.

When $0° \leqslant \alpha \leqslant 90°$ (Figs. 5.21 (a) & (b)), $F_{\tau p}$ is on the plane $x_b' \ O_b' \ y_b'$ and the fiber could be highly rigidly supported by hole wall material and fiber bends little. Meanwhile, the force $F_{\sigma p}$ of the tool along the fiber axis imposes a tensile stress on the fiber, and the high stress appears in the tool-fiber contact area due to the high rigidity of fiber and the small contact area. This stress concentration makes fiber easier fracture in the affinity of tool nose (Fig. 5.23 (a)). In this case, the hole surface roughness and subsurface damage are small [19, 20]. When the fiber is subjected to the component force $F_{\tau a}$ along the hole axis and toward the underneath of the workpiece surface, the fiber could also be highly rigidly supported by bottom material of the hole during cutting process. The angle between the fiber axis and the cutting direction of $v_{\tau a}$ is also equal to 90°. It is desired to make the fiber fracture in the affinity of tool nose, hence high hole surface finish can be achieved.

On the other hand, the fiber is subjected to $F_{\tau p}$ and $F_{\tau a}$ for $90°<\alpha<180°$ in plane $x_b' \ O_b' \ y_b'$ (Figs. 5.22 (a) & (b)). $F_{\tau p}$ is normal to the fiber axis while the $F_{\tau a}$ is a downward force along the axis of hole. Initially, as shown in Fig. 5.23 (b) the fiber comes into contact with the rake face of tool end cutting edge at the position 1 in plane $x_b' \ O_b' \ y_b'$ and later the fiber will deform as cutting tool moves. At position 2, the fiber will fracture when the shear stress τ due to $F_{\tau a}$ and $F_{\tau p}$ is beyond the allowable stress $[\tau]$ of fiber. The process continues unless the fiber is cut away by the tool. Supposing that the fiber starts to bend at position D, based on Eq. (5.7) the precession angle of tool φ_B (positive: counterclockwise) can be computed when the fiber fractures under the force $F_{\tau p}$ in plane $x_b' \ O_b' \ y_b'$ [21]. It follows that

$$\varphi_B = \frac{\left([\tau]A\right)^2 l^2}{2EI} - \frac{\left(F_c \sin\beta\right)^2 l^2}{2EI}\sin^2\theta \tag{5.10}$$

where A is the area of fiber cutting, l the length of BD, E the Young's modulus, I the moment of inertia.

In the helical milling process, $0° < \beta < 180°$ [11]. One can know from Eq. (5.10) that φ_B will decrease with increasing θ. So greater θ will induce smaller φ_B for $\theta > 0°$ in THM, that is to say, the less the fiber bends and debinds, the less the hole is damaged in the hole-drilling of CFRP. In the case of $\theta = 0°$ (i.e. CHM process), φ_B reaches the maximum, as a consequence of which the fiber bends and debinds most severely and the hole surface is most damaged in CHM [20].

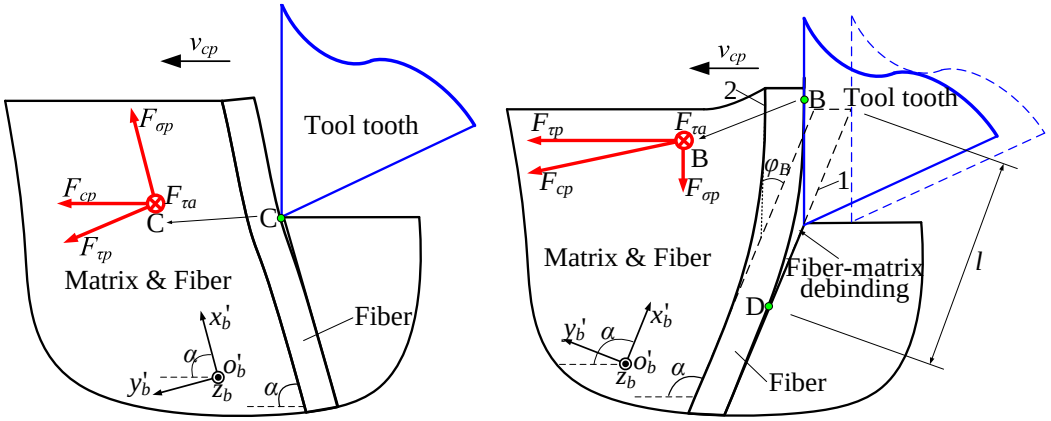

(a) $0° \leqslant \alpha \leqslant 90°$ (b) $90° < \alpha < 180°$

Fig. 5.23 Fiber fracture in the cutting of CFRP on x_b' O_b' y_b' plane

5.4 Summary

The surface finish of CFRP hole obtained by tilted helical milling (THM) was investigated theoretically. Experiments were performed to verify the theoretical analysis. From the theoretical and experimental results, some conclusions can be drawn as following:

(1) The thrust force in THM ($\theta = 5°$) is only ~50% of that in conventional helical milling (CHM) ($\theta = 0°$) and features smaller fluctuation.

(2) By comparison with CHM, THM not only inhibits entrance tearing and exit delamination but also improve the hole diameter accuracy.

(3) In CHM, rugged hole surface was observed for instantaneous fiber cutting angle $90° < \alpha < 180°$. But the hole surface is smooth for all α in THM.

(4) In CHM, a large amount of fiber bending and fiber-matrix debinding probably happen for $90° < \alpha < 180°$, which can be ameliorated greatly by THM. The larger

the angle θ, the more significant the amelioration.

(5) THM is able to achieve better roughness uniformity of hole surface than CHM.

References

[1] Wang, H.J., Sun, J., Zhang, D.D., Guo, K., Li, J.F., "The effect of cutting temperature in milling of carbon fiber reinforced polymer composites," Compos. Part A APPL. S., Vol. 91, pp. 380–387, 2016.

[2] Cheng, H., Zhang, K.F., Wang, N., Luo, B., Meng, Q.X., "A novel six-state cutting force model for drilling-countersinking machining process of CFRP-Al stacks," Int. J. Adv. Manuf. Technol., Vol. 89, No. 5–8, pp. 2063–2076, 2017.

[3] Zitoune, R., Krishnaraj, V., Collombet, F., "Study of drilling of composite material and aluminium stack," Compos. Struct., Vol. 92, No. 5, pp. 1246–1255, 2010.

[4] Wei, J.C., Jiao, G.Q., Jia, P.R., Huang, T., "The effect of interference fit size on the fatigue life of bolted joints in composite laminates," Compos. Part B Eng., Vol. 53, pp. 62–68, 2013.

[5] Alberdi, A., Artaza, T., Suarez, A., Rivero, A., Girot, F., "An experimental study on abrasive waterjet cutting of CFRP/Ti6Al4V stacks for drilling operations," Int. J. Adv. Manuf. Technol., Vol. 86, No. 1–4, pp. 691–704, 2016.

[6] Khashaba, U.A., "Delamination in drilling GFR-thermoset composites," Compos. Struct., Vol. 63, No. 3–4, pp. 313–327, 2004.

[7] Liu, D.F., Tang, Y.J., Cong, W.L., "A review of mechanical drilling for composite laminates," Compos. Struct., Vol. 94, No. 4, pp. 1265–1279, 2012.

[8] Pereira, R.B.D., Brandao, L.C., Paiva, A.P., Ferreira, J.R., Davim, J.P., "A review of helical milling process," Int. J. Mach. Tool. Manuf., Vol. 120, pp. 27–48, 2017.

[9] Liu, J., Chen, G., Ji, C.H., Qin, X.D., Li, H., Ren, C.Z., "An investigation of workpiece temperature variation of helical milling for carbon fiber reinforced plastics (CFRP)," Int. J. Mach. Tool. Manuf., Vol. 86, No. 89–103, 2014.

[10] Iyer, R., Koshy, P., Ng, E., "Helical milling: an enabling technology for hard machining precision holes in AISI D2 tool steel," Int. J. Mach. Tool. Manuf., Vol. 47, No. 2, pp. 205–210, 2007.

[11] Denkena, B., Boehnke, D., Dege, J.H., "Helical milling of CFRP–titanium layer compounds," CIRP J. Manuf. Sci. Technol. Vol. 1, No. 2, pp. 64–69, 2008.

[12] Eguti, C.C.A., Trabasso, L.G., "Design of a robotic orbital driller for assembling aircraft structures," Mechatronics, Vol. 24, No. 5, pp. 533–545, 2014.

[13] Shan, Y.C., He, N., Li, L., Zhao, W., Qin, X.J., "Orbital milling hole of aerospace Al-alloy with big pitch," Transactions of Tianjin University, Vol. 17, No. 5, pp.

329–335, 2011.

[14] Wang, H.Y., Qin, X.D., Li, H., Ren, C.Z., “Analysis of cutting forces in helical milling of carbon fiber-reinforced plastic,” P. I. Mech. Eng. B-J Eng., Vol. 227, No. 1, pp. 62–74, 2013.

[15] Wu, Y.B., Wang, Q., Nomura, M., “Proposal of tilt helical milling method for hole creation of carbon fiber reinforced plastic (CFRP),” Adv. Mater. Res., Vol. 1136, pp. 190–195, 2016.

[16] Wang, Q., Wu, Y.B., Bitou, T., Nomura, M., Fujii, T., “Proposal of a tilted helical milling technique for high quality hole drilling of CFRP: Kinetic analysis of hole formation and material removal,” Int. J. Adv. Manuf. Technol., Vol. 94, No. 9–12, pp. 4221–4235, 2018.

[17] Zhu F., Xu X.P. and Kang R.K., “Drilling C/E Composites with Electroplated Diamond Abrasive Tool and its Damage Evaluation Method,” Key Engineering Materials, Vol. 487, pp. 371-375, 2011.

[18] Wang H.Y., Qin X.D., Li H., Ren C.Z, “Analysis of cutting forces in helical milling of carbon fiber–reinforced plastics,” P. I. Mech. Eng. B-J. Eng., Vol. 227, No. 1, pp. 62–74. 2012.

[19] Karpat, Y., Bahtiyar, O., Deger, B., “Mechanistic force modeling for milling of unidirectional carbon fiber reinforced polymer laminates,” Int. J. Mach. Tool. Manuf., Vol. 56, pp. 79–93, 2012.

[20] Wang, X.M., Zhang, L.C., “An experimental investigation into the orthogonal cutting of unidirectional fiber reinforced plastics,” Int. J. Mach. Tool. Manuf., Vol. 43, No. 10, pp. 1015–1022, 2003.

[21] Xu, W.X., Zhang, L.C., “Mechanics of fiber deformation and fracture in vibration-assisted cutting of unidirectional fiber-reinforced polymer composites,” Int. J. Mach. Tool Manuf., Vol. 103, pp. 40–52, 2016.

[22] Gupta V., “An introduction to mechanics of materials,” Oxford, U.K. : Alpha Science Intl, pp. 710-711, 2013.

Chapter VI
Conclusions

6.1 Dissertation Conclusions

A so-called tilted helical milling (THM) method was proposed for drilling CFRP products with high quality and high efficiency. Firstly, a theoretical analysis of the hole forming process and material removal rate during THM was performed and experiments were conducted to verify its basic processing properties and strengths. Secondly, the exit formation of the hole was studied, and the inhibition mechanism of the hole exit formation on the exit delamination defect was figured out. Further, both cutting force and cutting temperature can produce a significant effect on the CFRP processing quality. A string of plans was adopted to measure the cutting temperature during THM processing, and the effects of cutting force and cutting temperature were analyzed in different machining conditions. Lastly, the processing quality of hole entrance, exit and inner surface in different processing conditions was assessed to optimize the processing conditions and provide guidance for potential industrial application. The obtained results can be summarized as follows:

(1) THM can avoid the zero speed point problem, reduce thrust force/cutting temperature, and remove chips easily.

(2) Comparison with CHM, THM not only inhibits the entrance tearing and exit delamination but also improve the hole surface quality.

(3) Through the experimental studies on the effect of processing parameters on the hole quality, the advantage of THM over CHM has been confirmed.

According to the above results, high quality holes can be successfully obtained with high efficiency by THM.

6.2 Future Recommendations

The research in the THM is still in preliminary stage. There are many topics and unclear points that need to be investigated to ensure the reliability to apply this technology on the actual machining. In what follows, some recommendations and notes were list for future work.

(1) Dynamic analysis in tilted helical milling (THM) process should be studied.

(2) The reason how the critical thrust force cause hole exit delamination failure should be studied.

(3) The influence of different tool geometry parameters on the machining quality should be studied. The special tools for THM should be developed.

(4) The ultrasonic-assisted THM technique should be used to obtain the burr-free hole.

This page intentionally left blank.

ACKNOWLEDGEMENTS

I would like to sincerely thank many people who have contributed to the completion of this work. First, I wish to express my gratitude to my supervisor Prof. Yongbo Wu for his supervision throughout this research, for his encouragement regarding my professional development and for his advice on organizing and writing this thesis. Next, I want to thank my second supervisor Prof. Teruo Bitoh. Without his undeserved kindness, there is no hope to finish my last year of Ph.D study. He has walked me through all the stages of last school year. Without his consistent and illuminating instruction, this thesis could not have reached its present form.

I want to thank Prof. Dong Lu, Prof. Mitsuyoshi Nomura, Prof. Tatsuya Fujii and Prof. Jia Gu for their valuable advice on this research and I appreciate the enormous amount of time they spent with me discussing my research and correcting this dissertation. I am also grateful to Prof. Tsunehisa Suzuki for discussing my research at lab meetings and for his advice on writing this dissertation. I would like to thank Mr. Shigeo Miura, Mr. Seiichi Kimura and the other members of the AMT Group for their support and help. Furthermore, a deep thank is also given to Mr. Junfei Huang (Shimadzu (China) Co., LTD. Shenzhen Branch) for his help on the experimental works of CT-scans.

Finally, I thank my parents and my wife, who have always believed in me, encouraged me, and given me all their support whenever I have needed it.

List of Publications

Monograph:

1. Y. Wu, Q. Wang, S. Li, and D. Lu, “Chapter 4: Ultrasonic Assisted Machining of Nickle-based Superalloy Inconel 718” in Superalloys for Industry Applications, ISBN 978-1-78923-539-5, InTech Publishers, 2018.

Journal Papers:

1. Q. Wang, Y.B. Wu, T. Bitoh, M. Nomura, T. Fujii. Proposal of a tilted helical milling technique for high quality hole drilling of CFRP: Kinetic analysis of hole formation and material removal. The International Journal of Advanced Manufacturing Technology, Vol. 94, No. 9–12, pp. 4221–4235, 2018.
2. Y.B. Wu, Q. Wang, Nomura M. Proposal of tilt helical milling method for hole creation of carbon fiber reinforced plastic (CFRP). Advanced Materials Research, Vol. 1136, pp. 190–195, 2016.
3. Q. Wang, Y.B. Wu, J. Gu, D. Lu, Y.B. Ji, M. Nomura. Fundamental Machining Characteristics of the In-base-plane Ultrasonic Elliptical Vibration assisted Turning of Inconel 718. Procedia CIRP, Vol. 42, pp. 858-862, 2016.
4. Q. Wang, Y.B. Wu, T. Bitoh, D. Lu, M. Nomura, T. Fujii. Proposal of a tilted helical milling technique for high quality hole drilling of CFRP: Kinetic analysis of hole exit formation. Machining Science and Technology. LMST-2018-0048. Re-submitted after revision. 2018.
5. Q. Wang, Y.B. Wu, Y.G Li, D. Lu, T. Bitoh. Proposal of a tilted helical milling technique for high quality hole drilling of CFRP: Analysis of hole surface finish. The International Journal of Advanced Manufacturing Technology. JAMT-D-18-01723. Re-submitted after minor revision. 2018.

The Domestic Conferences Proceedings:

1. Q.Wang, Y.B.Wu, Nomura, et al. An experimental study on thrust force in hole drilling of CFRP by tilt helical milling. Proceedings of the Japan Society for Precision Engineering, 13-17, March 2017. Tokyo, Japan.
2. Q.Wang, Y.B.Wu, Jia Gu, et al. On the hole formation in the hole creation of CFRP by tilt helical milling. Proceedings of the Japan Society for Precision Engineering, 15-17, March 2016. Tokyo, Japan.
3. Q.Wang, Y.B.Wu, Nomura, et al. Influence of tool eccentricity in hole creation of CFRP by tilt helical milling, Proceedings of the Japan Society for Precision Engineering, 01-06, September 2015. Sendai, Japan.
4. Q. Wang, Y.B.Wu, S.L. Xu, T. Bitoh. A study of tilted helical milling technique for hole drilling of CFRP. The 14th Conference on Machining & Advanced Manufacturing Technology. 9-12, June 2017. Shen Zhen, China. (In Chinese)

The International Conference Proceedings:

1. Q. Wang, Y.B.Wu, S.L. Xu, T. Bitoh. Fundamental Investigation on the tilt helical milling of carbon fiber reinforced plastics (CFRP). Proceedings of the 20th International Symposium on Advances in Abrasive Technology. 3-6 December 2017 Okinawa, Japan.
2. Q. Wang, Y.B. Wu, J. Gu, D. Lu, Y.B. Ji, M. Nomura. Fundamental Machining Characteristics of the In-base-plane Ultrasonic Elliptical Vibration assisted Turning of Inconel 718. 18th CIRP Conference on Electro Physical and Chemical Machining (ISEM XVIII). 19-22 April 2016 Tokyo, Japan.
3. Y.B. Wu, Q. Wang, M. Nomura. Proposal of tilt helical milling method for hole creation of carbon fiber reinforced plastic (CFRP). Proceedings of the 18th International Symposium on Advances in Abrasive Technology. 4-7 October 2015 Jeju Island, Korea.

Patent

1. A tilt helical milling unit and tilt helical milling equipment. Authorized in China. No.2017214485492. 2017.11.02.
2. A table and processing equipment for tilt helical milling. Authorized in China. No. 2017214525413. 2017.11.02.
3. A tilt helical milling unit and equipment. Authorized in China. No. 201721460805X. 2017.11.02.
4. A spindle unit with ultrasonic cavitation function. Authorized in China. No.2018200300669. 2017.12.18.
5. A tilt helical milling unit, processing equipment and processing method. Under review in China. No. 201711065912.7. 2017.11.02.

Awards & Travel Grants:

1. Excellent paper award, The 14th Conference on Machining & Advanced Manufacturing Technology, 12 June 2017.
2. 本荘由利産学振興財団国際交流助成, May 2015.